DIPARTIMENTO DI INGEGNERIA MECCANICA E AEROSPAZIALE

CORSO DI LAUREA MAGISTRALE IN

INGEGNERIA AEROSPAZIALE

Conception and realisation of a wind sensor for application onboard a stratospheric balloon

---

Candidato:

Martina Schenetti

Relatore:

Piero Gili

Correlatore:

Pascal Roches

Anno Accademico 2022/2023

Abstract

The present paper aims at presenting the work performed by the author within the company CNES.
The overall context of the internship is characterised by the design of a new category of stratospheric balloons that will ensure the ability to control the flight direction. The objective is to manoeuvre the aerostats thanks to altitude excursions so as to exploit favourable winds to reach the desired destination or maintain the position above a specific point of interest. It is therefore essential to know the wind profile in the balloons' vicinity.

The internship here described addresses this need by developing a prototype system capable of providing information about the wind direction and intensity, while maintaining reduced costs in economic terms and also from the point of view of the additional weight introduced.
To do so, two different methods have been developed to calculate the wind profile, based on numerical strategies that take as inputs the readings from multiple sensors. The instrument system consists mainly of a GNSS module and an IMU, which have been integrated into the electronics assembly.

To ensure the system's operation, sophisticated programs to be executed by the electronics have been developed, as well as a transmission system to enable the communication with the ground. Moreover, the system's thermal and mechanical design have been performed, together with the power supply sizing.

Keywords: Wind sensor, Stratospheric balloons, CNES, Electronics integration, Numerical analysis

Sommario

Il presente elaborato ha come obiettivo quello di presentare il lavoro svolto dall'autrice presso la compagnia CNES.
Il contesto generale in cui il tirocinio si inserisce è caratterizzato dal progetto di una nuova categoria di palloni stratosferici che garantirà la possibilità di controllare la direzione di volo. L'intento è quello di manovrare gli aerostati grazie ad escursioni di altitudine in modo da sfruttare venti favorevoli al fine di raggiungere la destinazione desiderata, o di mantenere posizione stazionaria al di sopra di un punto di interesse specifico. Di conseguenza, risulta essenziale conoscere il profilo del vento nei dintorni dei palloni stratosferici in questione.

Il tirocinio in esame risponde a tale necessità tramite lo sviluppo di un prototipo in grado di fornire informazioni in merito a direzione e intensità del vento nell'ambiente operativo del pallone, pur mantenendo costi ridotti sia in termini economici, sia in termini di masse addizionali introdotte.
A tale scopo, due differenti metodologie sono state individuate e implementate per determinare il profilo del vento. Entrambi gli approcci si basano sull'impiego di strategie di analisi numerica che consentono di calcolare direzione e intensità del vento a partire da dati in input collezionati da vari sensori a bordo del pallone stratosferico. Più precisamente, il sistema di strumenti utilizzato consiste principalmente di un modulo GNSS e di una unità IMU, i quali sono stati entrambi integrati nell'assemblaggio elettronico del prototipo sviluppato.

Per assicurare l'operatività del sistema, si è reso necessario programmare i componenti elettronici in modo tale da far sì che eseguissero precise routine di attività. Allo stesso tempo, si è sviluppato un sistema di trasmissione delle informazioni raccolte a bordo del pallone al fine di permettere la comunicazione con il gruppo di lavoro al suolo. In aggiunta, si sono progettati il design meccanico del sistema nel suo complesso e un sistema di protezione termica, infine si è condotto il dimensionamento del sistema di alimentazione.

Parole chiave: Sensore del vento, Palloni stratosferici, CNES, Integrazione elettronica, Analisi numerica

Résumé

Ce document vise à présenter le travail effectué par l'autrice au sein de l'entreprise CNES.
Le contexte général du stage est caractérisé par la conception d'une nouvelle catégorie de ballons stratosphériques qui assureront la capacité de contrôler la direction du vol. L'objectif est de manœuvrer les aérostats grâce à des excursions d'altitude afin d'exploiter les vents favorables pour atteindre la destination souhaitée ou maintenir la position au-dessus d'un point d'intérêt spécifique. Il est donc indispensable de connaître le profil du vent à proximité de ballons.

Le stage décrit ici répond à ce besoin en développant un système prototype capable de fournir des informations sur la direction et l'intensité du vent, tout en maintenant des coûts réduits en termes économiques et aussi du point de vue du poids supplémentaire introduit.
Pour ce faire, deux méthodes différentes ont été développées pour calculer le profil du vent, basées sur des stratégies numériques qui prennent en compte les relevés de plusieurs capteurs. Le système d'instruments se compose principalement d'un module GNSS et d'un IMU, qui ont été intégrés dans l'ensemble électronique.

Pour assurer le fonctionnement du système, des programmes sophistiqués à exécuter par l'électronique ont été développés, ainsi qu'un système de transmission pour permettre la communication avec le sol. En outre, la conception thermique et mécanique du système a été réalisée, ainsi que le dimensionnement de l'alimentation électrique.

Mots clés: Capteur de vent, Ballons stratosphériques, CNES, Intégration électronique, Analyse numérique

Table of contents

Table of figures

List of Tables

Introduction

The present memoir has the aim to report the End of Studies Project performed by the author, Martina Schenetti. The project has taken place within the company CNES, Centre National d'Études Spatiales. More precisely, the internship has been performed within the Balloons Department of the site located in Toulouse, France.
In compliance with the undersigned agreement, the internship has started on March 1st 2023, and lasted six months, until August 31st 2023.

The general objective of the End of Studies Project is to enable the student to autonomously apply knowledge and personal soft skills acquired during the academic formation in a professional context. As regards the specific project under discussion, it is focused on the "Conception and realisation of a wind sensor onboard a stratospheric balloon".

The internship is placed within a global context which is characterised by the project of a new category of stratospheric balloons. The innovative generation of aerostats is identified with the name "BALMAN", which stands for "ballons manœuvrables", as it will ensure the ability to control the balloons' direction of flight.
The aim is to obtain the possibility of manoeuvring the aerostats thanks to altitude excursions, in order to exploit favourable winds to reach the desired destination or to hover the balloon above a point of interest, thus allowing a reduced energy consumption. It is therefore essential to know the wind profile in the vicinity of the balloon's operating environment.

Generally, HAPS (High-Altitude Platform Systems) are strongly dependent on weather conditions, and in particular on the winds encountered during their missions. However, the available data provided by weather forecasting are characterised by several problems. In fact, their resolution at the altitudes of interest is usually low, and the adopted models are generally affected by significant errors. As a consequence, improving the knowledge of the HAPS' flight environment is of crucial importance in order to optimise the mission, both in terms of flight safety and from a commercial point of view.

To date, some techniques and technologies have partially met this necessity, for example the use of local radiosondes - which however work only if the sensor is in the vicinity of the system

-, or of heavy and expensive instruments, such as LIDAR (LIght Detection And Ranging) and RADAR (RAdio Detecting And Ranging).

The main purpose of the internship is therefore to address the need to know the wind intensity and direction below stratospheric balloons, by developing the prototype of a system capable of providing such information while maintaining reduced costs not only in terms of economic expenses, but also from the point of view of the additional weight introduced by the developed system.

The final objective of the global project is to evaluate the performance of the wind sounder and compare the HAPS steering manoeuvres with and without its additional information.

Reading guide

The present report is organised in Chapters that aim at describing in detail all the activities that have been performed, but also at explaining in which context the project has been developed.

Therefore, this paper is organised as follows: first, a general introduction to the End of Studies Project, its main purpose and its subject is provided. Later, Chapter 1 focuses on the working environment, providing information about the company where the internship has taken place, and more specifically about the department of interest.
Chapter 2 then deals with the analysis of the need that is addressed by the project, with detailed descriptions of the state of the art of the technologies that are currently in use to handle the problem, together with their advantages and drawbacks.
Afterwards, Chapter 3 is dedicated to the characterisation of the identified solution, and to the description of the project's plan, which phases are deeply outlined.
The main body of the present report is represented by Chapters 4 and 5. The first of these two describes the implementation of the solution identified for the wind's determination, with appropriate reference to the choices that have been made and to their justifications. Whereas Chapter 5 focuses on the characterisation of the subsystems that have been designed to make the wind sensor operational.
Then, Chapter 6 aims at discussing the project's achievements, presenting a critical view on the work that has been performed, and emphasizing the next steps to reach the final goals.
Finally, some conclusions are given on the ground of the activities carried out and the results obtained, with the purpose of summarising the project's development, along with potential improvements to be implemented in the future.

1. Working environment

1.1 The company

CNES - the Centre National d'Études Spatiales - is the French Space Agency, a governmental organisation founded in 1961, which is responsible for shaping and implementing France Government's space policy within the framework of international cooperation, particularly within Europe. The nation's space strategy is implemented in fields of scientific, strategic, and economic importance. Additionally, the agency is actively involved in the assets of defence space, security, and global monitoring for environment, thus playing an important role within the framework of major international schemes.

Since its foundation, CNES has been taking part in scientific programmes in conjunction with European and international research organisations. Furthermore, it has implemented various operational and commercial applications stemming from space technologies such as Earth observation, telecommunications, and navigation.

CNES purpose is to extend the influence of French space policy, a target that is pursued thanks to its 2500 employees, which are distributed in its four centres in Paris, Toulouse, and French Guyana, and thanks to the agency's founding values of excellence, enthusiasm, and its desire to address the current needs and to face the future challenges. To this end, CNES coordinates scientific work with research laboratories, and cooperates with the industrial world, enabling continuous development of advanced technologies.

The company's activities are divided into 5 areas of intervention which cover all the skills needed to define and implement the French space policy: launchers, telecommunications, defence, science, and Earth's observation. Within the fields of scientific research and Earth's observation it is possible to place the operations and missions carried out by the Balloons Department of CNES, where the internship here described has taken place.

1.2 Balloons Department

CNES covers the role of one of the most active agencies in the world as regards the field of scientific balloons, since it represents one of the foremost experts worldwide in the design,

development, launch and operation of stratospheric balloons. Moreover, the company is prime contractor for balloon activities in France.

Generated under the impetus of the scientific community in the early 1960s, the balloons activity consists of designing and operating aerostatic vehicles to carry scientific instruments with automatic operation. The Balloons programme provides access to scientific research and allows the development of innovative missions through inexpensive, ecological, and reliable methods.

Stratospheric balloons are better suited and more efficient than any other means of atmospheric exploration. Indeed, they present many advantages: they are considerably cheaper than planes, satellites and sounding rockets; they can be easily launched from a great variety of sites, without the need for heavy infrastructure; they are usually carried by the current during flight, meaning they do not require a propulsion system; they are subjected to a less hostile atmospheric environment; their gondolas and payloads can often be recovered and re-utilised; they are completely free, without any link to the ground, and unmanned, carrying automatically operating scientific instruments. Moreover, balloons can explore parts of the atmosphere that are inaccessible to the other tools, therefore they can be used to complement satellite observations and measurements taken from the ground.
In simple words, balloons constitute a unique tool for exploration, measurements, and experimentation, and they represent a huge benefit for an extensive international scientific community.

With the balloon programme, CNES conducts important scientific research and feeds the possibility of technological innovations: each year more than 60 people work on aerostat systems that are dedicated to French and international scientific research.
At the moment, several campaigns are going on, which are characterised by different objectives and various features. Balloons are currently launched from various sites all over the world (Aire sur l'Adour, France; Kiruna, Sweden; Timmins, Canada; Seychelles; Antarctica; etc.), depending on the scientific objectives and on the existent constraints.

2. Analysis of the need

2.1 Project's objective

As already mentioned, the project under description is focused on the "Conception and realisation of a wind sensor onboard a stratospheric balloon".
The principal objective of the internship is to address the need to know the wind profile below stratospheric balloons. Therefore, the project aims at designing the system and realising its first prototypes to validate the different concepts of use and/or limitations towards the aerostat's interfaces.

The developed system is intended to find application in the next stratospheric balloons' generation BALMAN, which innovative potential relies in their manoeuvrability.
The basic concept of these aerostats is shown in Figure 1.

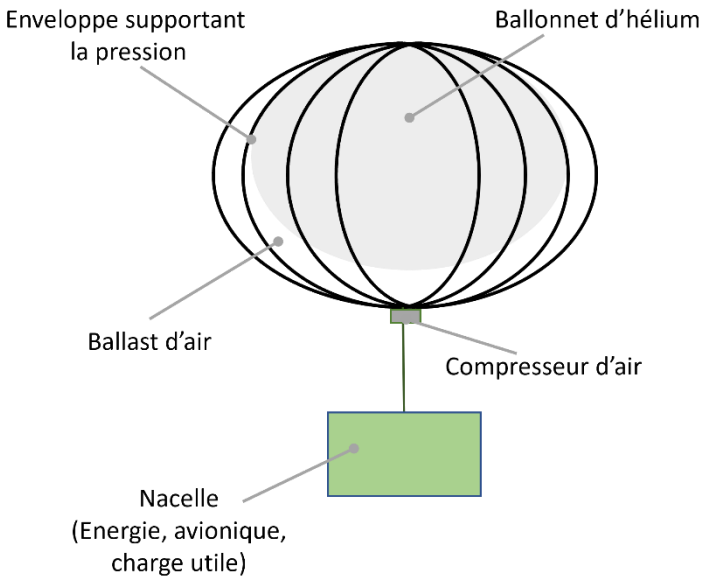

Figure 1: BALMAN concept (Department Balloons, 2022)

BALMAN working principle is the active control of the balloon's altitude, which is currently the focus of multiple studies and projects in the field. Among these, it is relevant to mention the Thunderhead Balloon System, a steerable multipurpose platform recently developed by Raven Aerostat, which has navigational capabilities and the possibility to maintain persistent flight over areas of interest (Thunderhead flight - Developed by Aerostar, 2023).

Another interesting study is reported in (Huafei Du, 2019), where the analysis of flight performance simulation and station-keeping endurance for stratospheric super-pressure balloons in real wind field is performed. The mentioned paper proposes an approach that catches the wind in different directions by changing the balloon's float altitude in order to control the balloon's position and fix it within a specific district of interest. The research has led to the development of a numerical model that simulates the flight performance and analyses the station-keeping endurance of the aerostat considering the wind speed and direction throughout the troposphere and stratosphere. After the establishment of a theoretical model, a computer program has been implemented for the simulation, taking as initial conditions the real wind field data, measured by the employment of a radiosonde balloon, and assuming that the wind field is relatively stable for several days. The results show that choosing the proper flight altitude has a direct and significant impact on the travelled horizontal distance, due to the unavoidable altitude fluctuations caused by the temperature oscillations of the Helium during the day-night cycle (Huafei Du, 2019).

The mentioned examples clearly show the interest of actively changing the balloon's altitude in order to take advantage of the winds. This is the purpose of BALMAN generation of balloons. Figure 1 shows that the new aerostats consist of two envelopes, the inner one contains Helium and takes the name of "ballonet", whereas the outer one is inflated with air and serves as ballast. The balloon can be controlled and piloted thanks to a compressor that can adjust the balloon's inflation (introducing or removing air) to conduct altitude excursions among $16km$ and $22km$ above the sea level, to levels where the winds can help in manoeuvring the balloon towards the desired direction or in maximising the station-keeping period above an area of interest.

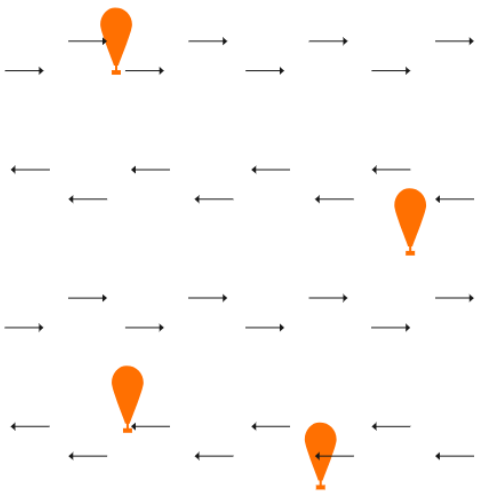

Figure 2: Wind stratification (Department Balloons, 2022)

This kind of stratospheric balloons is developed by the company HEMERIA[1] and is intended to be able to pilot and adjust its own trajectory in the stratosphere.
BALMAN considerable potential is represented by the possibility of not only facilitating access to space at a lower cost and a lower environmental impact, but also of flying over areas of interest for longer periods of time, with a beneficial reduction of logistical and operational constraints. In fact, the ultimate aim of BALMAN systems is to be able to fly over inhabited land, taking advantage of cross winds, which speed and direction change with altitude and are here assumed to be horizontally stratified as shown in Figure 2.
In order to develop such technology, a deep knowledge of the surrounding environment is needed; more specifically, it is crucial to provide awareness of the wind profile among 0 and $1km$ below the balloon, at least as regards the wind direction.

The aim of the project here described is intended to be reached with the realisation of a device capable of measuring different physical quantities and of bringing such information back to the wind intensity and direction below the aerostat. The mentioned system is planned to be lowered from the balloon's nacelle through a mechanical cable which deployment is controlled by a reeling system driven by a motor located in the nacelle.

2.2 State of the art

The ability of manoeuvring balloons represents a great advantage for several reasons. Firstly, it constitutes a meaningful improvement of the mission's safety, which is always of primary concern; secondly, it enables general profits for the scientific activities that are carried out, for example the efficient planning of measurements, as well as the definition and maintenance of a desired trajectory, which is also linked to the possibility to recover the system once the mission is completed. For these reasons, BALMAN project meets not only scientific interests, but also strategic and industrial demands.

In order to monitor a stratospheric balloon's trajectory, it is generally necessary to have access to a numerical weather prediction model (with the aim of forecasting the evolution of the

[1] HEMERIA is a European leader in the design and manufacture of stratospheric balloons intended to carry scientific and technical missions in the stratosphere, and it represents the main partner of CNES Balloons Department.

operating environment), and to define a model of the aerostat's behaviour (a flight physics model) (Valérian Jewtoukoff, 2016).

Computer simulation is one of the most efficient methods to forecast the motion processes of stratospheric balloons. Two famous programs have been developed by the National Aeronautics and Space Administration's Balloon Program Office, the Scientific Balloon Analysis Model (SINBAD) and Balloon Ascent, which are used to predict balloons flight profiles based on the operating system and operating environment, taking into account features such as the distinction among super-pressure and zero-pressure balloons, wind direction and speed, material properties. Additionally, the Italian Aerospace Research Centre (CIRA) has developed the software ACHAB (Analysis Code for High Altitude Balloons), which is capable of predicting horizontal and vertical motion, as well as the balloon's thermal behaviour (Huafei Du, 2019).

Currently at CNES, the knowledge of the wind's profile in the balloon's operating environment is provided by the weather forecast and is generally corrected with meaningful data collected by the balloon's instrumental payload (telemetry data). As an example, during the Strapolété campaign[2] it was assumed that the aerostat is capable of tracing the wind along the trajectory; indeed, the balloon's three-dimensional position was collected periodically by a GPS (Global Positioning System) receiver in the flight chain, and the horizontal wind speed was deduced from the balloon's successive positions (Le magazine d'information du centre national d'études spatiales, 2009).

In recent years, a great effort has been devoted to the improvement of atmospheric flows predictions, for which purpose several methods and strategies have been adopted. A relevant example is constituted by the use of radiosondes, which are small telemetry instruments generally carried by balloons into the atmosphere. These sensors can measure air characteristic quantities such as pressure, temperature, and relative humidity, and send the recorded information to a ground receiver through a radio transmitter. In this way, they allow the direct collection of real data in the aerostats' operating environment.

Considering the specific project under discussion, it is however clear that using radiosondes would be too expensive and inefficient, since several measures would be needed at different altitudes and at different moments during a single mission.

[2] A large-scale balloon campaign which was part of International Polar Year in 2009, conducted from Kiruna, Sweden.

Another possibility that has been explored is to forecast the balloon's trajectory by using high-resolution mesoscale models, as reported in the study (Valérian Jewtoukoff, 2016). Despite the scientific interest represented by the cited research, one of the main outcomes of this investigation is that very large errors are present in the predictions when the balloon flies in the lower stratosphere.

It is relevant to mention that other studies about how to measure the winds around stratospheric balloons exist and are currently under development. For instance, the U.S. Defense Advanced Research Projects Agency (DARPA) has tested a wind sensor called "Strat-OAWL" (Stratospheric Optical Autocovariance Wind Lidar) for application onboard aerostats. The system's working principle is based on LIDAR technology: the instrument is carried within the balloon's payload during the mission; the system is capable of sending pulses of laser light towards the stratosphere and of gathering the reflected beam (which represents only a small fraction of the transmitted signal) through a telescope. The wind speed and direction can be determined by measuring the Doppler shift[3] between the transmitted beam and the received one (DARPA Tests Wind Sensor for Stratospheric Balloons, 2019).
Although this project is of high scientific importance and interest, it does not represent a suitable solution to address the problem under discussion. Indeed, the main requirement here is to develop a system capable of determining the wind speed in order to improve the performance of BALMAN generation of aerostats. Consequently, the principal objective is to optimise such auxiliary system in terms of additional weights and volumes, costs, and complexity.

A simple and plausible solution to measure the wind speed could be to integrate anemometers within the aerostat's payload. Some examples of their use for atmospheric balloons are found in the available literature. An interesting case is represented by the experiment conducted in 2017 which studied the application of sonic anemometers[4] at high altitudes (Maruca BA, 2017). Similarly, in 2021 a mission was launched to measure the wind speed around a stratospheric

[3] The Doppler effect or Doppler shift is the apparent change in a wave's frequency which is produced by the movement of the signal's source.
[4] A sonic anemometer uses ultrasonic sound waves to determine instantaneous wind speed by measuring how much the sound waves traveling between a pair of transducers are sped up or slowed down due to the effect of the wind (H., 2012).

balloon. During the study, a cup anemometer[5] was successfully used to collect the wind's measurements.
In both cases, the anemometer resulted to have troubles taking measurements around $17km$ of altitude, while the collected information was very commonly poor from $18km$ above the sea level.

From the previous considerations, it is evident that the need for a simple, low-cost, low-power and highly efficient system is still actual. The following Chapter is thus dedicated to the description of the solution identified to answer the problem, together with the methodological choices that have been consequently implemented and the justification of the conducted actions.

[5] A cup anemometer is a device which consists of three or four cups mounted on a horizontal rotor that rotates when exposed to the wind: by measuring the number of revolutions over a specific period of time, it is possible to determine the wind speed (How to use cup anemometer, s.d.).

3. Identified solution and project plan

3.1 Identified solution

The concept behind the identified solution is based on the same principle of a previous similar experiment: the Stratéole 2 experiment. This consisted of a series of long-duration ballooning campaigns aimed at studying the tropical tropopause layer through a constellation of super-pressure balloons circling the Earth at the Equator.

The cited field of experiments led to the design of specific sensors that were lowered below the operated balloon. Indeed, a reel-down instrument system for profile measurements of water vapor, temperature, clouds, and aerosol beneath constant-altitude scientific balloons has been developed and tested during the mission (al., 2021).

This work represents a relevant source of information, due to the analogy with the project being performed. Therefore, it has been taken as reference in order to understand in detail the assumptions and hypothesis that have been made, the design of the developed devices and their modes of operation.

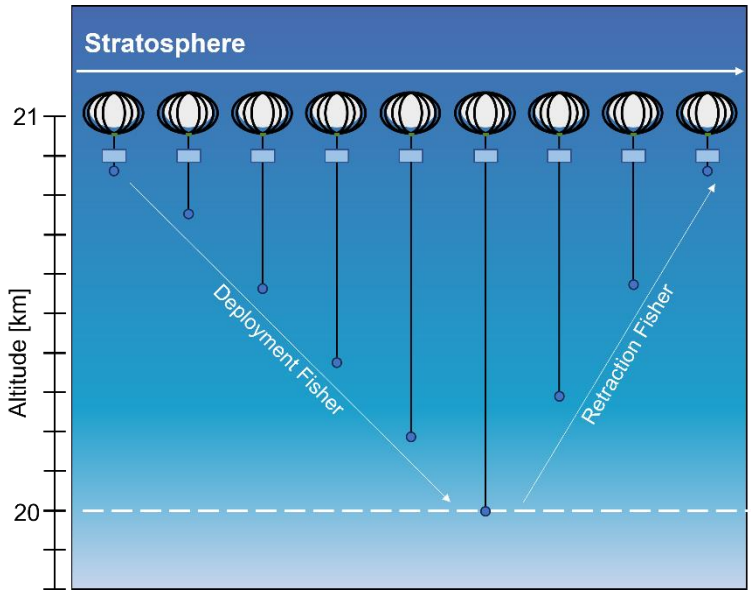

Figure 3: Wind Fish basic concept

The basic concept is the same, as illustrated in Figure 3: the instrument system is designated as "Wind Fish" or "Fisher" and is intended to be lowered below the stratospheric balloon through a cable in order to take relevant measurements. The design includes a controlled winching system which is capable of repeating the lowering and raising actions several times.

The Wind Fish is planned to be designed in the form of a sphere since this shape has been deeply studied in wind tunnel experiments, and therefore its behaviour within an air flow is well known and predictable. Moreover, the sphere is a blunt body, thus it generates an aerodynamic force that is mainly oriented along the flight direction (mostly drag component). In this way, the wind speed measurement is facilitated.

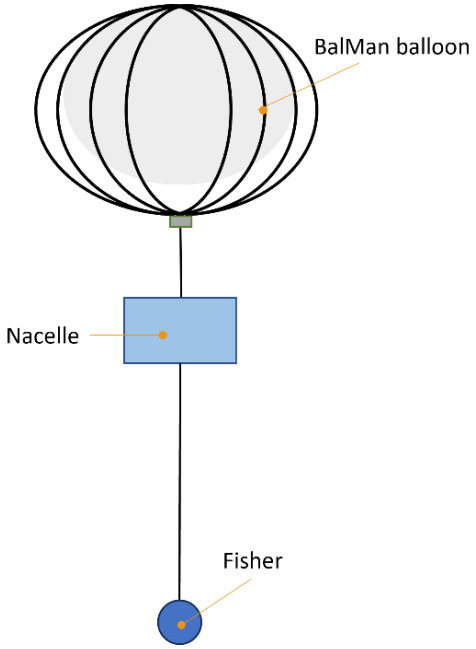

Figure 4: System's general architecture

Figure 4 illustrates the devised system, showing a simplified schematic of the balloon's envelope, the main payload inserted within the nacelle, and the system of sensors that constitute the Wind Fish. The actual and complete architecture of a stratospheric balloon is more complicated, and it includes also additional devices such as the parachute system, which however are not of interest for the specific project under study.

The probe must be oriented with the wind direction, therefore a rudder is meant to be mounted on the system, as shown in Figure 5.

Finally, the prototype is intended to be electrically supplied by a small solar panel, as illustrated in the picture below.

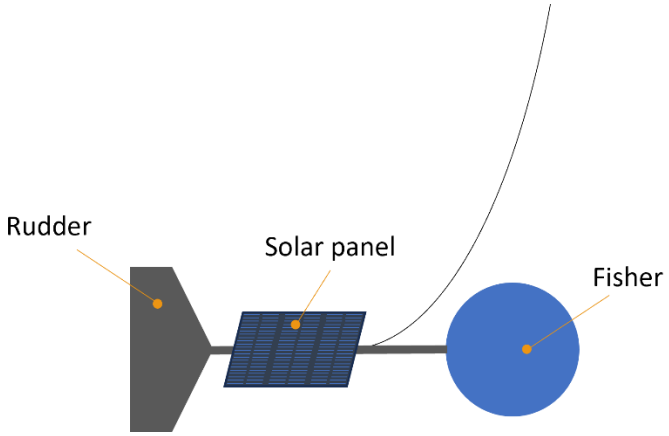

Figure 5: Wind sounder's architecture

Since the aim of the project is to enable the knowledge of the wind speed below stratospheric balloons in order to limit the energy consumption related to the balloon's manoeuvring, it is necessary to equipe the Wind Fish with devices that will have a low impact on the aerostats, especially in terms of additional costs and weight. In particular, the components chosen at a first attempt are: a GNSS (Global Navigation Satellite System) receiver, a differential pressure sensor, and a 9-DoF[6] Inertial Measurement Unit (IMU).

More specifically, the GNSS device is a differential GPS system, thus it is capable of measuring the Wind Fish position. Besides usually the latitude and longitude information are very accurate, the altitude measure is generally affected by a considerable uncertainty. This has been taken into account during the project's implementation, therefore the sensor has been used to obtain the three-dimensional distance between the probe below the balloon and the balloon's gondola, since considering relative measurements instead of absolute measurements results in an improved accuracy.

The differential pressure sensor is a digital airspeed sensor that can measure the environmental pressure and temperature thanks to a transducer and a Pitot tube. The component's operation is based on Bernoulli's principle: the relative wind speed is determined from the difference between the dynamic pressure and the static pressure in the considered environment. This device is commonly used to measure aircrafts speed; however, once left the troposphere and entered the stratosphere, the air becomes thinner and therefore the hypothesis of air as a perfect gas may be too approximate. After some comparisons with data coming from a flight simulation, it has been verified that this assumption does not allow to provide reliable and

[6] DoF stands for "Degrees of Freedom". This means that the cited instrument is equipped with a three-axis accelerometer, a three-axis magnetometer, and a three-axis angular rate sensor.

sufficiently accurate measurements of wind speed in the stratosphere, and more precisely at altitudes of interest (among 19 and $21km$ of altitude).

The IMU is intended to measure the Wind Fish attitude and orientation. Particular attention is given to the information about the pitch and the magnetic orientation, which are both fundamental to determine the wind direction. This is done through the combination of a gyroscope, an accelerometer, and a magnetometer. It is important to notice that the sensors contained within the Inertial Measurement Unit must be calibrated before their usage in order to obtain meaningful values from them. Additionally, the magnetometers require a further correction relative to the magnetic declination, which changes over time and location. These considerations are detailed in Section 4.1.4.

The mentioned sensors have to be properly connected to an ESP32 electronic board, and integrated into a single device assuring that it is not affected by interferences and that the measurements of each component remain reliable.
The ESP32 board is intended to be powered through a Lithium-Ion battery that will be charged by solar panels; therefore, it is crucial to analyse the amount of needed power with the aim of developing the correlated solar panels' sizing.

The Wind Fish board is also linked to a device that enables LoRa communications to another electronic card located in the balloon's nacelle. This latter is connected to a series of additional components: a GNSS receiver for the position determination; a device to enable the communication with the ground station through Iridium link; and a motor to perform the cable's deployment. The intent is indeed to gradually lower the Wind Fish below the balloon through a thin cable spooled around a reel-down instrument, with steps of $50m$ interspersed with periods of detection by the sensors, up to reach $1km$ below the balloon's altitude. Consequently, it is required to determine the appropriate function that correlates the actual cable's deployment to the number of revolutions completed by the motor's shaft, as well as to identify the most appropriate speed of rotation. The implemented function is described in detail in Section 5.3.1. These analyses were conducted only after the completion of the reeling system design, for which an external team was responsible (company 441 Engineering, of members Nicolas Poupat and Guilhem Tournie).

It is important to highlight that the developed system is capable of measuring the relative speed among the Wind Fish and the surrounding air. Therefore, the collected data consists not only of

the wind speed, but also of the balloon's one. In order to exclusively determine the wind speed, it is necessary to combine the obtained measures with the information about the balloon's speed, which is known since the balloon is tracked thanks to the instrumental payload it carries, and especially a GPS module.
Furthermore, it has to be underlined that the main objective is to monitor the wind direction. Consequently, both the balloon's heading[7] and the Fisher's attitude have to be taken into account.

Finally, the project's implementation has been based on the assumption that all the electronics will work under the operating conditions. For instance, the GPS is supposed to work properly and with enough precision, which constitutes a critical hypothesis, especially with regard to the system's numerical analysis developed in MATLAB programming language, as described in detail in the dedicated Section of the present paper.

3.2 Project's plan

The End of Studies Project under discussion is characterised by the variety and multidisciplinary of the topics involved. This is the reason why the project plan foresees to carry out in parallel multiple activities, in order to develop a solid and deep understanding of the interactions between the different physical systems and theoretical concepts that are involved.

The main purpose of the internship is to progress as far as possible in the proposed project. This latter is classified into three macro phases, which activities and key milestones are described in the next Sections. It is important to highlight that the End of Studies Project's objective is mainly to reach the development of the first of these phases, given the available time to perform the project.

3.2.1 First phase

The first identified phase is the design and manufacture of a Wind Fish prototype. This phase is thus articulated in the following activities: definition of the electronic inputs and outputs; encapsulation and electronic integration of the sensor, and consequently PCB's design; behavioural simulation and algorithms; 3D CAD design of the complete and integrated sensor;

[7] Heading indicates where the balloon is pointing relative to the magnetic north.

realisation of the first prototypes through 3D printing; analysis of the complete system's mass balance.

This part of the project was mainly focused on the components involved, and in particular on sensors potentially usable to detect significant data. Therefore, during the first period the internship has prioritised the study of the available sensors, making use of Arduino IDE and Visual Studio Code software in order to obtain relevant information from such devices.
This phase involved not only the coding aspect, but also the physical welding of the components, as well as the study of electrical connections and interference. The mentioned activities have taken place in the electronic room within the Balloons Department of CNES.

3.2.2 Second phase

The second macro phase is represented by the ground functional validation. More precisely, the included steps are meant to be: thermal simulations; manufacturing of $3-5$ Wind Fish prototypes; ground validation of the algorithms developed for the winds' deduction; and mechanical tests of the prototypes.

Concerning the prototypes' manufacture, this is planned to be performed through 3D printing, with the aid of technical experts. While the algorithms' validation is intended to verify that the obtained measurements are reliable, and to set the appropriate corrections in case of errors such as biases, noises, and wrong calibration of the sensors. For example, it is known that the magnetometer readings are affected by magnetic field induced by electric current; therefore, it is fundamental to test the best calibration code in order to obtain valid data from the sensors.

Finally, the mechanical tests are aimed at verifying that the prototypes can sustain mechanical stresses and vibrations without permanent damage. This is of great relevance due to the assembly's sensitivity, particularly at the moment of the balloon's launch.
As a reference, in the previously mentioned Stratéole 2 mission, the sensor release was more dynamic than planned due to calm winds at launch that required the rapid movement of the gondola. The consequence led to minor damage of the connector between the nacelle and the assembly of sensors. This remarks the importance of conducting tests on the strength and resistance of the cable, which will eventually lead to a market analysis in order to identify the most appropriate choice. The same concept is valid for all the other physical and electronic components.

3.2.3 Third phase

Finally, the last phase is the qualification in the stratospheric environment during flight. This comprehends: the qualification in a cold oven and at low pressure; the flight validation onboard balloons based on previous technologies; the in-flight application for the specific mission (new balloons' generation).

The aim of this phase is to verify that the sensor can actually survive in the environment that characterises the mission, at first with simulations on ground, and afterwards through in-flight tests. This is of fundamental importance in order to inspect the potential issues and risks related to the real mission.

4. Implementation of the solution

After the general picture of the electronic components under use given in Section 3.1, a in-depth characterisation of the measurement system is here provided.
Then, the Chapter concentrates on describing the methods which have been implemented for the actual determination of the wind speed through numerical algorithms. In particular, the simplified hypotheses and the basic assumptions adopted for the definition of appropriate models of the system are here illustrated. The Chapter concludes with the comparison of the obtained results with realistic data provided by a flight simulator.

4.1 Measurement system

As it has been introduced in Section 3.1, the measurement system is composed of multiple sensors which provide information about different quantities and have been chosen among the COTS (Commercial Off The Shelf) components available on the market.
The devices that have been tested and which use has been implemented are described in the present Section, with the aim of explaining their working principles and their logic of use.

4.1.1 Electronic board

As already mentioned, the core of the developed system is the electronic card ESP32. The ESP32 is a series of low-cost and low-power System on a Chip (SoC) microcontrollers designed by Espressif.
This development board represents the brain of the electronic assemblies in the Fisher and in the balloon's nacelle, since it controls all the other devices, and their operation, and it is responsible for monitoring the mission's status by enabling the communication among the two subsystems and also towards the ground segment.

To be more precise, an ESP32 Lolin32 Lite has been used for the system in the Wind Fish, whereas an ESP32 DEVKIT DOIT has been chosen for the assembly in the gondola. The two boards are represented in Figure 6 a) and b), respectively.

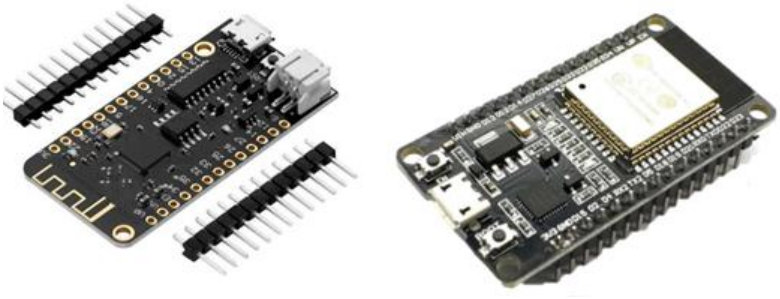

Figure 6: a) ESP32 Lolin 32 Lite (AZ-Delivery); b) ESP32 DEVKIT DOIT (ESP32 Projects)

It is relevant to note that the intent was firstly to use the same board for the two systems, an ESP32 Lolin32 Lite, since it presents some advantages in terms of lighter weight, smaller dimensions, and reduced power consumption with respect to the normal ESP32 board. Moreover, it operates at a lower voltage ($3.3V$, compared to the ESP32 DEVKIT DOIT $5V$), and it can be powered through sources of $2.2 \div 3.6V$. Nevertheless, it was necessary to modify the initial choice for the system in the nacelle in order to adapt it to the need for matching the other electronic devices – in particular, the Iridium modem and the assembly associated with the motor – as it will be explained in Chapter 5.

The two boards can anyway operate synchronously and successfully communicate with each other, since they both belong to the ESP32 family.

4.1.2 GNSS module

The component used to provide the information about the position is a differential GNSS module from Beitian and is shown in Figure 7.

Figure 7: GNSS module (BN-220 GPS Module + Antenna Datasheet)

GNSS stands for Global Navigation Satellite System, and it is used to refer to a constellation of satellites working as navigation system. GNSS's purpose is to provide navigation services, which means that they are intended to transmit information to determine the location of the receiver (user).

GNSS provides data on the satellites' position, which together with the distance measurements allow the receiver to determine its position in four dimensions, space and time.
In order to do so, a minimum of four satellites is needed: three are used to determine the X, Y, and Z coordinates (trilateration principle), while the fourth serves as a time reference, since satellites contain precision atomic time watches.

The main advantages of GNSS are that they provide a global coverage which is available in any weather conditions, and the transmitted data are very accurate over time. These navigation systems are however subject to radio interference, due to the fact that radio signals are characterised by low power: as a consequence, the signals are vulnerable to intentional and unintentional interference, as well as they are subject to temporary blackouts caused by loss of visibility of the satellites. Though these might represent considerable drawbacks for ground positioning - a temporary loss of navigation solution may be unacceptable for some applications - they do not constitute a big disadvantage concerning the project under work, whose operating environment is the stratosphere.
The use of a GNSS receiver is therefore considered a valid option for the project's development.

The chosen device enables the knowledge of the system's position in terms of latitude, longitude and altitude; it provides the data and time information as well as the speed over ground and course to a specified location. Being based on differential GNSS, the component is able to receive more accurate and reliable positioning data with respect to the normal GNSS receivers. Indeed, differential satellite positioning systems not only make use of the information transmitted by the constellation of satellites, but they also integrate such information with additional data coming from reference stations (Differential GPS: What It Is and How to Use It Effectively, 2023).
For the specific component under use, the augmentation system is of type SBAS (Satellite-based augmentation system), which means that the extra information is provided by geostationary satellites. Augmentation systems serve to reduce the positioning errors obtainable with GNSS systems due to disturbances encountered by electromagnetic signals in the atmosphere.[8]

[8] The thorough description of these systems' operation falls outside the scope of the present report; for further details, see references (Holfmann-Wellenhof B., 1992), (E., 1996), (Pratap Misra P., 2006).

The information is transmitted to the receiving modules as NMEA (National Marine Electronics Association) messages. These are comma-delimited text formats that consist of rows of data referred to as “sentences”. There exist a variety of diverse languages of NMEA, which can be distinguished and recognised by the first five letters of each message. Depending on the message’s structure, different additional information can be extracted from the sentence (for example, number of satellites that are seen, their identification numbers, precision indices, etc.). In order to extract any data from the transmitted messages, the GNSS device uses a serial interface, with Receive (RX) and Transmit (TX) connections. Moreover, it requires the use of two specific libraries in Visual Studio Code environment, which are the specific versions of TinyGPSPlus and SoftwareSerial for the ESP32 family.

4.1.3 Differential pressure sensor

At a first attempt, some studies have been focused on a digital pressure sensor.
The chosen component is from Pixhawk and is reported in the following Figure. It is possible to see that the integrated device is composed of a pitot tube, a pressure transducer and a rubber tube. The transducer is the small, ceramic based, PCB mounted MS4525DO, from Measurement Specialties.

Figure 8: Differential Air Pressure Sensor (Pixhawk PX4 Differential Airspeed Sensor Kit - Pitot Tube)

The analysis of the device’s datasheet allowed to identify the transfer functions from the sensor’s digital outputs (electric signal) to meaningful data concerning temperature and differential pressure. This information is provided in the form of two graphs and their corresponding laws, reported in document (MS4525DO Measurement Specialties, 2023).

To obtain information about the system’s speed, the introduction of an appropriate function taking into account the Bernoulli’s equation was required. In fluid dynamics, Bernoulli’s

principle states that the combination of pressure and the sum of kinetic and potential energy densities is constant not only over time, but also along a streamline. This principle is valid only for incompressible and frictionless flows, and it can be written as a pressure balance between two flow sections a and b:

$$\frac{1}{2}\rho_a v_a^2 + p_a + \rho_a g h_a = \frac{1}{2}\rho_b v_b^2 + p_b + \rho_b g h_b$$

where ρ, v, p are the fluid's density, velocity and static pressure respectively, and h is the height of the flow section (Pitot Tube Wind Speed and Airspeed Indicator - Theory and Experiments, 2023).

The pitot tube can measure the stagnation pressure $p_{stagnation} = \frac{1}{2}\rho v^2 + p_{static}$, which includes both the static pressure and the incident pressure on the bend. Additionally, it can determine the static pressure p_{static} separately, thanks to the static ports – which are perpendicular to the flow direction. Consequently, the fluid's speed can be obtained as:

$v = \sqrt{\frac{2(p_{stagnation} - p_{static})}{\rho}}$.

From this formula, it is evident that the speed's computation requires the knowledge of the air density of the working environment. Therefore, it has been fundamental to choose a suitable source of such input.

With the aim of avoiding auxiliary components, the choice was the adoption of an atmospheric model to obtain the air density information at the system's altitude. Consequently, the ISA (International Standard Atmosphere) atmospheric model has been introduced at the software level[9].

This component was first studied since the hypothesis of a working system was made – as mentioned in Chapter 3. Initially, it was assumed that the digital chip would be positioned inside a thermal protection to avoid exposure to the cold stratospheric environment. Reasonably, the dynamic and static ports were meant to be placed outside this isolating box, in order to expose them to the air's flow. Even though it was predictable that this sensor's accuracy is not sufficient for the operating environment, it was decided to study it anyway with the aim of exploring and testing several devices and solutions.

[9] The reference model has been taken from sources (Earth Atmospheric Model - Metric Units, 2023) and (International Standard Atmosphere, 2023).

Given that the described sensor can accurately measure pressure from $1psi$ to $150psi$ while the Wind Fish is intended to fly at altitudes where the atmospheric pressure is around $4000 \div 6000Pa$[10] - falling in a range which is lower than the device's sensitivity -, it has been decided to not rely on its measurements. Indeed, not only the information provided by the device will inevitably suffer from errors, but also the computation of the speed will amplify the inaccuracy due to rounding errors introduced by the calculations (caused by the representation of numbers on the calculator), and to their propagation through the computational algorithm.
Moreover, the principal aim of the present work is to collect information about the wind direction, which is considered more important than knowing the air flow's intensity: this means that the differential pressure sensor cannot operate without the integration of an additional device capable of measuring the orientation of winds.

4.1.4 Inertial measurement unit

The component used as Inertial Measurement Unit is the LSM9DS1 Breakout from SparkFun, shown in Figure 9. This versatile motion-sensing device houses a 3-axis accelerometer, 3-axis magnetometer, and 3-axis gyroscope, being able to monitor movement and orientation according to 9 degrees of freedom (acceleration, magnetic force and angular rotation along three axes).

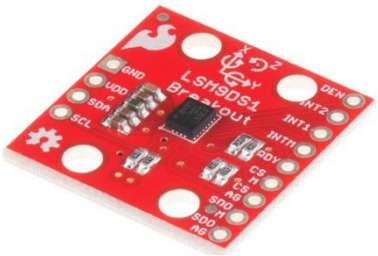

Figure 9: Inertial Measurement Unit (LSM9DS1 - iNEMO inertial module: 3D accelerometer, 3D gyroscope, 3D magnetometer, 2023)

The instrument is based on MEMS (Micro Electro-Mechanical Systems) technology, comprehending a set of devices of various nature integrated in a highly miniaturised form on the same substrate of semiconductor material. Electro-mechanical microsystems present numerous practical applications, thanks to their extremely small size and their considerably low

[10] More precisely, $6400Pa = 0.93psi$ at $19km$ and $4700Pa = 0.68psi$ at $21km$, where $1psi = 6894.75729Pa$.

cost. However, an important downside of using such hardware is their lower accuracy with respect to sensors based on other technologies.

The used chip is equipped with a flexible digital interface, supporting both I^2C (Inter-Integrated Circuit) and SPI (Serial Peripheral Interface) communication protocols[11]. For the specific project under interest, the I^2C protocol has been adopted to simplify the circuit, since it requires a smaller number of connections and wirings.
Additionally, to extract data from this inertial unit, it has been necessary to use a specific Library in the Visual Studio Code environment, the SparkFunLSM9DS1. The Library's functionalities enable the reading of the most up-to-date information from the three inertial sensors, and the translation from the raw data to meaningful values that are properly scaled and dimensioned.

As regards the project under discussion, there is no need to collect all the measurements available from the LSM9DS1 device, for example the data about accelerations and angular rates; whereas crucial values are represented by the pitch and roll angles. In fact, these values affect the system's aerodynamics, and thus the speed's computation. Even the magnetic heading represents a fundamental value, which provides a direct information about the wind direction, since the Fisher is connected to an external rudder so that it tends to orient itself according to the wind it is subject to.

There exist several methodologies to specify the orientation of a body; the most commonly used strategies are the attitude's matrices (directional cosine matrices), the Euler angles, and quaternions. For the project under discussion, it has been chosen to adopt the Euler angles, since they constitute a highly appreciated method of attitude's representation due to their instinctiveness of use and understanding. These angles are denoted as *pitch* ϑ, *roll* ϕ, and *yaw* ψ (also called heading or azimuth)[12] and are constrained by the following relations (in order to obtain a unique solution for any orientation instead of multiple configurations):

$$\begin{cases} -90° \leq \vartheta \leq 90° \\ -180° \leq \phi \leq 180° \\ -180° \leq \psi \leq 180° \end{cases}$$

Such limits are integrated at the software level by using the $atan$ function for the pitch computation, and the $atan2$ function for the roll and heading computations.

[11] These two ways of communication are described in detail in Section 5.1 of the present report.
[12] For the theoretical definition and practical meaning of these angles, see references (Ozyagcilar, 2015) and (Computing tilt measurement and tilt-compensated eCompass, 2023).

These angles are referenced to the local horizontal plane, which is perpendicular to the Earth's gravity. Heading is defined as the angle with respect to the magnetic north pole; if the heading with respect to the geographic location is needed, then the declination angle at the user's current geographic location must be added/subtracted from the magnetic heading, as explained in the following.

Underlying the use of accelerometer and magnetometer to obtain the device's orientation is the fact that the measurements obtained from the sensors in the IMU are all referred to the reference system integral to the body. The accelerometer can be used to obtain the value of pitch and roll angles, whereas the heading is obtained by using the magnetometer.
The final equations that relate these angles with the accelerometer's and magnetometer's readings are the following[13]:

$$\begin{cases} \tan\vartheta = -\dfrac{a_{m,x}}{\sqrt{{a_{m,y}}^2 + {a_{m,z}}^2}} \\ \tan\phi = \dfrac{a_{m,y}}{a_{m,z}} \\ \tan\psi = \dfrac{B_{m,z}\sin\phi - B_{m,y}\cos\phi}{B_{m,x}\cos\vartheta + B_{m,y}\sin\phi\sin\vartheta + B_{m,z}\sin\vartheta\cos\phi} \end{cases}$$

The last equation derives from the fact that since the sensor can have an arbitrary orientation, the compass heading cannot be computed simply as $\tan\psi = -\frac{B_{m,y}}{B_{m,x}}$. To compensate for this effect, it is possible to combine the accelerometer's readings to measure the tilt angles of pitch and roll, and therefore level the magnetometer's readings (Computing tilt measurement and tilt-compensated eCompass).

During experimental activities, it was observed that the magnetometer is oriented differently with respect to the accelerometer, fact that has been taken into account with the adaptation of the above equations coherently. Precisely, while the accelerometer and gyroscope axes orientations share a right-hand rule relationship with each other, the X and Y axes of the magnetic sensor are flipped.

[13] The detailed explanation and derivation of such relations fall out of the scope of this report, and can be found in (Ozyagcilar, 2015) and (Computing tilt measurement and tilt-compensated eCompass).

In order to obtain a meaningful value from the magnetometer's readings, a compensation of the magnetic declination[14] is needed. Since this quantity is a function of longitude, latitude and time of the year, it is necessary to introduce a statement at the software level that keeps track of its actual value at the balloon's location and at the moment at which the mission occurs.
There exist several ways to determine declination, for example from a magnetic chart (maps of the Earth's magnetic field are available from the National Geophysical Data Centre (NGDC) of the National Oceanic and Atmospheric Administration (NOAA)), from dedicated executable software (as instance WMM (World Magnetic Model) Software and Coefficients, from NOAA)[15], or from online calculators (Magnetic Field Calculators from the National Centres for Environmental Information (NCEI) of NOAA)[16]. These methods generally take as input the geographical location of the system and the temporal moment of interest.

For the specific project under discussion, a possibility is to indicate the magnetic declination as a variable which value is given as input depending on the actual mission (computed indicating the real operating location, altitude, and period of the year). Since balloons are not static vehicles, it might be argued that the magnetic declination changes along the aerostats' trajectory. However, a possible solution could be to update the value of the aforementioned variable depending on the mission's status (position and date). One option could be to compute the declination in discrete points along the balloon's path; an alternative - given the desired balloon's trajectory for a specific mission - would be to collect as many estimates of the declination across the planned path as possible, and to fit a smooth function to them. This could be done for example by adopting a dedicated and open-source Library in Arduino environment that implements a model, found at (ArduPilot - AP_Declination). Though this Library assumes that the altitude of interest is $0km$ above the sea level, it has been observed that there is not a big difference in case of stratospheric trajectories. Indeed, this verification has been made taking into consideration the data about the Stratéole 2 mission's path. Considering a mission lasting one year, it has been observed that there is almost no difference in the magnetic declination at $0km$ and at $20km$ above the sea level.

[14] Magnetic declination is simply defined by the angle between the magnetic north and the true north.
[15] See the reference website (WMM Software and Coefficients).
[16] See the reference website (Magnetic Field Calculators).

A further option could be to use a different GNSS module, in fact some devices are capable of measuring the magnetic declination. For instance, according to its datasheet the GPS BN 880 is provided with an integrated compass.

In addition to the described correction about the magnetic declination, it is necessary to also introduce a compensation for the errors related to the metallic devices located next to the component, which presence affects the magnetometers' readings. Indeed, in addition to the geomagnetic field, the magnetometer measures the magnetic field of the system, the host vehicle, and any carried equipment.
During the tests conducted to verify the proper integration of the electronic components, it has been observed that the heading is highly affected by the vicinity of other devices. In particular, this phenomenon has been manifested with greater intensity after the introduction of an external power source.

The sensor is factory calibrated and the corrective values are stored in non-volatile memory, internal to the instrument. Every time the device is turned on, the parameters are loaded to the internal registers to be employed during active operation, which allows using the device without further calibration made by the user. On the other hand, a meticulous calibration must be carried out to consider the particular magnetic environment of the sensor at its final location. In fact, this environment can severely disturb the Earth's magnetic field reading.
In order to reduce the mentioned effect, proper calibration of the magnetometer is required once all the components have been integrated together. This calibration must be performed in place, which means where the sensors will be used. In fact, data are mostly confused by the immediate environment, so the calibration can be done just once after mounting the system.
The calibration procedure consists in collecting a large number of measurements of the magnetic field on the three axes for all the possible positions of the sensor. To do this, after connecting the magnetometer to a microcontroller, it is necessary to upload an elementary sketch that sends the raw values of the magnetic field and to start it while manually rotating the sensor. The output must be in the appropriate format so as to use it in a tool that calculates the calibration parameters. For this purpose, there exists a dedicated function in the SparkFun Library, which has been implemented at the software level, showing an improvement in the

heading's reading. Another possibility is to use more sophisticated methods to find very precise calibration parameters, for example open-source software such as MotionCal or Magnetov1,2.[17]

Since the aim of this project is to obtain information about the system's attitude and to combine it with the data provided by the GNSS module for the wind speed computation, it has been decided to maintain the software implementation as simple as possible. Consequently, it has been chosen to adopt the SparkFun built-in function to perform the instrument's calibration, and to integrate the heading measure collected by the Inertial Measurement Unit with the value obtained from the computational algorithm (described in the following Section).

Another possibility could be the implementation of a sensor fusion between the inertial and satellite systems, in order to obtain precise information about the Wind Fish motion (position, speed, and attitude). However, this would represent a costly operation at the level of the software's development, due to its high complexity and elevated time consumption. Moreover, it would fall out of the scope of the present project, which is not the resolution of a navigation problem.

4.2 Simulations and algorithms

To introduce this Section, it is crucial to note that the cable is considered as one dimensional, perfectly flexible, and completely inextensible.

It is important to mention that the International Standard Atmosphere model has been adopted in the algorithms to account for the specific working environment characterising stratospheric balloons. Moreover, it has been assumed that the wind stratification is horizontal, which means that the wind does not have any vertical component, as illustrated in Figure 2, and also that it is constant, meaning it is the same in each layer during the complete cycle of measurements.

As explained previously, the implemented components are capable of measuring different quantities related to the balloon's operating environment, but not directly the wind direction and intensity. To obtain this information, it is necessary to identify the physical problem that characterises the system, and afterwards to build the corresponding mathematical model based on simplified hypothesis.

[17] For further information, see references (Digital compass) and (Improved magnetometer calibration).

The idea is therefore to create a 3D model of the system and solve it through numerical analysis strategies, considering the information coming from the available instruments in order to obtain the accurate computation of the wind speed. The main problem to be faced is indeed the definition of a mathematical model. Two approaches have been identified and implemented: a mechanical chain approach and a suspended cable approach, which will be described separately in the following.

The principle behind the calculus is to compute the wind speed once every time the cable is lowered of $50m$, thus 20 times until the achievement of $1km$ below the balloon.

In both cases, the solving algorithms have been determined considering the information coming from the electronic components and the equilibrium of the forces acting on the system: tension on the cable, weight of the cable and of the sensors attached to it, air drag generated by the cable and by the probe. It must be specified that, since the probe is meant to have the shape of a sphere, it is assumed that it does not generate any lift component of the aerodynamic force.

The two methods have led to the definition of two problems consisting in two systems of nonlinear equations. These problems can be internally solved by MATLAB by creating the corresponding optimisation problems that minimise the sum of squares of the components of the residual vector: the process to find a solution is iterative, and the built-in solver must be adapted to the specific case under study in terms of tolerances, maximum number of iterations, starting point, etc.

In the case of the work of interest, the optimisation problems which have been created for the two approaches are solved by *@solve* with the algorithm Levenberg-Marquardt. More precisely, the *@lsqnonlin* solver has been adopted: this is an iterative nonlinear least-squares method, which starts from a specified initial point and ends when a minimum of the sum of squares of the optimisation function is found.[18]

Overall, several attempts and methods have been explored, among which the chosen one has showed to provide the most precise and reliable outcomes.

[18] For further details about the principle behind the algorithms and its resolution, see references (K., 1944) (D., 1963).

Levenberg-Marquardt method

The detailed description of the theory behind the adopted numerical analysis strategies falls out of the scope of the present paper. Therefore, only a general introduction of the implemented approach is reported here.

Levenberg-Marquardt methods are one of the well-known techniques that are used to solve the classical problem of finding a solution to the constrained system of nonlinear equations:

$$F(x) = 0 \; so \; that \; x \in X$$

where $X \subseteq \mathbb{R}^n$ is a nonempty, closed and convex set, and $F: \mathcal{O} \to \mathbb{R}^m$ is a given mapping defined on an open neighbourhood $\mathcal{O}$ of the set X (Christian Kanzow, 2004).
In order to solve this problem, the related optimisation problem is generally considered:

$$\min_x f(x) \; \; so \; that \; x \in X$$

where $f(x) := \|F(x)\|_2^2 = \sum_i F_i^2(x)$ denotes the natural merit function corresponding to the mapping F, where $\|...\|$ represents the Euclidean norm.

Problems of this type occur in many practical applications, for which the residual $\|F(x)\|$ is likely to be small at the optimum, and can be minimised using a general, unconstrained minimisation technique. Nevertheless, it is often possible to exploit certain characteristics of the problem in order to improve the iterative efficiency of the solution procedure.
In particular, introducing the gradient and Hessian matrix of the optimisation equation can represent an advantage. Indeed, it is possible to write (Least-Squares (Model Fitting) Algorithms, 2023):

$$G(x) = 2J(x)^T F(x)$$

$$H(x) = 2J(x)^T J(x) + 2Q(x)$$

where $G(x)$ is the gradient vector of $f(x)$, $J(x)$ is the m-by- n Jacobian matrix of $F(x)$, and $H(x)$ denotes the Hessian matrix of $f(x)$. The matrix $Q(x)$ is given by $Q(x) = \sum_{i=1}^{m} F_i(x) \cdot D_i(x)$, where $D_i(x)$ represents the Hessian matrix of each $F_i(x)$.
A particular property is that when the residual $\|F(x)\|$ tends to zero as residual x_k approaches the solution, residual $Q(x)$ also tends to zero. Therefore, when $\|F(x)\|$ is small, an effective method is to use the Gauss-Newton direction as a basis for an optimisation procedure.

At each major iteration k, the Gauss-Newton method obtains the search direction d_k as a solution of the linear least-squares problem:

$$\min_{d_k \in \mathbb{R}^n} \|J(x_k)d_k + F(x_k)\|_2^2$$

The direction derived from this method is equivalent to the Newton direction when $Q(x) = 0$. The algorithm uses the search direction d_k as part of a line search strategy to ensure that the function $f(x)$ decreases at each iteration.

The Gauss-Newton method often encounters problems when the second-order term $Q(x)$ is not negligible. The Levenberg-Marquardt method overcomes this problem by adopting a search direction that is a cross between the Gauss-Newton direction and the steepest descent direction. The Levenberg-Marquardt curve-fitting method is indeed a combination of these two minimisation strategies. As seen, in the Gauss-Newton method the sum of the squared errors is reduced by assuming the least-squares function is locally quadratic and finding its minimum. Whereas in the gradient descent method, the sum of the squared errors is reduced by updating the parameters in the steepest-descent direction.
The Levenberg-Marquardt method acts similarly to a gradient-descent method when the parameters are far from their optimal value, while it acts more like the Gauss-Newton method when the parameters are close to their optimal value (D., 1963).

More precisely, the Levenberg-Marquardt method uses a search direction that is a solution of the linear set of equations:

$$(J(x_k)^T J(x_k) + \lambda_k I)d_k = -J(x_k)^T F(x_k)$$

where I is the identity matrix, and λ_k is a scalar which controls the magnitude and direction of d_k. When λ_k is zero, the search direction is identical to the one obtained from the Gauss-Newton method. As λ_k tends to infinity, d_k tends to the steepest descent direction, with a magnitude approaching zero. Consequently, for sufficiently large values of λ_k, the relation $\|F(x_k + d_k)\| < \|F(x_k)\|$ is true. Therefore, it is possible to control the term λ_k to ensure descent of the residual value even when the algorithm encounters second-order terms (meaning that $Q(x)$ is not negligible), which restrict the efficiency of the Gauss-Newton method.
If the step is successful (gives a lower function value), the algorithm sets $\lambda_{k+1} = \lambda_k/10$, whereas if the step is unsuccessful, the algorithm sets $\lambda_{k+1} = \lambda_k * 10$ (Least-Squares (Model Fitting) Algorithms, 2023).

4.2.1 Mechanical chain approach

The first method considers the cable as discretised in parts which number equals the number of iterations: at the first iteration, only one element of cable is considered, of length $50m$; at the second iteration, two elements of cable are considered, each of them is $50m$ long; etc.

This approach leads to the definition of a rectangular system of nonlinear equations, with more equations than unknowns (overdetermined problem). The complexity of this problem is very high, since the system to be solved changes at every iteration, and its size increases (the number of equations rises).

At every iteration, the first three equations of the system are derived from the information about the Wind Fish and nacelle positions. For the first iteration, these equations can be written as:

$$\begin{cases} L \sin\vartheta_1 \cos\alpha_1 = \Delta x_{GPS} \\ L \sin\vartheta_1 \sin\alpha_1 = \Delta y_{GPS} \\ L \cos\vartheta_1 = \Delta z_{GPS} \end{cases}$$

where Δx_{GPS}, Δy_{GPS} and Δz_{GPS} represent the distance between the nacelle and the Fisher projected along the X, Y and Z axes respectively, which is provided by the GNSS modules. The angles ϑ_1 and α_1 are clearly defined in Figure 10, and they represent the only unknowns of the system.

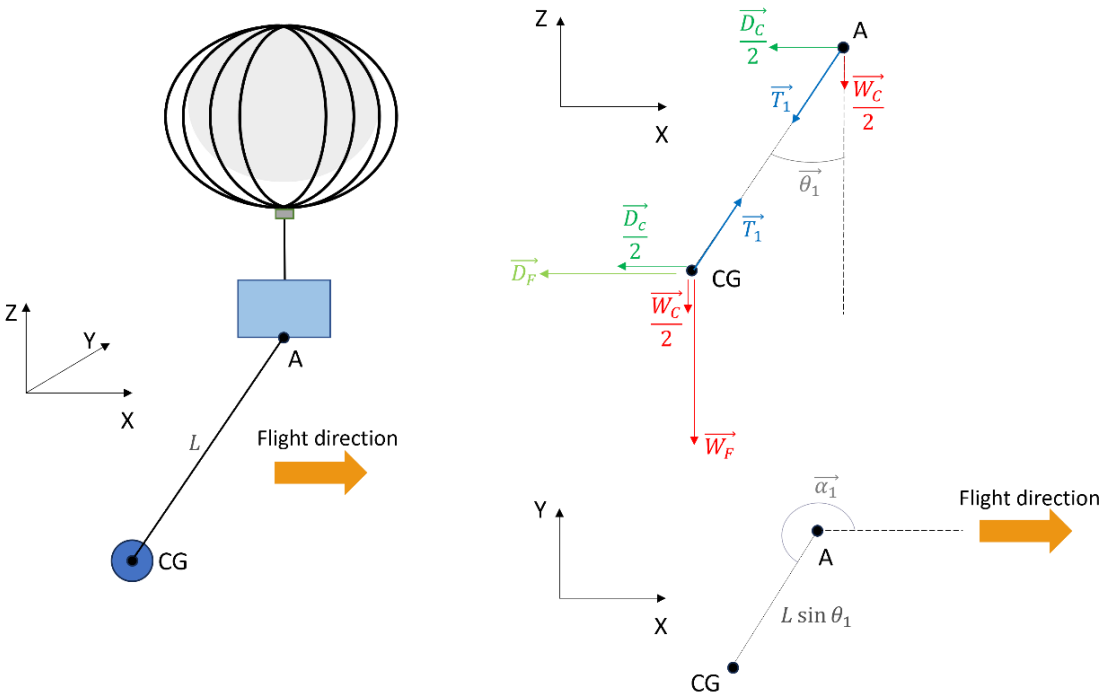

Figure 10: Mechanical chain approach - first iteration

For the generic i^{th} iteration, the above system becomes:

$$\begin{cases} L\sin\vartheta_1\cos\alpha_1 + L\sin\vartheta_2\cos\alpha_2 + \cdots + L\sin\vartheta_{i-1}\cos\alpha_{i-1} + L\sin\vartheta_i\cos\alpha_i = \Delta x_{GPS} \\ L\sin\vartheta_1\sin\alpha_1 + L\sin\vartheta_2\sin\alpha_2 + \cdots + L\sin\vartheta_{i-1}\sin\alpha_{i-1} + L\sin\vartheta_i\sin\alpha_i = \Delta y_{GPS} \\ L\cos\vartheta_1 + L\cos\vartheta_2 + \cdots + L\cos\vartheta_{i-1} + L\cos\vartheta_i = \Delta z_{GPS} \end{cases}$$

To determine the wind speed, some additional equations are needed. Such information is obtained by writing the equilibrium of forces acting on the cable.

Considering that point A belongs to the balloon's nacelle, its balance is assumed to be guaranteed through the other forces acting on the gondola. Only the equilibrium at point CG is therefore considered. The following system can thus be written for the first iteration:

$$\begin{cases} -T_1\sin\vartheta_1\cos\alpha_1 + D_F\cos\alpha_1 + \frac{1}{2}\mathrm{D_C}\cos\alpha_1 = 0 \\ -T_1\sin\vartheta_1\sin\alpha_1 + D_F\sin\alpha_1 + \frac{1}{2}\mathrm{D_C}\sin\alpha_1 = 0 \\ T_1\cos\vartheta_1 - W_F - \frac{1}{2}W_\mathrm{C} = 0 \end{cases}$$

where the three equations correspond to the equilibrium of forces projected along the X, Y and Z axes respectively. T_1 is the cable's tension applied on point CG; W_F and W_C are the Fisher weight and the weight of the segment of cable deployed under the balloon, accordingly; D_F and D_C are the drag components of the aerodynamic forces generated by the Fisher and the portion of cable lowered, respectively. These two quantities can be written as: $D_F = \frac{1}{2}\rho S_F c_{D_F} v_F^2$ and $D_C = \frac{1}{2}\rho S_C\, c_{D_C} v_F^2$, where ρ is the air density at the Wind Fish altitude; S_F and S_C are the wet surfaces[20] of the probe and of the segment of cable, respectively; c_{D_F} is the Fisher's drag coefficient (considered to be the one of a sphere, 0.47) and c_{D_C} is the drag coefficient of one element of cable (considered to be the one of a cylinder, 0.82); v_F is the speed of the air with respect to the Fisher (considering the Fisher as steady in an inertial reference frame)[21].

During the simulation's activity, it has been observed that the solutions' accuracy decreases after the first iteration. Consequently, several considerations on how to improve the system were made, and multiple analyses and tries were performed to describe the same problem in a better way.

---

[19] The sign – is here entered since the tension $\overrightarrow{T_1}$ here considered is directed from point CG to point A, therefore it forms the angle $(\alpha_1 - 180°)$ with respect to the X axis.

[20] The wet surface in aerodynamics is simply the surface which is exposed to the flux.

[21] The speed of the Fisher relative to the air if this latter is considered as steady in an absolute reference frame.

For example, the possibility to combine dependent equations of the system was studied so as to remove redundancies and improve the system's conditioning. Though this led to the reduction of the system's size, it was not possible to obtain a square system (with the same number of equations and unknowns), since it would have led to a non-acceptable loss of information.
Combining the first two equations of the system results in the equation: $-T_1 \sin\vartheta_1 + D_F + \frac{1}{2}D_C = 0$, which corresponds to the equilibrium of forces projected on the XY plane.
The first iteration's system is therefore composed of five equations in four unknowns: the two angles ϑ_1 and α_1, the tension on the cable T_1, and the air speed v_F.

As already explained, the number of cable's nodes increases at each iteration; therefore, the number of equations rises accordingly (at least two equilibrium equations can be written for each node). At the second iteration, the solving system is made of seven equations in six unknowns:

$$\begin{cases} L\sin\vartheta_1\cos\alpha_1 + L\sin\vartheta_2\cos\alpha_2 = \Delta x_{GPS} \\ L\sin\vartheta_1\sin\alpha_1 + L\sin\vartheta_2\sin\alpha_2 = \Delta y_{GPS} \\ L\cos\vartheta_1 + L\cos\vartheta_2 = \Delta z_{GPS} \\ -T_1\sin\vartheta_1 + T_2\sin\vartheta_2 + \frac{1}{2}D_{C_1} + \frac{1}{2}D_{C_2} = 0 \\ T_1\cos\vartheta_1 - T_2\cos\vartheta_2 - W_C = 0 \\ -T_2\sin\vartheta_2 + D_F + \frac{1}{2}D_{C_2} = 0 \\ T_2\cos\vartheta_2 - W_F - \frac{1}{2}W_c = 0 \end{cases}$$

The first three equations represent the position's determination, enabled thanks to the information of the GNSS modules. The fourth and fifth equations express the equilibrium of forces at node B. Finally, the last two relations represent the equilibrium of forces at node CG. The symbols' meaning is analogous to the one already explained, and clearly illustrated in Figure 11.

It has to be pointed out that $D_{C_1} = \frac{1}{2}\rho S_C\, c_{D_C} v_{F_1}^2$ and $D_{C_2} = \frac{1}{2}\rho S_C\, c_{D_C} v_{F_2}^2$ are different, since the wind is stratified (therefore v_{F_1} and v_{F_2} are distinct).

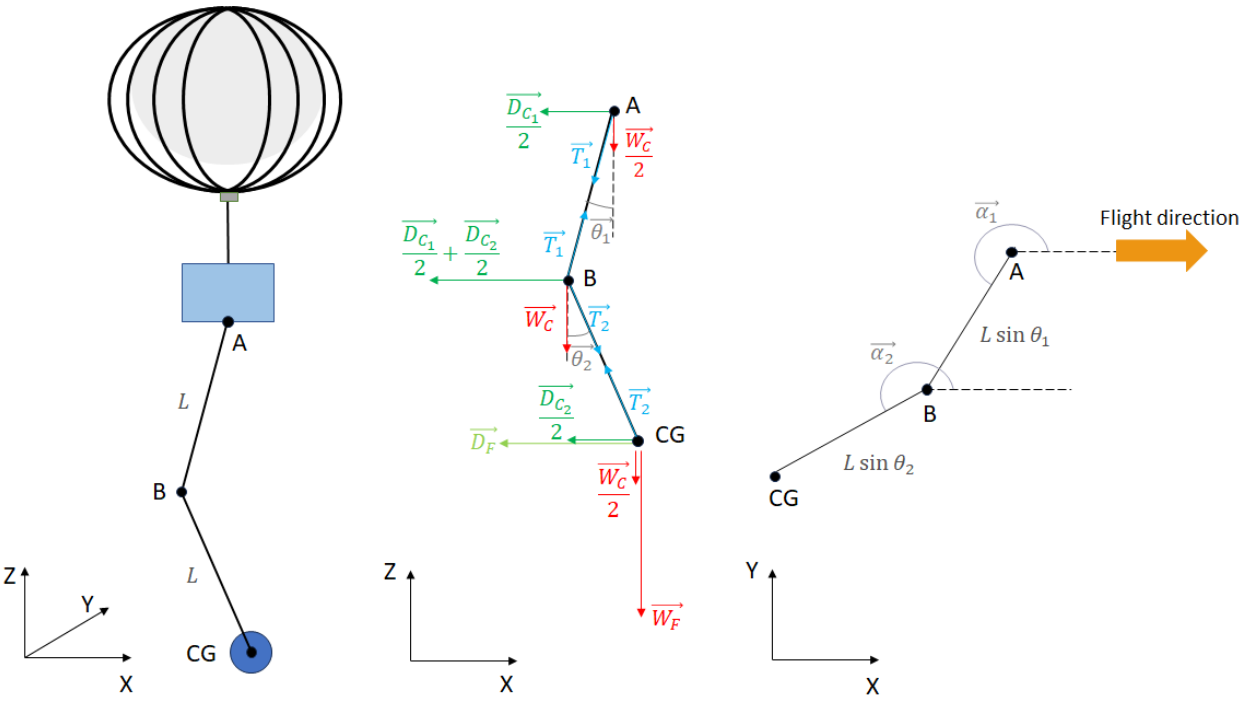

Figure 11: Mechanical chain approach - second iteration

The unknowns in this case are ϑ_1, T_1, ϑ_2, T_2 and v_{F_2}. It is important to highlight that ϑ_1, T_1 are different at each iteration since more cable is lowered below the balloon, which means that its total weight increases and the equilibrium of forces changes; as a consequence, the cable assumes a different configuration to guarantee such equilibrium. On the contrary, the angle α_1 and the speed v_{F_1} (in general, α_n and all v_{F_n} for n: 1 to $(i-1)$ at the i^{th} iteration) are assumed to be the same for all the duration of the data collection; indeed, it is hypothesised that the wind intensity and direction remain constant over time.

As mentioned, several other methods have been explored and tested.

At first, the idea was to use the function *@fsolve* (another common nonlinear systems solver). The method has been tested, showing that already at the second iteration the solution completely loses accuracy. This is due to the fact that the solver is not suitable for rectangular systems of equations.

Trials were made also with *@fmincon* solver with the algorithm Interior-point, which however showed to be less precise than the approach here implemented: in fact, the solver presents warnings about badly scaled or closed to singular matrices, implying that the solution cannot be accurate.

Finally, the described algorithm has been compared with an existing code capable of solving nonlinear systems of equations. Even though the solution of a constrained and non-square system of equations has not been subject of intense research, it was possible to make a comparison with the TRESNEI[22] method, a MATLAB implementation of a trust-region Gauss-Newton approach for bound-constrained nonlinear least-squares problems described in (Benedetta Morini, 2010). The available code has been run on the problem already generated, providing results that showed no improvements with respect to the solver autonomously implemented, whereas a loss of accuracy was observed.

Some attempts have been made considering the cable's drag as negligible. Although this did not show any meaningful improvement, it led to the definition of another approach, which is described in the below Section.

4.2.2 Suspended cable approach

The second method assumes that the cable is an ideal wire, which mean a particular type of continuous one-dimensional body that satisfies two properties: the moment of the contact forces is equal to zero, and the inner effort has a tension character. An ideal cable does not have an internal structure able to realise a twisting or bending moment of the wire; moreover, it only reacts to tensile stresses but does not respond to pressure exerted on its sections.

Moreover, the drag component of the aerodynamic force generated by the cable is considered to be negligible with respect to the other forces acting on the system. Therefore, the cable's positioning is not discretised anymore, but it is modelled as a hyperbolic cosine.

For this approach, the problem leads to the definition of a square system of nonlinear equations, which updates at every iteration, but without an increment in the number of equations.
Again, the assumption is made that the GNSS module provides very good information about the Fisher's position and speed. Additionally, it is hypothesised that the cable is inextensible, continuous, one-dimensional and perfectly flexible.

[22] Acronym for Trust-Region Solver for Nonlinear Equalities and Inequalities.

This method is based on the principle that the segment of deployed cable assumes the shape of a homogeneous catenary[23]. This curve is simply a hyperbolic cosine arc, which general equation is (Catenary, 2023):

$$f(x) = \ z = a\cosh\left(\frac{x}{a}\right) = a\left(\frac{e^{\frac{x}{a}} + e^{-\frac{x}{a}}}{2}\right)$$

where x and z represent the coordinates of a generic point belonging to the curve, expressed in a cartesian reference frame which origin corresponds to the catenary's vertex. It is crucial to underline that this method is 2D, as the previous equation shows.

The main idea is that each time a portion of cable is lowered below the balloon, it assumes the shape of a new curve. The parameter a is the one that accounts for this variation.
Since the length of the cable increases at each iteration and the wind speed is different at different altitudes, it is not possible to assume that the new curve's vertex is located always in the same point, nor that is corresponds to the Fisher centre of gravity (which would represent a great simplification). Therefore, in order to determine the shape (coefficient a) assumed by the cable at every iteration it is necessary to solve a system of three equations generated by imposing that the curve passes through two known points and that its length is assigned.
These equations are written in a reference system that is different at each new step, oriented as the one represented on the top left side of Figure 12.

[23] A catenary, also known as funicular curve, is the curve that an idealised cable - supposed homogeneous, flexible and non-stretchable - assumes when supported only at its extremities and subject to a uniform distribution of parallel forces.

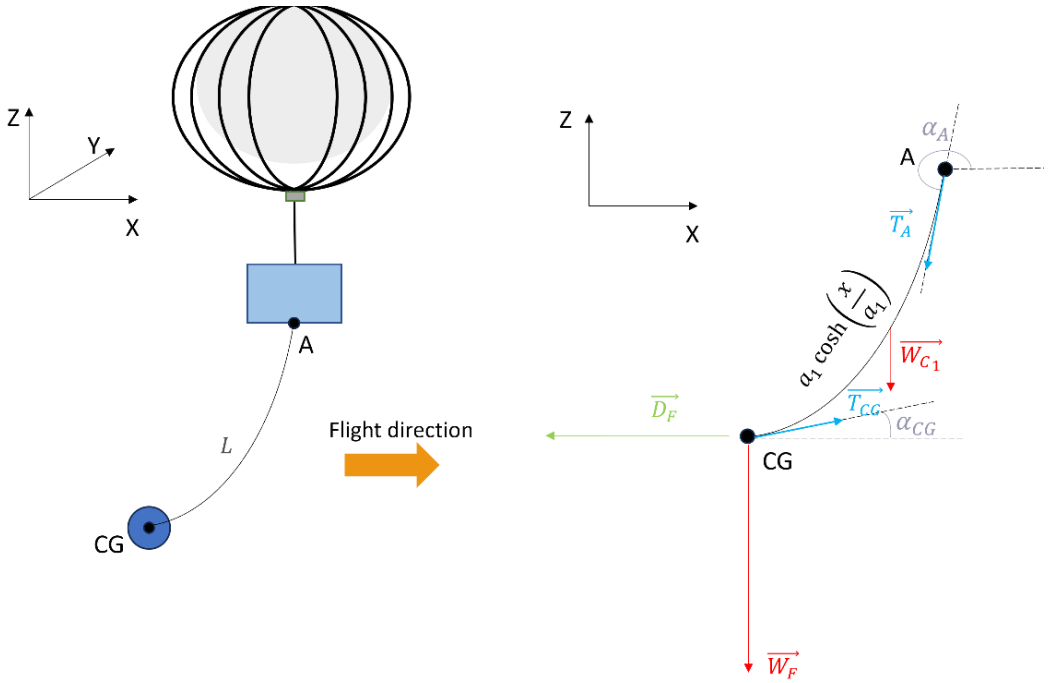

Figure 12: Suspended cable approach - first iteration

Considering that the length of a segment of cable is $i * L$, the cable starting point is denoted as A and the other end is indicated as CG, at the i^{th} iteration the aforementioned system of equations can be written as:

$$\begin{cases} x_A - x_{CG} = \Delta x_{GPS} \\ z_A - z_{CG} = \Delta z_{GPS} = \dfrac{a_i}{2}\left(e^{\frac{x_A}{a_i}} + e^{-\frac{x_A}{a_i}} - e^{\frac{x_{CG}}{a_i}} - e^{-\frac{x_{CG}}{a_i}}\right) \\ i * L = abs\left(\left[a_i \dfrac{e^{\frac{x}{a_i}} - e^{-\frac{x}{a_i}}}{2}\right]_{x_A}^{x_{CG}}\right) \end{cases}$$

where the unknowns are x_A, x_{CG} and a_i, while Δx_{GPS} and Δz_{GPS} represent the information provided by the GNSS modules about the distance between the nacelle and the Fisher in the horizontal and vertical plane[24], respectively.

The first equation is simply derived from the GNSS information. The second relation results from imposing that the two points A and CG belong to the curve: it is immediate to observe that it corresponds to the definition of the catenary curve which vertex is located in the origin of the considered reference frame.

[24] Though the terms "horizontal" and "vertical" are not meaningful from an absolute point of view, here it is considered that the horizontal plane corresponds to the one formed by the axes X and Y represented in Figure 12, while the vertical plane is generated by the axes X and Z.

The last equation is obtained knowing that the length of the curve between the points A and CG can be calculated as (Arc Length, 2023):

$$i * L = abs\left(\int_{x_A}^{x_{CG}} \sqrt{1 + |f'(x)|^2}\, dx\right) = abs\left(\int_{x_A}^{x_{CG}} \sqrt{1 + \sinh^2\left(\frac{x}{a_i}\right)}\, dx\right)$$

Since the written system is made of three equations in three unknowns, it can be classified as a closed system and easily solved.

In order to determine the wind speed, it is then necessary to consider the intrinsic equations for a cable so as to determine the tensions and external forces applied to it. The following three equations can be therefore identified:

$$\begin{cases} T_A \cos\alpha_A + T_{CG} \cos\alpha_{CG} - D_F = 0 \\ T_A \sin\alpha_A + T_{CG} \sin\alpha_{CG} - W_C - W_F = 0 \\ -D_F|\Delta z_{GPS}| + W_F|\Delta x_{GPS}| + W_C\left|\frac{\Delta x_{GPS}}{2}\right| = 0 \end{cases}$$

where the first two relations represent the equilibrium of forces projected in the X and Z axes, respectively, while the third represents the momentum equilibrium written with respect to the pole A. T_A and T_{CG} correspond to the tension on the cable's extremities; D_F indicates the drag component of the aerodynamic force generated by the Wind Fish (defined as in the first approach); W_F is the Fisher's weight force; W_C is the weight of the cable's portion that has been lowered. Apart from W_F, which is always the same, these quantities vary at each iteration.
It can be observed that α_{CG} and α_A are the angles formed by the X axis with the tangent lines to the curve in points CG and A, respectively[25]. Such angles can be therefore determined as:

$$\alpha_{CG} = \operatorname{atan}\left(\sinh\left(\frac{x_{CG}}{a}\right)\right)$$

$$\alpha_A = -\operatorname{atan}\left(\sinh\left(\frac{x_A}{a}\right)\right)$$

The system is thus composed of three equations in the three unknowns D_F, T_A and T_{CG}.

[25] This property derives from the fact that the cable has been assumed perfectly flexible, which means it cannot resist to any torque. Consequently, the internal stress on the wire at each point is always directed along the tangent line to the cable in that point (the stress is completely axial).

$$\begin{cases} -T_A \cos\left(atan\left(\sinh\left(\frac{x_A}{a}\right)\right)\right) + T_{CG} \cos\left(atan\left(\sinh\left(\frac{x_{CG}}{a}\right)\right)\right) - D_F = 0 \\ -T_A \sin\left(atan\left(\sinh\left(\frac{x_A}{a}\right)\right)\right) + T_{CG} \sin\left(atan\left(\sinh\left(\frac{x_{CG}}{a}\right)\right)\right) - W_C - W_F = 0 \\ -D_F|\Delta z_{GPS}| + W_F|\Delta x_{GPS}| + W_C\left|\frac{\Delta x_{GPS}}{2}\right| = 0 \end{cases}$$

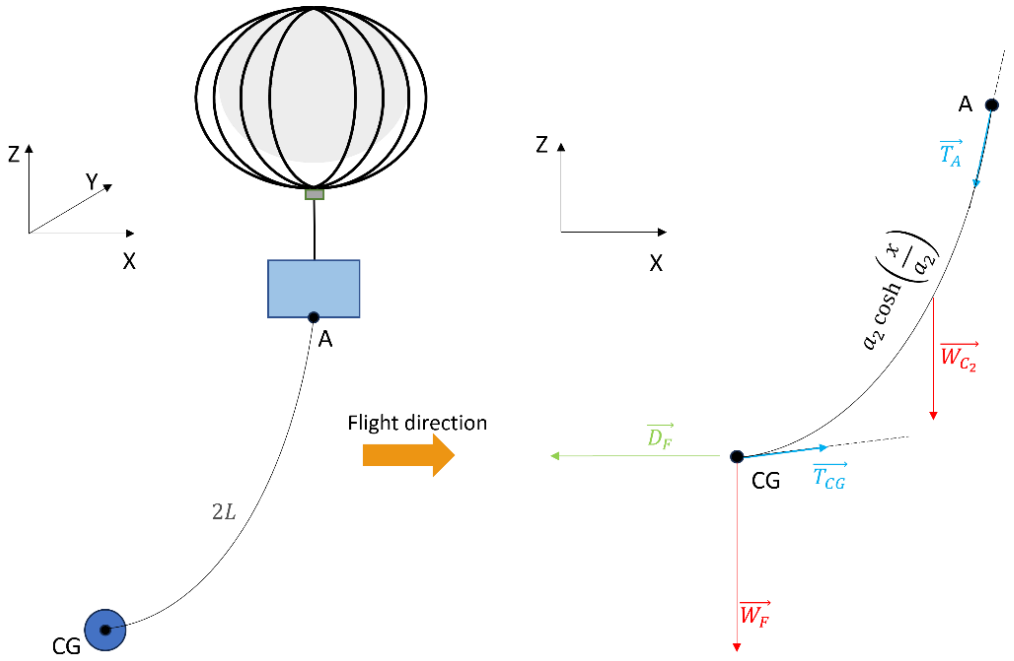

Figure 13: Suspended cable approach - second iteration

4.2.3 Analysis and comparison of the two methods

The present Section aims at analysing the two approaches that have been implemented.
At first, general observations are reported about the methods' working principles, together with comments about how they affect the algorithms' outcomes. This is done by focusing on the common aspects that the two approaches share, while underlying the points of extreme distinction. Afterwards, the results obtained from a series of simulations performed on the basis of data generated at CNES flight simulator are reported and described in detail.
The comparison is illustrated in Figures from 14 to 17, and in the graphs in Annex A.

It has been observed that both methods' results are strongly dependent on the chosen starting points. This is coherent with the fact that both approaches are based on optimisation problems, therefore their outcomes are highly affected by the initial guess. If the first estimate is not realistic enough, and not close enough to the real value, then the algorithms cannot find the

solution. This is the reason why the option of using multiple starting points was adopted in both methods. Such points are chosen as series of values around a reasonable guess. As regards the wind speed intensity, it has been considered as the speed value measured by the differential GNSS module. Concerning the wind direction, it has been ascertained that this value is less affected by the initial choice with respect to the wind speed.

It is important to highlight that both codes require to provide the GNSS information about the position to the MATLAB scripts in an appropriate format. Indeed, the GNSS module gives this information in the form of two angles corresponding to latitude and longitude (measured in degrees), whereas the two algorithms need such data in the form of distances measured in meters. A possibility is to use the built-in function *distanceTo* of the TinyGPSPlus Library to compute the horizontal projection of the distance between the nacelle and the Wind Fish. It has to be noticed that the mentioned function calculates the distance between two points located on the Earth's surface. This means that in order to obtain the right value for the application under discussion, it is necessary to build a similar function (or modify the existing one) to account for the altitude above the sea level in addition to the Earth's radius. Beside this consideration, it has been observed that there is a very small difference in the calculus, around 0.31%.
Another option is to simply consider that the distances dx and dy required as input by the MATLAB scripts are calculated as the product among the Earth's radius added with the balloon's altitude, and the sine of the differential angles obtained as the differences in latitudes and longitudes.
Analogously, focusing on the determination of the wind direction, it is possible to use the function *courseTo* of the aforementioned Library. In this case, attention must be paid to the point considered as reference. For instance, if the course is computed from the gondola's position to the Fisher's one, then its value is referenced with respect to the gondola.

Finally, in both cases the speed obtained from running the scripts is the relative speed of the air with respect to the Wind Fish. As a consequence, this measure consists not only of the wind speed, but also of the balloon's speed. In order to know the effective wind profile, it is necessary to combine the collected information with the balloon's speed, which is known through telemetry data.

The focus is now put on the comparison of the two methods based on the information given by the flight simulator. Four cases of study have been considered and taken as reference point to

analyse and compare the results of the two approaches. These samples correspond to the implementation of the methods starting from four different altitudes: more precisely, case A corresponds to an altitude for the first iteration of $21050m$; example B to $20570m$; sample C represents an altitude of $20090m$; and for case D the first iteration occurs at $19465m$. It is important to note that these altitudes have been chosen given the available data provided by the company's flight simulator, and initially considering segments of cable of length $L = 50m$.

The comparison among the two approaches has been performed only for the first three iterations of the algorithms. The results are illustrated in Figures from 14 to 17, which show the wind speed and direction obtained from running the scripts with respect to the ones generated by the flight simulator. More precisely, Figures 14 and 15 report a comparison of the absolute values obtained from the two strategies, whereas Figures 16 and 17 illustrate the confrontation of the resulting relative errors (calculated with respect to the data coming from the simulator).

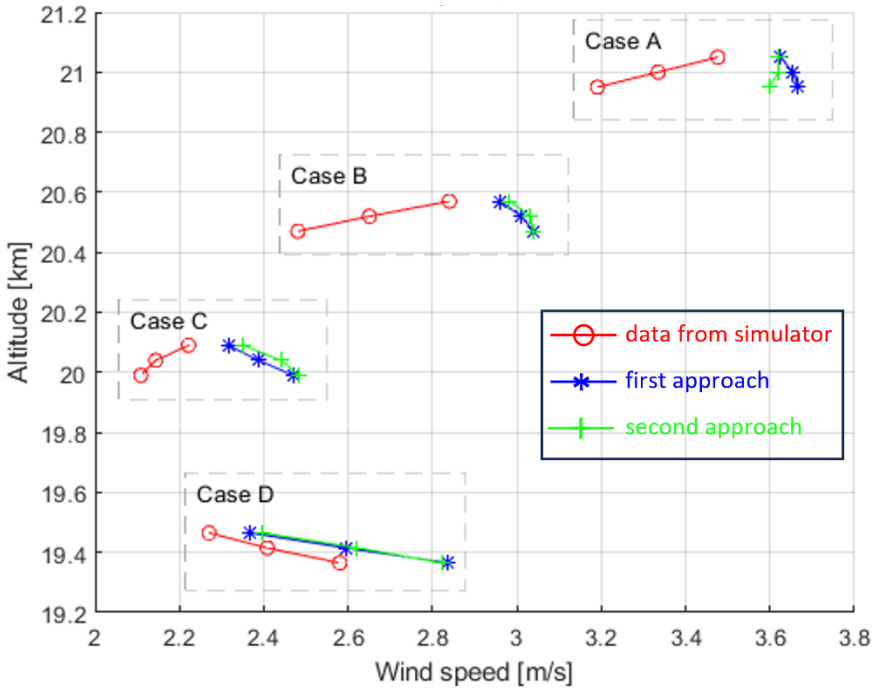

Figure 14: Comparison of wind speed for L=50m

The graphs exposing the outcomes on the wind direction are illustrated over the range from $-180°$ to $+180°$ for clarity of exposition, despite the fact that the real data and the calculated values are represented in the range $[0; 360]°$.

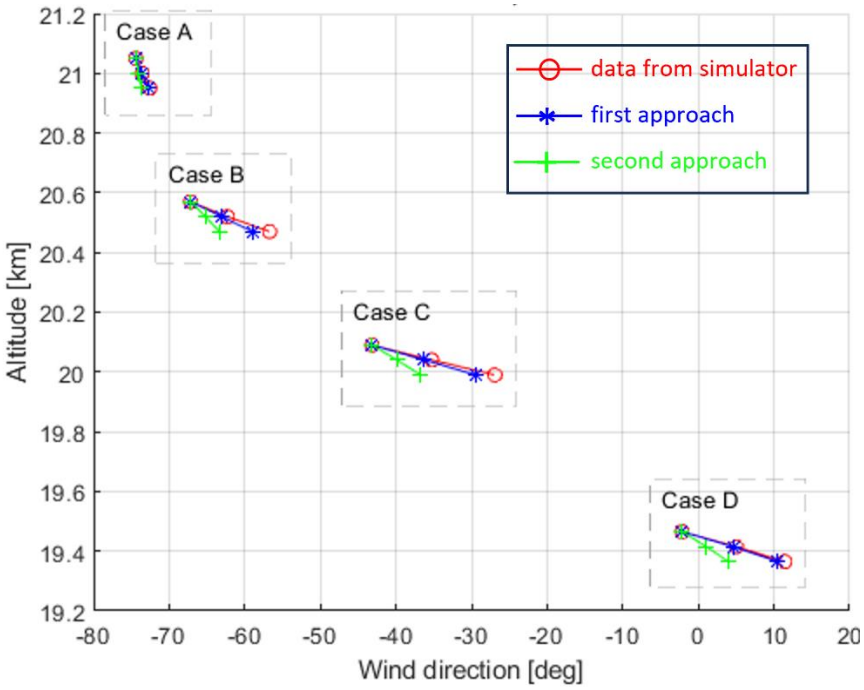

Figure 15: Comparison of wind direction for L=50m

As regards the first method, the accuracy of the results clearly decreases with the number of iterations. The reason behind this lies in the fact that some outcomes of each iteration are used as input for the following ones, causing a progressive loss of precision at every iteration.

The same effect generally verifies also for the second approach. Nevertheless, the reason behind the increasing errors in this situation is different. Indeed, for the second method each iteration is completely independent from the others (both from the previous ones and from the successive ones). Notwithstanding this, the graphs show that the error tends to increase with the number of iterations (although this is not always the case). This is because the second approach relies on the approximation of the cable's placement with a catenary curve. Hence, the loss of accuracy is caused by the method's difficulty in finding an appropriate curve that models the shape of the wire. This is a result of the fact that at each iteration the cable is intuitively positioned almost vertically, given its very small mass and reduced dimensions[26] (surface area exposed to the relative flow), especially in comparison with those of the probe[27]. As a result, the two cable's extremities are not enough spaced apart in the horizontal plane for this approach to accurately model the shape assumed by the wire.

[26] The cable's specifications are reported in Section 5.3.
[27] For information about the Wind Fish initial sizing, see Section 5.7.

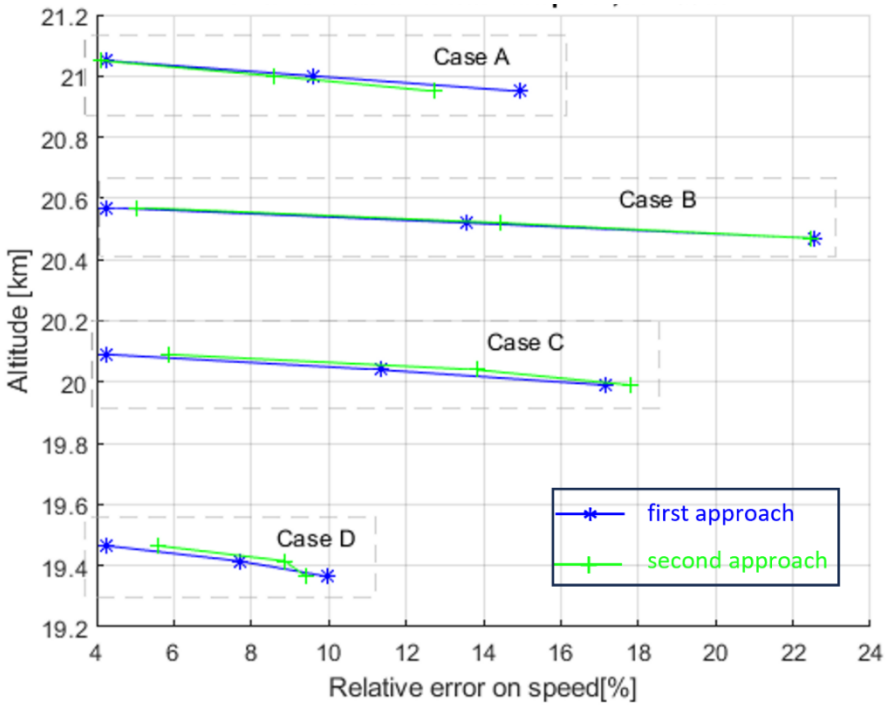

Figure 16: Comparison of relative errors on wind speed, L=50m

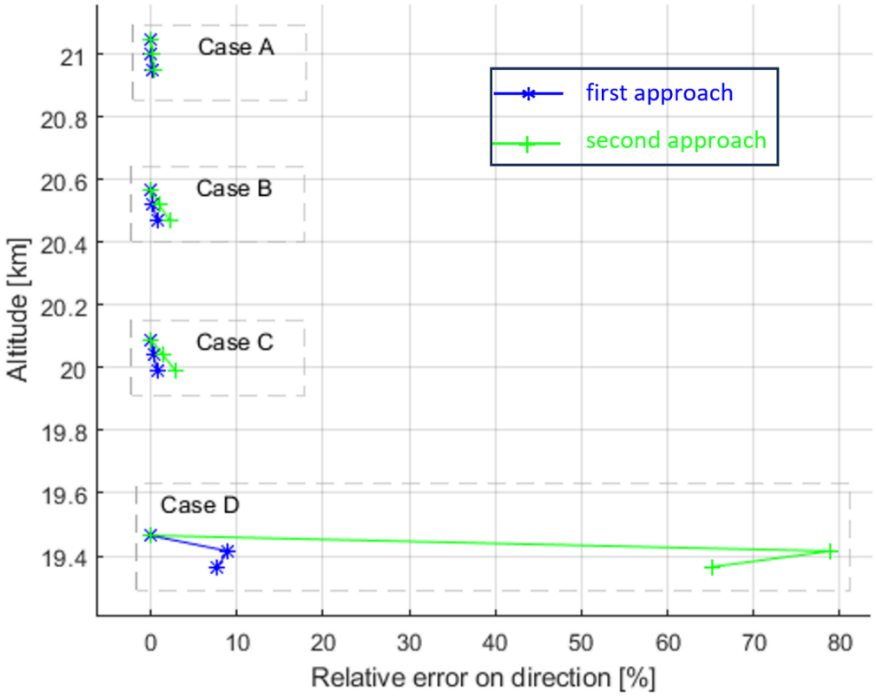

Figure 17: Comparison of relative errors on wind direction, L=50m

From the reported pictures, it appears evident that the second approach is less accurate in terms of wind direction, especially when the heading angle is low (see Figure 17, case D). Again, the reason behind this can be traced back to the difficulty of the cable's shape modelling when the projections of its ends in the horizontal plane are not relevantly distanced.

A possible improvement in the wind direction outcome can be achieved by integrating the heading calculation of this approach - based on the data provided by the GNSS module - with the heading information given by the Inertial Measurement Unit, as mentioned in Section 4.1.4.

In general, it can be stated that the relative error on the wind direction is lower than the one on the wind speed. The cause for this is probably the fact that the wind intensity at the altitudes of interest is of small value (as observed from the data provided by the flight simulator) - normally in the order of magnitude of $1 \div 5 m/s$ -, while the wind direction is variable over a wider range - all the $360°$. As a result, the computer approximation of the data is worse for the velocity, and the error is further propagated by the numerical algorithms.
This is valid apart from the exceptional case D, where the poor accuracy of the wind direction measurement is related to the fact that the involved angles are very small, which is likely to cause errors' propagation in the computational algorithm.

With the aim of exploring different methods to improve precision, several tests have been performed and numerous expedients have been adopted. Among these, a relevant enhancement was obtained by considering a diverse length of the portion of cable that is lowered below the balloon. Precisely, it has been observed that the results are more accurate if the segment of cable is increased from $50m$ to $125m$. This is probably due to the fact that in case the variable L is bigger, the numerical quantities which the algorithms are dealing with are less subject to numerical cancellation and error's propagation, and in general the matrix conditioning of the solving system of equations is better.
The corresponding results are reported in the form of graphs in Annex A.

Something that is not visible from the presented graphs, but appears clearly from the methods' description, is that the second strategy is much simpler and easier to implement. Indeed, while for the first approach every iteration is dependent from the previous ones, this is not true for the second method. In this case, each iteration is independent from the others and the solving system of equations is always the same, without an increase in the numerical problem's complexity. This is the reason why it seems preferable to carry out the second approach for the final implementation.

5. Systems design

The present Chapter aims at describing which activities and studies have been carried out in order to implement the project. Given the multidisciplinary nature of the internship, for the present report it has been decided to illustrate the performed activities by grouping them according to a logical scheme of subsystems. Consequently, the current Chapter is organised into several Sections that are focused on describing in detail the different subsystems in which the project has been articulated.

Firstly, the attention is placed on the communication system, which has been realised in order to allow the transmission of information from the probe to the balloon's nacelle and from this latter towards the ground station. It is important to mention that the communication system is highly related to the necessity of defining suitable timelines of operation by the two subsystems involving the gondola and the probe, with the objective of ensuring their mutual synchronisation. As a consequence, a detailed description is provided of the arrangements adopted at the software level concerning the logic and temporal operation schemes of the two electronic boards.

Subsequently, the Chapter provides a precise explanation of the system designed for the spooling and unspooling of the cable through which the probe is connected to lower it below the stratospheric balloon. As already mentioned, such reeling system has been developed in collaboration with an external working team, precisely belonging to the company 441 Engineering.

The following Section is focused on the power supply systems that have been developed for the two electronic assemblies in the nacelle and in the probe. This also represents an introduction to Section 5.6, which deals with the analysis of the thermal problem. Indeed, the design of the powering system is closely related to the need to supply a heater to enable the electronic components' operation in the working environment. Furthermore, the thermal analysis is strictly dependent on the overall sizing of each subsystem (nacelle and probe), which is determined from the design of the electronic PCBs and therefore influenced by the number of batteries required for the power supply, as well as by the thermal problem itself. The mentioned interdependencies are illustrated in Sections 5.5, 5.6 and 5.7.

5.1 Communication system

5.1.1 LoRa

As mentioned above, the measurements taken by Fisher are intended to be transferred to the board located in the balloon's nacelle through LoRa communication., as shown in Figure 18.

The term LoRa stands for "Long Range Wide Area" and it refers to a low-power wireless network protocol. This wireless data communication technology uses a radio modulation technique that can be generated by LoRa transceiver chips.

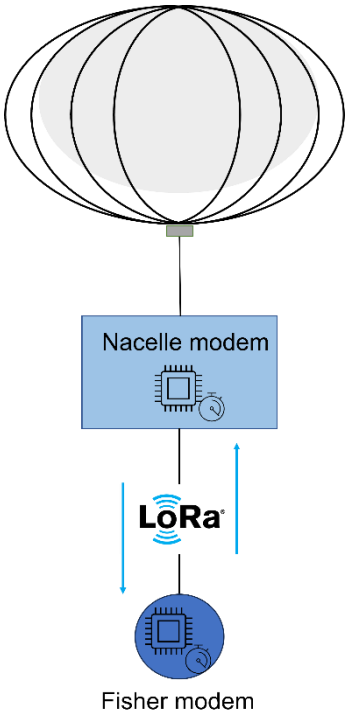

Figure 18: LoRa link

LoRa protocol provides the capability to achieve long distance communication without using much power, and is characterised by a high immunity to interference. Obviously, LoRa comes with its own drawbacks: to achieve high distance with low power requirements, LoRa operates on very low bandwidth. The maximum bandwidth for LoRa enables the transmission of only small amounts of data. Nevertheless, such amount is enough to transmit sensor values - as in the application described in the present dissertation.

During the project's development, it has indeed been noticed that there is a limit in the length of the message that can be received via LoRa communication - hence, the string containing the

information has to be smartly generated in order to reduce the number of characters while still being meaningful.

The device that is used for this point-to-point communication is the SEMTECH transceiver SX1278 (LoRa SX 1276/77/78/79, 2023) showed in Figure 19, which typical bandwidth is $433MHz$.

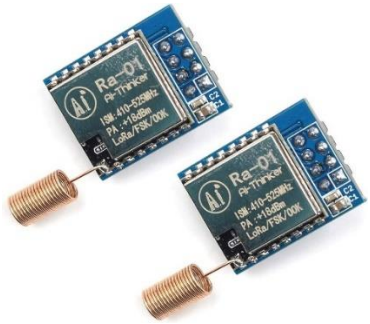

Figure 19: LoRa modems (LoRa SX 1276/77/78/79, 2023)

The illustrated component is connected to the electronic board through the synchronous serial data protocol SPI[28]: the LoRa modem represents the peripheral device (slave), while the ESP32 is the controller (master), which both can send and receive data at the same time to and from the other one.

The frequency at which the signal can be sent is regulated depending on the area where the modem is operating. For the project under analysis, the frequency of $433MHz$ has been considered generally valid (it is a matter of interferences with other vehicles and users); this value is allowed in France, and its validity has been extended for the case of a real flight.

In order to establish the LoRa link, it is mandatory that the two LoRa modems are initialised with the same band, as it has been observed during some tests, which showed the impossibility of communication in case the devices operate with different frequencies.

5.1.2 Iridium

As regards the communication between the balloon and the ground segment, it is planned to occur via Iridium link. Iridium is a global satellite communications system which provides access to voice and data services anywhere on Earth. The Iridium constellation consists of

[28] To better understand the concept behind this communication protocol, see reference (ESP32 SPI Communication).

66 Low Earth Orbit (LEO) satellites, and several in-orbit spares, which enable global coverage and mobility everywhere. This architecture is considered a meshed constellation of interconnected, cross-linked satellites so that each satellite can communicate with the other nearby satellites in adjacent orbits (Iridium Network).

The device used to ensure this communication for the project under description is RockBLOCK9603, which works with the Iridium Satellite System and the Rock Seven Servers to enable the connection between two points. The component is illustrated in Figure 20.

Figure 20: Iridium modem (RockBLOCK 9603 - Datasheet Small, 2023)

The module allows a low latency, SBD (Short Burst Data) communication. SBD is a bandwidth-limited messaging system, capable of transmitting 340 bytes per message sent; 270 bytes per message received, and with a send/receive frequency of approximately once every 40 seconds with a good view of the sky. The device is therefore suitable for applications which need to regularly send or receive small amounts of information, typically tracking, telemetry, system control and monitoring applications (RockBLOCK 9603 - Datasheet Small, 2023).

The logical architecture behind the Iridium link is illustrated in Figure 21: the RockBLOCK 9603 communicates with the Iridium satellites to send/receive data; then the Iridium satellites communicate with ground-based stations to send/receive data between space and Earth; next, data is sent between the Iridium ground stations and the Rock Seven Servers. It is possible to access this server via a web interface, or to directly receive the information via email.

There are two possibilities to enable the Iridium link: one requires the connection to an external antenna, which can be attached to the modem through its SMA connector; the other option is represented by the use of the ceramic patch antenna integrated on one side of the device - and it has been implemented in the described project.

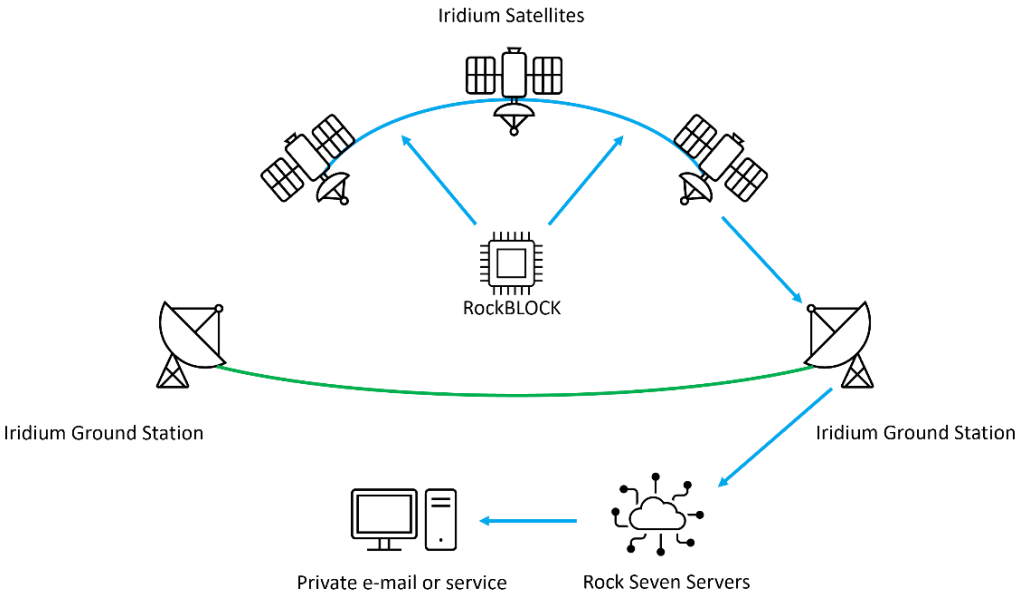

Figure 21: Iridium link

Data can flow in either direction. Messages transmitted from the RockBLOCK mobile device can either be delivered to the indicated email address, either sent to a private account on Ground Control's web service. For the project under discussion, the first of these options has been adopted.

Additionally, only one way of communication has been set, from the balloon's nacelle to the ground station. Further improvements could include programming the reciprocal communication route, from the ground to the nacelle, with the aim of sending instructions and commands to start the cycle of measurements.

The basic principle behind the Iridium connection is to utilise this network in order to send the collected data to the working team in charge for the mission development, and also to transmit updates about the system's operating status. For instance, in case a failure happens in the communication between the two boards, the Iridium modem in the nacelle is set to communicate the occurred malfunction - as well as any other issue.

During the project's development, the use of this component has generated some difficulties. Ineed, the first modem used was not able to work. To identify the cause of the issue, it has been necessary to deeply study the component's documentation available online, but also to contact some experts within CNES company - Moral Romain and Sandra Dussez.

Initially, the issue was reported as some errors related to the power system, which led to checking the connection of the modem with the board - that was in the first place an ESP32

LOLIN32 Lite, working with $3.3V$. To ensure the modem's outputs to be at logic $3.3V$ as well - the modem being powered by an external supply with the required $5V$ - it has been necessary to introduce a level shifter (Using The Logic Level Converter, 2023). However, the error kept manifesting even with the described modification. Indeed, the modem under use was not properly working since the internal current limiter was inactive, and this compromised one of the charging capacitors. Such problem was only visible when the small component's damage became big enough to appear evidently (the damaged capacitor started to expand).
Through careful analyses and observations and thanks to the help of the consulted experts, it was possible to identify the solution: not only the use of a different - functioning - device, but also of a different electronic board - an ESP32 WROOM 32, which supports $5V$ logic inputs.

It is important to underline that some aspects need to be considered to ensure a continuous operation of the Iridium modem. In the first place, it has to be guaranteed that the Iridium modem is completely charged despite the board sleep loops so as the supercapacitors stay powered (Power Supply, 2023). Moreover, it is necessary to use the appropriate libraries to program the device, which have been identified in the IridiumSBD Library and SoftwareSerial Library. Since this latter has been used also for the GNSS module, it is important to identify two different objects at the software level, and to associate them with different pins of the electronic board (both devices communicate to the board through a two-wires serial configuration).

Also, although the modem provides an approximate GPS location, this might be wrong of several kilometres, and therefore it is not reliable for the computation here implemented.

5.2 Timings and synchronisation

An important aspect that has to be taken into account is that the two electronic subsystems must follow highly precise operating logic schemes. Furthermore, since they have to communicate with each other, their activities must be well coordinated.
Consequently, it is essential to define hypothetic timelines for the two boards, taking into consideration all the different actions that each of them must perform, and scheduling precise periods of time for every operating task. As an example, some cautiousness has to be taken at the software level in order to enable the LoRa communication between the two electronic systems by keeping their synchronisation during the mission.

The described need has been deeply analysed, showing that it is crucial to identify logic and temporal sequences to monitor the activities of the two subsystems, which are reported in Figures 22 and 23.

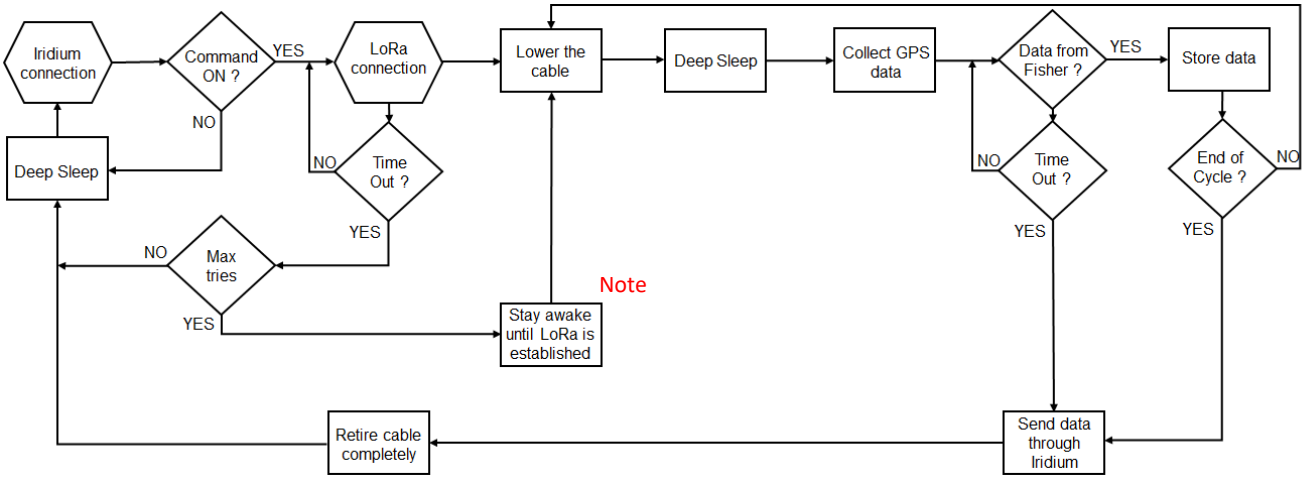

Figure 22: Nacelle's operation scheme

Since the aim is to ensure the boards' coordination, there is the exigence to adapt their functioning schemes with different periods of activity and of sleep mode. This means that some intervals are set in which one board is performing a task (e.g., establishing the Iridium connection in case of the nacelle's subsystem), while the other is simply waiting or sleeping. This necessity is addressed by setting different sleeping intervals and using timers to keep the systems busy with a single task for a specified amount of time as to avoid the uncertainty of not knowing what one of them is doing at a certain moment.

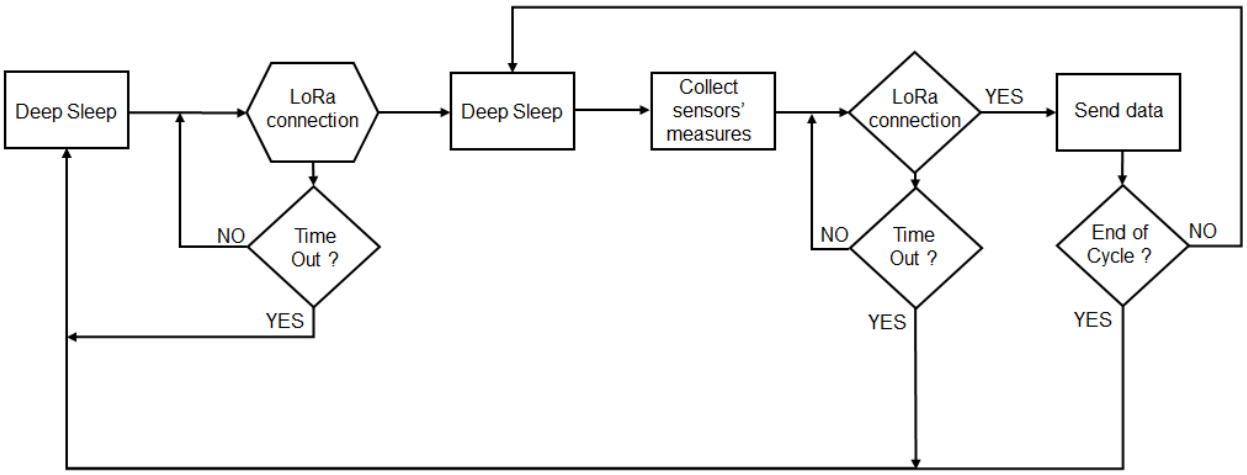

Figure 23: Wind Fish' operation scheme

5.2.1 LoRa logic

The necessity to accurately set the boards' operating schedules has been observed during some tests performed to verify the LoRa link, which have shown the strong dependence of the communication's success from the boards' synchronisation. In fact, several problems and difficulties have been encountered while trying to ensure that the two boards are able to communicate with each other.
A lot of analyses and trials have been necessary in this regard.

Since the communication is a two-way link, the boards have to look for each other: this means that in both their timelines precise intervals are planned for sending and receiving a message, after which completion the boards go on with the following tasks. This evidently implies the loss of some time wasted to ensure the boards' coordination.
Different possibilities have been explored, for instance running concurrent tasks to receive and send messages at the same time; though this would save a lot of operating time, it is in contrast with the aim of maintaining the systems' synchronisation, for which instead specific periods of time have to be dedicated to a single task. Specifically, not to lose the possibility of connecting the boards via LoRa link, periods of time in which both systems are busy with this activity must be set, even though the communication might be established very soon after the initialisation. Otherwise, one of the boards might go to sleep after sending a message, while the other would still be looking for the answer - it is not possible to determine in advance when the link is going to be fixed.

The main idea behind the adopted solution is the following: the code is set so as the board in the nacelle sends a message to the Wind Fish for a dedicated interval (see Annex B); the board in the Fisher wakes up and listens for the same period of time, after which it sends a message to answer (only in case it has received the sentence) for again the defined interval. During this period, the board in the nacelle is now listening, and if it receives something it then replies for the dedicated period. The three described "ping-pongs" (from nacelle to Wind Fish, from Wind Fish to nacelle, and again from nacelle to Wind Fish) are sufficient to ensure that each subsystem can send and receive messages from the other at least once, so that the connection is assumed to be working and it is possible to proceed with the successive activities.

It can be agreed that the synchronisation might be lost anyway due to multiple causes, such as internal delays at the software level, problems within the electronics' hardware, or human errors during the initial setting. Therefore, the possibility that the LoRa link is not established at some point during the operations still exists. If the communication fails and the two boards go to sleep separately, their coordination is lost, and it can occur that it is not restored. This is the reason why a setting has been added at the software level for the system in the gondola (indicated with a red note in Figure 22), which keeps the board awake in case the LoRa communication fails more than three times consecutively, so as to re-establish the connection with the Wind Fish. Such strategy has been successfully tested by forcing the loss of connection between the two subsystems.

5.2.2 Iridium logic

An analogous reasoning applies to the other activities in general, and specifically to the Iridium link. For example, it has been fundamental to identify the interval of time needed to establish such connection and then to send a message from the RockBLOCK modem.
This has required several tests, especially due to the fact that the modem does not work inside buildings, and sending messages necessitates a good view of the sky. In fact, the Iridium network operates in the microwave L-band, which means that successful data transmission relies on having an unobstructed line-of-sight view of a satellite. The RockBLOCK modem is able to calculate the signal quality based on the view it has of the Iridium constellation, and it is generally set to send the signal only over a minimum level of quality.

The modem's operation has been examined in multiple occasions and within different environments. The first tests have taken place within CNES Lagrange building, where it has been observed that opening the window and placing the device as to orient the integrated antenna towards the sky is sometimes sufficient to reach a good signal quality. Nevertheless, being inside a building usually causes the transmission to be very slow.
In order to reproduce a more realistic test, closer to the actual operating environment - without this kind of external impediments - some examinations have been performed within a laboratory provided with a connector for the modem's antenna, and with an internal GPS repeater. These tests main outcome is that sending a message can take several minutes, which has to be taken into account in the aforementioned timelines at the software level.

The ideated functioning is shown in Figures 22 and 23, and in Annex B. Assuming that the electronic board in the nacelle wakes up at time 0 in an absolute time reference frame, it first tries to establish the Iridium link, for example for an interval of $1.5mins$, during which the system in the Fisher is in deep sleep. In case this communication fails, the board goes to sleep; otherwise, it starts to transmit a message to institute the LoRa link, which clearly highlights that the board in the Wind Fish should be woken up at time 1.5, when it suddenly begins to listen at the other. In this way, the two boards are looking for each other at the same time.

5.2.3 Deep sleep

As it can be observed from Figures 22 and 23 and Annex B, certain periods of time are dedicated to Deep Sleep. This electronics' mode is set in order to reduce the power consumption: in particular, the ESP32 has different power-saving modes, which are based on disabling some of the board's features. The Deep Sleep mode is fundamental especially for the Fisher's electronics system, where the power usage has to be optimised in order to limit the number of required batteries (and therefore the global weight and size of the system). Moreover, setting some periods of Deep Sleep mode represents a considerable improvement of the batteries' performance and of the application's power efficiency.

This mode sets the board in a rudimentary state: only the ULP (Ultra Low Power) processor is active and the RTC (Real Time Clock) memory is powered, consuming very little energy (magnitude in the order of $10\mu A$) and being able to perform just basic actions (Save energy on the ESP32 with Deep Sleep, 2023).

The board can be woken up with various methods, as for example a timer, a touch pad, external interrupts, or the ULP coprocessor itself, and it comes out of Deep Sleep with a reset that starts the program execution from the beginning. As for the specific project under discussion, the wake-up source has been chosen to be always a timer, decision which underlines how crucial it is to precisely define the two boards' timelines. Since the boards must follow specific sequences of actions, it has been necessary to introduce some settings to prevent them from continuously repeating the same code's execution. This was done through the help of some *if* statements and variables that take into account the number of times the sketch has been already run[29].

[29] Another possibility that has been explored is to use the Light Sleep mode instead of the Deep Sleep, since in this case the board wakes up and goes on with the execution from the point where it left. However, this option has been excluded since it is not suitable for the objective of saving a big amount of energy.

Specifically, data that have to be used over sleep mode must be defined as global variables[30] stored in the RTC memory with the corresponding attribute.
The Deep Sleep mode is also useful to avoid the collection of measurements during the cable's deployment, since they would be highly affected by errors related to the Wind Fish movements.

In addition to the use of Deep Sleep mode, it has been decided to optimise the active time of each board, by minimising it whenever possible. With this aim, it has been necessary to adopt the strategy of running multiple tasks simultaneously.
Tasks are the building blocks of real time operating systems: they execute on their own context and are independent from each other. Concurrent tasks can be run on the ESP32 two separated cores, or even on the same one, making the board multitasking. Each task is then associated with a function that contains the code to be executed. Moreover, it is possible to control when a task is being enabled, to suspend its execution and then to resume it when desired, or to definitively delete it.
Several concurrent tasks have been created in the Fisher's software so as to enable contemporaneous measurements taken by the different sensors (GNSS module, differential pressure sensor, and IMU); whereas at the nacelle's level, an idea could be to retire the cable while sending an Iridium message containing the collected information after the cycle of measurements has ended.

5.3 Reeling system

For the final implementation of the reeling assembly, the main idea has been to develop a system as simple as possible in order to limit the risk of breakdowns and mechanical problems.
With this aim, the 441 Engineering team has conducted several tests on different winding systems, as reported in document (Tournie, 2023).
The dimensions of the coil, and particularly its width and diameter, have been chosen based on the outcomes of the several conducted tests.[31] The final design has been achieved with the objective of optimising the winding of the cable around the coil in a perfectly uniform manner,

[30] A global variable is a variable that can be accessed by any function in the code, and which cope extends to the whole program's execution. To create a global variable, it is sufficient to declare it outside the setup, loop and custom functions of the code.
[31] The coil's diameter is $160mm$ and its width is $10mm$; with the cable completely wound around the coil, the total diameter becomes $190mm$.

without protrusions or depressions. To this end, it has been necessary to include a system that prevents the wire from coming off the spool by minimising the risk of the wire becoming slack.

It was observed that the use of a spring system is not really effective, as it can enter into resonance. The found solution consists of using closed eyelets, which enable simple and effective wire guidance without the risk for the wire to come out of the spool. The system is shown in Figure 24, where the external polystyrene box that serves as thermal protection is also illustrated, and in Figure 25.

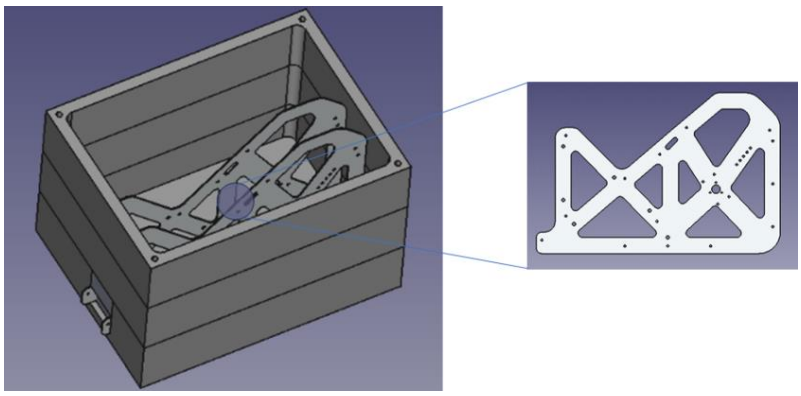

Figure 24: Nacelle's reeling system

The chosen cable is a thin wire generally used for fishing purpose. The cable has a diameter of only $0.1mm$ and is made of polyethylene, which is a very light material (density of $0.93g/cm^3$).

Figure 25 shows the frame, which is made of 2 aluminium plates connected by colonettes and numerous rotating axles. The interchangeable carbon mast is mounted on a pivot link and held in place at the top by a halyard.

Considering the wire routing, the cable passes inside a tube and then through a Z-shaped circuit via rings, before winding around the spool. Proper winding is ensured by the appropriate distance interposed between the last ring and the wheel, and by the presence of a roller.

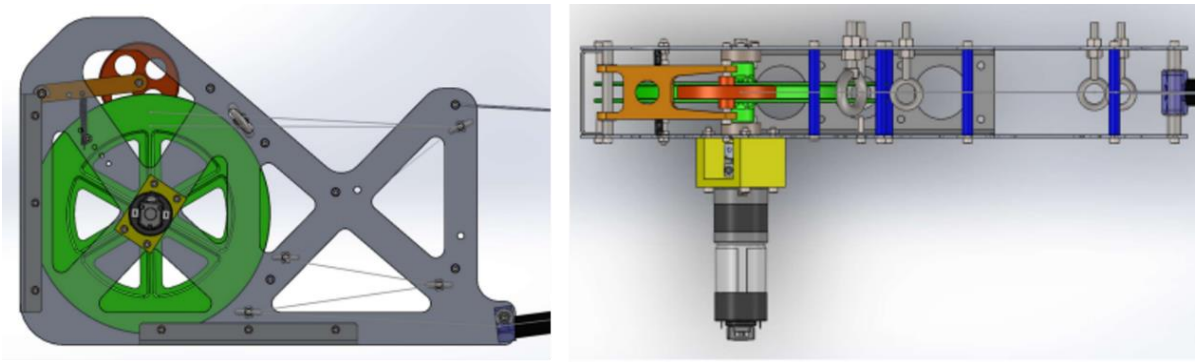

Figure 25: Reeling system (Tournie, 2023)

During the performed tests it has been observed that regular, constant tension in the wire is crucial for appropriate operation. Therefore, in order to ensure permanent tension on the cable, different solutions have been studied and proposed by the external team: the insertion of a roller against or at the end of the line, controlled by a force-sensor or a potentiometer; the use of a spring-mounted plate that opens the electric circuit according to the cable's tension and switches off the motor; the electric motor's control according to its current readings. The finally chosen solution is to do nothing at the mechanical level but to intervene at the software level whenever necessary, by controlling the precise motion of the motor.

It is relevant to mention that, after the preparation a system to test the cable's deployment mechanism[32], it was found impossible to use the stepper motor initially chosen (component 28BYJ-48), even though it can be easily and accurately controlled. Indeed, the conducted experiments have made explicit the need for a different and more powerful motor. A DC (Direct Current) planetary gear motor has been chosen as alternative system (device E192.12.125, shown in Figure 26), and it has been associated to a driver (device Driver Shield L293D Expansion Board Module) to control its functioning through the ESP32 board, and to an encoder to precisely regulate the number of accomplished rotations.

[32] To test the system, it has been necessary to introduce an external input to set the direction of the motor's revolutions, and to start and stop the motor as wanted. In order to achieve these auxiliary degrees of freedom, different approaches have been examined. The final solution and its functioning have been appropriately described in a report that has been provided to 441 Engineering team to facilitate their tests.

Figure 26: Planetary gear motor (Technical data - series E192, 2023)

A driver is the object that comes between the motor and the electronic board: the input to a motor driver is the desired functionality communicated by the controller, and it has to respect the circuit's limits and kinematic capabilities. The driver's internal logic processes the request by providing suitable signals in output to drive the generic amplifier stage, which in turn reprocesses the electrical quantities in input, transforming them properly to drive the electric motor connected to its output.

The reasons why an appropriate motor driver is convenient/necessary are varied; one of the most relevant relates to the fact that usually the object handling the logic is not capable of directly driving a motor due to the electrical quantities involved. For example, a microcontroller cannot normally deliver enough current and voltage to drive a motor without the risk of a burning out (Andrea, 2023).

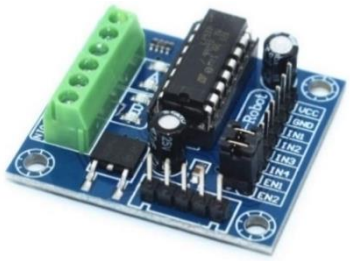

Figure 27: Motor driver module (L293D Motor Driver Module, 2023)

The selected driver is the L293D, which is illustrated in Figure 27. The device is a basic motor driver integrated chip, which consists of two H-bridge circuits (the simplest circuit for changing polarity across the load connected to it) and four high current and high voltage channels.

This component enables the possibility to drive a DC motor (or any other inductive load) in clockwise and counterclockwise direction, and also to control the speed of revolution - even though this functionality is not of interest for the project under discussion.

On the other hand, an encoder is a displacement and velocity transducer that transforms angular or linear mechanical motion into a series of digital electrical pulses. These pulses can be used to control the mechanical displacements that generated them and the corresponding speed by

using actuating devices. The opted component is a biphasic incremental rotary encoder, shown in Figure 28.

As the encoder's shaft rotates, the two outputs trigger periodically: by simply counting the encoder's pulses, it is possible to monitor the number of shaft's revolutions. Moreover, depending on the direction of revolution, one of the outputs triggers before the other, therefore it is possible to know in which sense the shaft is rotating.

Figure 28: Rotary encoder (38S6G5-B-G24N-Imprimante Incrémentale à Distance, s.d.)

The selected components have been tested with a series of different winding systems by the 441 Engineering team, showing that the assembly develops a sufficient amount of power to operate the reeling system.

To ensure that the proper tension is always maintained on the cable, the motor is controlled through the driver and feedback on its movement is provided by the encoder. To this end, the encoder's shaft is properly connected to the motor's one, in order to enable such supervision.

It has been decided to implement a simple function to monitor the effective motor's revolutions. No PID (Proportional Integral Derivative) controller has been implemented to set the speed, with the aim of maintaining the rotations per minute constant during each step and of keeping the software's complexity as low as possible.

The regulation is therefore achieved through the use of an interrupt that constantly checks the encoder's output and keeps track of the number of received pulses[33]. Knowing that - for the specific component under use - 600 pulses correspond to one rotation, it is possible to trace back with high accuracy the number of rounds completed by the motor's shaft. Then, the driver stops the motor as soon as the desired revolutions have been achieved.

[33] At the software level, the microcontroller monitors any change that occurs in the encoder's outputs, so as to count for the two directions of rotation, and also for the steady state condition.

Without any additional command, the motor's speed is automatically set as the maximum value that can be reached according to the supplied power. In the case of $12V$ power supply, the shaft's speed is $24rpm$ according to the datasheet, which means 2.5 seconds to complete one rotation (Technical data - series E192, 2023). The motor's speed has been tested and measured in both directions, confirming the technical specifications.

It is relevant to mention that the use of the encoder has initially caused the damage of one electronic board. For this reason, the component has been tested and its functioning verified with the use of an Arduino MEGA, which is considerably more powerful than ESP32. After the code's validation, the encoder outputs have been measured to ensure their compatibility with the ESP32 operating limits (in terms of input current and voltage). The experiments have shown that the encoder must be powered with not more than $5V$ in order to avoid peaks of current in its outputs that could damage the electronic card.

5.3.1 Cable's length and motor's revolutions

As underlined previously, it has been necessary to identify how to calculate the length of cable deployed with relation to the dimensions of the winding system, taking into account that the wind diameter changes as the cable is spooled or unspooled around it. To this end, two different methods have been implemented, which are described in the following. Both approaches are based on the idea that the motor's speed is kept constant, so that the motor's working period is automatically identified.

First approach

As regards the first approach, the main concept behind it is to determine the relation between the volume of cable that has been lowered and the occupied volume around the wind. Such relation has been identified assuming that the filling coefficient of the coiled cable stays constant. The filling factor represents the portion of available volume that is actually occupied by the cable: when the cable is spooled around the wind, some space is left empty as shown in Figure 29, where the yellow circles represent the windings (which section is circular).

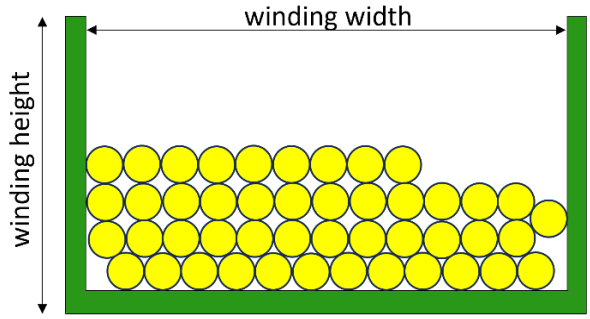

Figure 29: Cable's windings

The calculations that led to the determination of the number of motor rounds required to deploy $50m$ of cable at each step are reported in the following.

The cable's total volume is the one of a solid cylinder: $V_{real} = 20 * L * \pi * \left(\frac{d}{2}\right)^2$, where $20 * L$ is the cable's length ($1km$: $L = 50m$) and d is its diameter ($0.1mm$). The occupied volume is calculated as the volume of a hollow cylinder: $V_{occupied} = h * \pi * \left(\frac{d_{outer} - d_{inner}}{2}\right)^2$, where h is the cylinder height, corresponding to the coil's width, d_{outer} is the external diameter of the coil when the cable is completely spooled around it, and d_{inner} is the internal diameter of the coil.

It is therefore possible to calculate the filling coefficient as the ratio between the real volume of the cable and the volume which is effectively occupied around the coil:

$$filling_{coefficient} = \frac{V_{real}}{V_{occupied}} = 0.09523809523$$

Since this coefficient depends on the cable's shape and on the coil's sizes, it is assumed to be a constant value, that does not vary depending on the number of cable's windings.
Consequently, knowing that the cable is lowered in steps of $50m$, it is possible to determine the real volume of cable that is wound around the coil at each step:

$$V_{real_i} = \big(20 - (i - 1)\big) * L * \pi * \left(\frac{d}{2}\right)^2$$

Since i corresponds to the iterations' number, the previously introduced V_{real} denotes V_{real_1}.
The occupied volume can be determined at each iteration as:

$$V_{occupied_i} = h * \pi * \left(\frac{d_{outer_i} - d_{inner}}{2}\right)^2$$

where d_{outer_i} is the new outer diameter - corresponding to the portion of cable actually wound around the coil at the i^{th} iteration -, which value is unknown.

Again, $V_{occupied}$ indicates $V_{occupied_1}$.

The occupied volume can be calculated also as a function of the real volume:

$$V_{occupied_i} = V_{real_i} * \frac{1}{filling_{coefficient}}$$

Combining the last two equations, it is possible to determine the outer diameter at each iteration:

$$d_{outer_i} = \sqrt{\frac{V_{occupied_i}}{h * \pi} * 4 + d_{inner}{}^2} = \sqrt{\frac{V_{real_i}}{h * \pi * filling_{coefficient}} * 4 + d_{inner}{}^2}$$

Furthermore, it is immediate to see that the relationship between this value and the portion of unspooled cable is (formula for a circle's length):

$$L = d_{outer_i} * \pi * n_{rounds}$$

where n_{rounds} is the number of rounds completed to lower the cable's segment.

Therefore, the number of rounds necessary to lower $50m$ of cable at each step can be determined as:

$$n_{rounds} = \frac{L}{\pi * \sqrt{\frac{V_{real_i}}{h * \pi * filling_{coefficient}} * 4 + d_{inner}{}^2}}$$

$$= \frac{L}{\pi * \sqrt{\frac{\left[\left(20 - (i-1)\right) * L * \pi * \left(\frac{d}{2}\right)^2\right]}{h * \pi * filling_{coefficient}} * 4 + d_{inner}{}^2}}$$

Second approach

The second approach assumes that it is possible to identify a linear function that correlates each iteration with the number of motor's revolutions which correspond to lowering the cable of $50m$. Such relation has been determined by implementing an interpolation function for the deployed segment with a first order polynomial.

As previously observed, the number of motor's rounds is directly linked to the coil's diameter (comprehensive of the portion of cable wound around it), and therefore it can be brought back to the corresponding iteration.

The idea was initially to find a quadratic polynomial that could approximate the motor's revolutions. Nevertheless, since the real data to be fit are just two (the point corresponding to the first iteration, when the cable is completely spooled around the coil, and the one representing the end of the measurements' cycle, when all the cable has been lowered), it is only possible to develop a linear interpolation. It should be noted that the interpolation is made among the point corresponding to the real first iteration, and a hypothetical point corresponding to a 21st iteration (i.e., the end of the cable).

Both functions have been implemented at the software level so as to obtain the input value to the driver that controls the motor's rotations. More precisely, once the motor is activated, the encoder continuously checks the number of rotations effectively completed and compare this input with the desired number of rounds, which is computed with the aforementioned function.

The target number of revolutions obtained from the cited formula must be rounded to an integer value, otherwise the encoder is not capable of making the comparison with the actual number of rotations. The need to introduce this cautiousness has been observed during some tests of the coupling between the encoder and the motor, which have shown that the encoder does not recognise values that are not integer numbers.

The comparison between the two described approaches is shown in Figure 30 and Table 1.

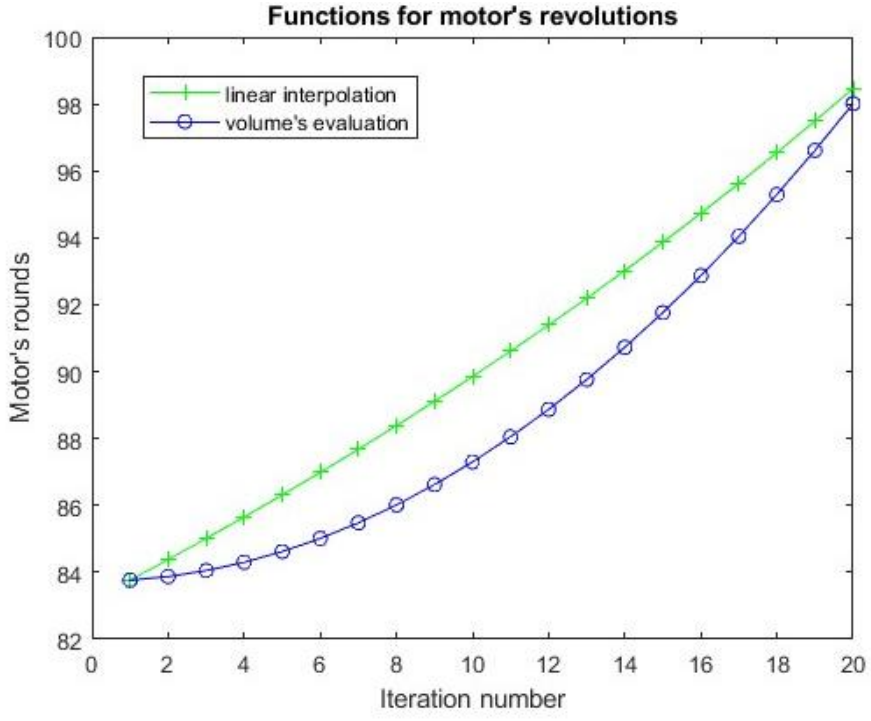

Figure 30: Comparison between the two approaches - from MATLAB script

Table 1 clearly shows that the difference between the two methods is evident from the third iteration and remains relevant until the 18th iteration - considering that the number of revolutions effectively completed is rounded to the closest integer value. Therefore, it has been chosen to implement the first approach, given that it is not based on an approximated interpolation of data. However, the intent for the future is to perform some experimental tests to verify which method among the two provides the most accurate estimate of the real number of revolutions.

Table 1: Comparison between the two approaches

Iteration number	Volume's evaluation method	Linear interpolation method	Iteration number	Volume's evaluation method	Linear interpolation method
1	83.7657595220502	83.7657595220502	11	90.6134252731660	88.0492358612460
2	84.3815847038229	83.8728464305301	12	91.3944296317411	88.8702354929251
3	85.0111948834755	84.0513246113299	13	92.1959830950017	89.7626263969243
4	85.6551121430012	84.3011940644497	14	93.0190028804284	90.7264085732433
5	86.3138866725676	84.6224547898894	15	93.8644645647615	91.7615820218823
6	86.9880987466116	85.0151067876490	16	94.7334069465675	92.8681467428412
7	87.6783608724297	85.4791500577285	17	95.6269374133448	94.0461027361200
8	88.3853201293452	86.0145846001280	18	96.5462378762278	95.2954500017188
9	89.1096607187574	86.6214104148474	19	97.4925713446224	96.6161885396374
10	89.8521067479159	87.2996275018867	20	98.4672892239533	98.0083183498761

5.4 Electronics integration

The electronics integration covers a role of fundamental importance in order to develop a unified sensor which is comprehensive of all the implied devices.

Incorporating several components together requires a good knowledge of their logical connections and ways of interactions, so as to ensure the absence of interferences among them. For this reason, it has been necessary to analyse how each device operates (in terms of communication protocol, data collection, etc.) and how it is interfaced with the core of the electronic system, the ESP32 board.

At first, every component has been properly connected to the electronic card in order to verify its appropriate functioning and interaction with the board. After testing each device separately,

an inspection of the proper operation of the complete electronic assembly was necessary so as to detect eventual malfunctioning and interferences among the sensors, and to eliminate them.

There exist several ways of interaction between electronic devices. Among these, the most commonly used are I^2C protocol and serial data communication. The I^2C protocol is a communication bus which is intended to allow multiple peripheral digital integrated circuits to communicate with one or more controller chips. I^2C is indeed a synchronous half duplex communication that supports multi master and multi slave; it is a simple two-wire serial protocol that uses its two lines for clock and data transmission.
The ESP32 supports I^2C communication through its two bus interfaces that can serve as master or slave depending on the user's configuration. Any pin of the electronic board can be configured to support the I^2C functionality. Additionally, with I^2C communication every sensor on the bus is associated with its own address, a hexadecimal identification number which is generally indicated in the component's datasheet. Therefore, it is possible to connect multiple I^2C sensors on the same bus of the electronic card: to avoid conflicts, it is sufficient to refer to each peripheral by its address.
On the other hand, SPI is an interface bus commonly used to send data between microcontrollers and small peripherals, which is full duplex (simultaneous sending and receiving of data) communication. SPI only supports single master, and it uses four wires (Difference Between I2C vs SPI, 2023).
For the project under discussion, it has been decided to adopt the I^2C communication protocol when possible, with the aim of simplifying the connections between the components and of reducing the number of wirings.

To report an example of electronics integration at the software level, it has been observed that the GNSS module does not work properly in case the code makes use of delays to separate the execution of different tasks. This is due to the fact that the *delay* function in C/C++ language is used to completely suspend the program's running, therefore the GNSS module is not able to continuously parse for packets of information. To solve this issue, a specific function inserting delays in the program without interrupting the GNSS module's activity, thus without losing information, was created.
A further inconvenient has been recorded for the IMU's readings once the integration of the Wind Fish electronic assembly has been completed. More precisely, it has been ascertained that

the information about the heading is highly affected by a massive presence of other electronic devices, and in particular of an external power source. The precautions that have been adopted to correct the resulting errors are reported in Section 4.1.4 of the present paper.

At the hardware level, there exist several recommendations that can and should be followed during the physical assembly of the electronic components to optimise their functioning and to avoid any conflicts and faults. For instance, it is highly advised to solder a $0.1\mu F$ ceramic capacitor among the positive and negative terminals of the DC motor in order to help smooth out any voltage spikes (ESP32 with DC Motor and L298 Motor Driver - Control Speed and Direction, 2023).

Regarding the preventive actions taken at the hardware level, these arrangements should be taken into account in the design of the PCB layout, as described in the following.

5.4.1 PCB layout

A PCB (Printed Circuit Board) is an electronic assembly that uses copper conductors to create electrical connections between components. Printed circuit boards provide a mechanical support for electronic components so that the device can be mounted in an enclosure.
The design of a printed circuit board involves a specific series of steps in line with the production process, the encapsulation of the integrated circuit and the bare board structure.

To start designing a PCB layout, it is first necessary to draw the schematic of the electronic circuit. The schematic is used as a blueprint for placing the components on the PCB and laying out their connections. The schematic symbols must be associated with the appropriate PCB footprints, corresponding to the real physical dimensions and characteristics of the used devices (such as the position of pads and holes). It is important to correctly wire the components in the schematic, and to verify the connections before creating the PCB layout.

There exist several rules that must be followed in the conception of a PCB. Here, only the fundamental recommendations that are relevant for the project under interest are reported.
In order to optimise the PCB's design, it is crucial to keep the connections as short as possible; in fact, long conductive traces can suffer from interference and noise due to other sources of electromagnetic radiation. Moreover, the different components should be supplied power with separated traces of approximately equal length (star configuration) so as to ensure that each device receives the same supply voltage.

As per the application under description, it does not imply specific and restrictive constraints as regards the PCB's size and shape; nevertheless, it has been chosen to design a simple rectangular shape (for both the nacelle's and the Fisher's board), and to keep its dimensions limited while ensuring enough distance between the components to easily position and solder them to the board.

The components have been placed following multiple criteria: the layout has been designed considering the component's connections and sizes, but also their working principles. For instance, for the LoRa modem it has been necessary to analyse the antenna's characteristics: indeed, it is required that the antenna's radiation pattern ensures the communication between the Wind Fish system and the one in the gondola. The adopted device (described in Section 5.1.1) is characterised by the use of a helical spiral spring antenna, as the specification states (Ra-01 Specification, 2019). Since the signal's wavelength is considerably bigger than the helix diameter[34], the antenna is considered to be a normal-mode helix which operates as a monopole antenna. This means that the radiation pattern is omnidirectional, hence the antenna radiates equal power in all directions perpendicular to its axis (Helical antenna, 2023).
A further point that has been accommodated is the fact that no metallic components should be placed around the antenna, otherwise they would represent obstacles in the signal's path.
Given these considerations, the LoRa modem has been properly positioned and oriented on the PCB layout.

Another aspect that has been taken into account is that the general recommendation for surface mounted devices is to place them on the same side of the board. This guidance has been followed for the PCB for the Fisher's electronics; while for the assembly in the nacelle, it has been chosen to position the GNSS module and the Iridium modem on the upper side of the board, and the other components on the opposite face. The reason behind this decision is to simplify the assembly of components and the tracing of their connections, while ensuring that the antennas face the sky.

Considering that the components under use are all characterised by low power consumption, the current that nominally flows through their connections is low (generally in the order of

[34] The signal's wavelength is calculated as the ratio between the speed of light, $c = 3 * 10^8 m/s$, and the signal frequency, in the order of $433MHz$; $\lambda = \frac{c}{f} = 69.284cm$. While the antenna's diameter is around $0.5cm$.

magnitude of tens of mA, and with maximum of some hundreds of mA); consequently, it has not been necessary to adopt specific carefulness for the traces' width.

As described in the dedicated Section 5.6, before designing the board in the Wind Fish it has been necessary to consider the necessity of a MOSFET (Metal Oxide Semiconductor Field Effect Transistor) circuit for the thermal control system. At first, the devised circuit has been tested to verify its correct functioning and adjust eventual mistakes; then, it has been included in the final design.

Finally, some holes have been inserted in the layout for mounting purpose, and more specifically to ensure stable attachment of the board to a containment casing in the final assembly of the prototype.

The latest versions of the printed PCBs are shown in Figures 31 and 32, where the components have been placed on the boards for illustrative purpose, whereas the drawn schematics are reported in Annex C.
The illustrated layouts have been designed with the software EasyEDA, which is well-documented and enables the functionality of exporting the Gerber files that can be directly uploaded on the printing machine or sent to the manufacturer.

Figure 31: Nacelle PCB

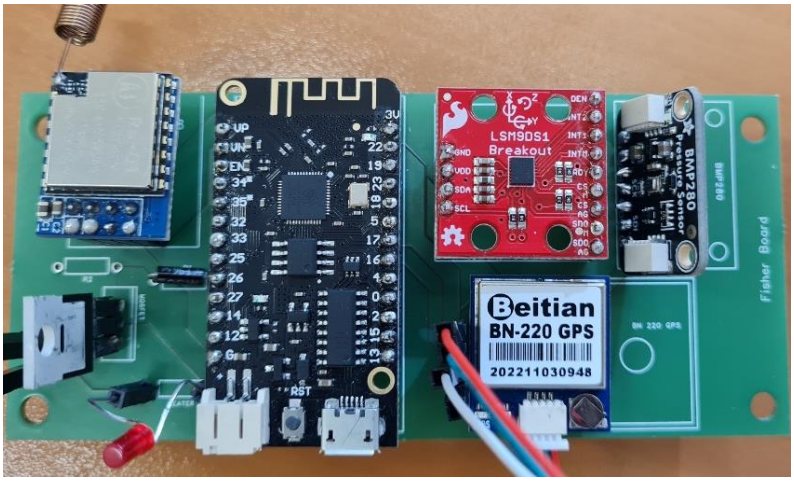

Figure 32: Wind Fish PCB

It is relevant to note that the PCB layout has to be designed taking into account appropriate settings to match the printer's characteristics. As an example, the number of layers in the layout has been limited to two (bottom and top layer) to match with the company's printer, and vias have been avoided due to the printer's limited capability. Indeed, at first the PCB's printing has been performed with the company's PCB printer, by the technical expert Manni Florant.
Moreover, the routing has been performed manually to simplify the printer's isolation process, and to avoid drawing traces close to each other or to other pads (verified with a software's functionality), with the general aim of maintaining the PCB's cost and complexity as low as possible.

Initially, the basic settings have been chosen for the route's width, with a subsequent modification due to the inaccuracy of the drilling system. Due to some technical problems, the company's printer was not able to manufacture two layers PCB (the two sides resulted to be disconnected); therefore, the designs have been ordered by an external provider. This has required the layouts' modification so as to adapt them to the design's rules of the supplier, and has considerably delayed the project, since the PCBs were delivered more than a month after the order was placed.
The PCB layouts have been ordered by the manufacturer AISLER, uploading the Gerber files and verifying that the design rules are met, and examining the ordered configuration with the website's inspector functionality.

The final boards have been visually inspected and have shown no apparent problem. Afterwards, continuity tests[35] have been performed with the electrical tester to verify the correctness of the connections between the components. Again, the verification has been successful.
Finally, female headers have been welded on the boards[36] to complete the electronics assembly and to check the correct execution of the developed programs (as already confirmed on the breadboards). The result was immediately positive for the nacelle's PCB, whereas for the Fisher's one it was necessary to remove one of the resistors of the MOSFET circuit, as shown in Figure 38. Despite the designed circuit had worked on the breadboard, it did not on the printed PCB; by simply removing the resistor between the gate and the source, the normal operation was re-established.
Moreover, the BMP280 (see Section 5.6.2) footprint was flipped with respect to reality, therefore it was necessary to solder the component on the opposite side as the one planned.

5.5 Power supply

An important aspect concerning the system's design is the power supply. Indeed, the power subsystem plays a fundamental role and therefore it has to be properly dimensioned and configured.

As regards the electronics in the Fisher, the idea is to power all the sensors directly through the ESP32 board (which provides 3.3V), connected to a rechargeable Li-Ion battery. This latter is intended to be charged by a small solar panel via an appropriate solar charger, as described in Section 5.5.2.

In the case of the system in the balloon's nacelle, the main board is going to power only the GNSS module and the LoRa modem (which both work with 3.3V); whereas the Iridium modem and the board itself will be powered by some batteries in series to provide the required 5V. Another possibility that has been explored is to power the 3.3V-working devices with the same 5V power source. However, this solution has been discarded due to its additional complexity,

[35] Continuity is the presence of a complete path for current flow, which confirms the two points under test are connected.
[36] The choice was made to avoid the direct soldering of the components to the board, to prevent the issue of having to desolder them in case of mistakes in the PCBs.

since it requires not only a voltage regulator, but also the use of two ceramic capacitors in order to stabilize the inputs/outputs and absorb eventual peaks of current.
Regarding the reeling system, since the encoder works with DC among 5 and 12V, it will be powered with the same group of batteries at 5V. This choice has been taken after some tests showed that the board would be damaged in case the encoder is working with voltages higher than 5V, since it would receive an input signal at too high current - resulting in ultimate damage of its voltage regulator.
As for the gear motor, it requires an external power supply of $12 \div 24V$, therefore it is powered by an additional group of batteries providing 12V. It is important to notice that the motor is powered through the driver, and the connection requires the introduction of a small capacitor between the input power and the ground, as previously observed. Additionally, it is fundamental to connect the driver ground to the same reference ground as the board's one, which is the common ground (this practice is mandatory for every electronic circuit - there must be only one ground reference).

As described in Section 5.6, the demand of a thermal regulation has underlined the need to design a power system for the heaters under use. Consequently, it has been necessary to proceed in an iterative loop to determine the number and size of required batteries, which evidently influences the thermal analysis (in terms of the system's dimensions and of the global thermal inertia), together with the required heater and its characteristics (in terms of generated heat and also electric source).

5.5.1 Batteries sizing

The type of batteries chosen and considered for the analysis is SAFT LSH20, which is generally used by the company for application within similar projects. Figure 33 reports an example of the product.

Figure 33: LSH20 battery (Primary Lithium Battery - LSH 20, 2023)

LSH20 is a type of primary lithium battery, working with Li-$SOCl_2$ (lithium-thionyl chloride) and providing $3.6V$ at a nominal capacity[37] of 13Ah.
These cells are commonly chosen since they are highly stable during their lifetime and application. Moreover, they are characterised by a wide range of operating temperature, which extends among $-60°C$ and $+85°C$. Additional benefits are represented by their easy integration into compact systems thanks to their cylindrical shape, and by their low self-discharge rate (Primary Lithium Battery - LSH 20, 2023).

As described in the previous Section, the implemented systems operate at voltages of 5V or 12V. Therefore, it is necessary to connect several batteries in series[38] to provide such power: more specifically, two batteries in series are needed to supply 5V, whereas four cells can provide 12V.
The number of required batteries depends not only on the voltage needed for the system's operation, but also on the mission's duration. To define this period, it has been considered that the first application of the implemented project will be the in-flight verification test. Consequently, it has been assumed that the mission will last around one week, during which the system must be autonomous.

To determine the number of needed batteries, it is required at first to calculate the total amount of loads (in Watts) which run directly on the storage energy of the cells. Such computation has been performed for the two subsystems in the Fisher and in the gondola, considering the specifications of the two assemblies of components in terms of operating voltage and current (including the heaters).
Moreover, it is necessary to identify the amount of hours per day in which the system is actually operational, since some periods of inactivity have been programmed with the aim of reducing the power consumption, as described in Section 5.2. The number of hours of operation is defined as backup hours: as this value increases, more batteries are needed.

An important parameter to take into consideration is the batteries' Depth of Discharge (DoD). The DoD is represented in percent (%) of total capacity of the battery, and it indicates the charging and recharging cycle of the battery. A deeper discharge shortens the battery's life, therefore the more discharging of a battery, the fewer cycles are completed.

[37] The capacity of a battery is the amount of energy charge in the cell that enables $1A$ of current to flow for $1h$.
[38] The DC voltage of the battery system is therefore 3.6V times the number of batteries in series.

For the specific application under discussion, a discharge safety of 20% has been considered (i.e., a DoD of 80%).

The requested battery capacity size is thus calculated with the formula:

$$Battery\ capacity\ [Ah] = \frac{Energy\ demand\ [W] * Autonomy\ days\ * Backup\ hours\ [h]}{DoD\ [\%] * DC\ voltage\ [V]}$$

Once this quantity has been identified, the number of required batteries has been determined consequently.

In order to provide more than the single battery's nominal capacity, it is necessary to connect multiple cells in parallel. Given the specific type of battery applied and the characteristics of the developed systems, the calculus have led to the following outcomes: two parallel groups of four batteries each are needed to power the heater in the Wind Fish; whereas two parallel groups of two batteries in series are needed to power the electronic system in the nacelle (main board, Iridium modem and encoder), and three parallel groups of four batteries each are required for the motor and the heater operation.

These results have been used to perform the first attempt mechanical design of the two subsystems, described in Section 5.7, and thus to identify realistic dimensions to consider for the thermal analysis.

5.5.2 Solar panels

The chosen solar panel is a small system that provides 5V (Mini Solar Panel - model 11585, 2023), illustrated in Figure 34. Besides the working environment, the device is assumed to work at a proper temperature (its operating range is among $-10°C$ and $+60°C$): the hypothesis is that the electronic components dissipate enough power to warm the panel up to an acceptable value of temperature.

Figure 34: Solar Panel (Mini Solar Panel - model 11585, 2023)

As mentioned, the solar panel is intended to charge a Li-Ion battery via a solar charger, and through the battery the ESP32 Lolin32 Lite board.

The solar charger that has been used is a CN3065 18650 Li-Ion Mini Solar Charger Module, shown in Figure 35. The device is a single lithium battery charge management chip that provides a simple and efficient way to recharge a single Lithium-Ion or Li-Polymer rechargeable battery through a solar panel.

Figure 35: Mini Solar Charger (CN306518650 Li-Ion Mini Solar Charger Module, 2023)

This complete linear charger operates at constant-current/constant-voltage, with thermal regulation to maximise charge rate without risk of overheating (Lithium Ion Battery Charger for Solar-Powered Systems, 2023). The regulation voltage is internally fixed at 4.2V with 1% accuracy, and it is adjustable with an external resistor, whereas the charging current is automatically adjusted based on the output capability of input power supply.

The module is provided with a pin which can sense the battery's voltage: the charge cycle is automatically restarted when the reading from this pin falls below the recharge threshold (4.1V).

The load, which for the specific project under interest is the ESP32 Lolin32 Lite board, should be connected in parallel with the battery. The only possibility to power the board is through its integrated battery connector. Indeed, it is important to notice that the ESP32 Lolin32 Lite cannot be powered directly from the 3.3V pin, which serves only as an output pin, not as an input.

Since the board has an integrated voltage regulator, the solar system is generally considered suitable for charging it (Introduction to CN3065 Mini Solar Charger, 2023). However, the solar charger power inputs and outputs have been tested to verify the appropriate functioning and to avoid any damage to the electronics. With the use of a multi-meter, it has been possible to

observe that the output voltage is exactly 4.2V[39] when the charge is complete. Therefore, there is no need for a voltage regulator.

Figure 36 illustrates the schematic of the designed system.

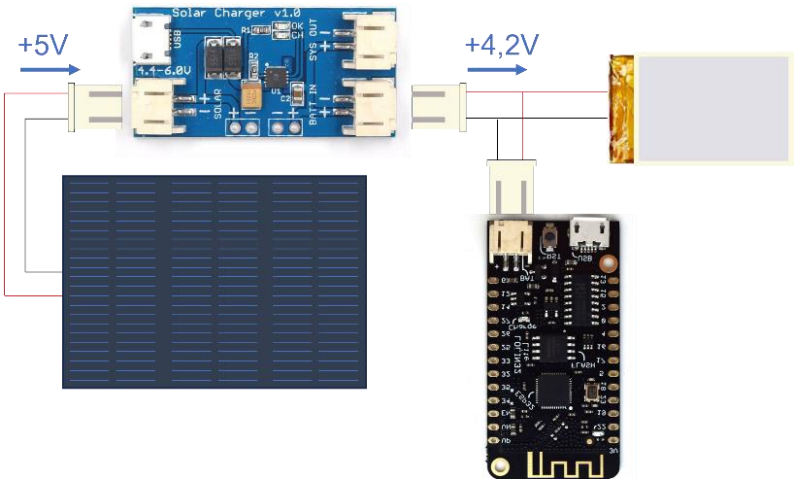

Figure 36: Solar charger circuit

5.6 Thermal control system

As per the thermal protection, the stratosphere represents a hostile environment for most electronic devices. Indeed, the majority of them cannot operate at very low temperatures such as $-55°C$, that characterise the layer of stratosphere located around $19 \div 21km$ above the sea level. Consequently, the need for a thermal protection must be analysed with the aim of identifying its appropriate design and manufacture. Additionally, the necessity of an integrated heater has to be investigated in order to keep the devices in their operative environment, while the demand of a temperature sensor to verify such situation has to be examined. These latter additional components must be properly chosen among the technologies available in the market, considering the requirements in terms of needed heating source and power supply, together with the availability of space where to place the components.

The thermal control system design process is indeed organised in the following steps: identification of thermal requirements and constraints; characterisation of thermal environment; definition of thermal challenges or problem areas; identification of applicable thermal control; determination of radiator and heater requirements; estimation of additional mass and power;

[39] Component SOT89-3 of the ME6211 series, which can tolerate input voltages in the range of 2V÷6V (High Speed LDO Regulators, High PSRR, Low noise, ME6211 Series, 2023).

documentation and iteration. Therefore, the activities to be carried out are: analysis of the system's configurations and of the mission's environment; design of suitable solutions to ensure that the equipment temperatures are within allowable ranges; verification to confirm, either by simulation and/or testing, the accuracy of the thermal analysis and of the temperatures prediction for the mission.

These activities have been performed for the two operating systems, the one in the balloon's nacelle and the one in the Wind Fish. More precisely, thermal simulations have been carried out to identify the heating power needed by each system and to choose the heater accordingly. With this aim, it has been necessary to devise two separated thermal models, taking into account the heat exchanges occurring within the two systems.

The conceived models have been implemented to run the thermal simulations, which have been executed with the software TN Solver[40]. For this purpose, it is necessary to describe the thermal models in text input files. Analogously, the simulation results are returned not only by the function but also in text output files for post-processing.

Two different concepts have been adopted for the temperature control within the systems in the nacelle and in the Wind Fish, even though in both cases isolating boxes in polystyrene material have been designed and manufactured.

The conducted analysis and the implemented principles are described in detail in the following Sections, while a general introduction to temperature control systems is provided below.

5.6.1 Thermal analysis

A stratospheric balloon interacts with the space environment through heat exchanges, namely, the flow of thermal energy caused by temperature differences, and the consequent temperature distribution and change. Heat exchanges occur in the forms of conduction, convection and radiation.

Conduction is caused by the collision between adjacent atoms or molecules, predominantly in a solid or liquid substance; it takes place inside individual bodies and between two bodies that are in contact.

[40] TN Solver is an open-source thermal network solver, written using Octave (the open-source implementation of MATLAB). It is available at (TNSolver - A Thermal Network Solver, 2023). The software has been developed by Washington University to conduct thermal computation at a pressure of $1013.25 hPa$; and it has been modified by Sergio Sosa-Sesma to adapt it to the balloon's operating environment (with a characteristic pressure of $4000 Pa$).

Convection occurs among a fluid (liquid or gas) and a solid interface. This type of heat transfer is caused by the movement of the fluid: it not only depends on the temperature difference between solid and fluid, but also on the flow's speed (the faster the flow, the higher the heat exchange).
Finally, radiation is the phenomenon of energy transmission from one body to another that occurs through electromagnetic waves; therefore, it does not require the presence of a mean of propagation. All bodies constantly emit energy via electromagnetic radiation, which intensity depends on numerous properties of the body (What is Heat Transfer?, 2023).

The objective of thermal analysis is to solve the general heat-transfer equation, which describes these thermal exchanges (T. L. Bergman, 2011):

$$Q_{out}[W] = Q_{solar_{direct}} + Q_{solar_{albedo}} + Q_{planet_{IR}} + Q_{int}$$

From the above formula, it is evident that the overall thermal control is usually achieved by balancing the heat emitted as Infrared Radiation (heat rejected by the system) against the heat dissipated by its internal components (heat generated internally) plus the heat absorbed from the environment.
Q_{out} depends on the system's surface exposed to space, and on its equilibrium temperature.
$Q_{solar_{direct}}$ is a function of the system's surface perpendicular to the sun vector, the solar irradiance and the distance from the Sun. Sunlight is the major source of environmental heating.
$Q_{solar_{albedo}}$ depends on the system's projected area to the planet, the solar albedo[41] of the planet and the visibility factor[42]. As any other object, the Earth is responsible for albedo phenomenon, because of which about 34% of energy hitting the Earth from the Sun is then diffused towards free space.
$Q_{planet_{IR}}$ is function of the planet's emission, which depends on the planet's local surface temperature, and of the view factor, that measures the fraction of radiation emitted from a surface and intercepted by another one. All the incident sunlight that is not reflected as albedo is absorbed by the planet and eventually re-emitted as IR (Infrared Radiation) energy or blackbody radiation.

[41] The albedo of an object is the extent to which it reflects light, defined as the fraction of incident sunlight on a planet reflected back to space. Planet's albedo depends on the planet's surface reflectivity characteristics, the view factor, and the system's orientation.
[42] The visibility factor is the fraction of albedo intercepted by the system, depending on its altitude, its attitude and view factor body-planet.

Q_{int} is the heat generated internally by the system. This is caused by several factors: the electronic equipment dissipates heat by Joule effect; power systems generate thermal dissipation, mainly due to chemical reactions (batteries); and thermal provisions (heaters or equivalent heating generators), which represent the power needed to maintain the equipment temperature requirements.

The general thermal analysis process requires firstly the definition of a geometric math model, which can be identified once the 3D design of the system has been conceived and thus can be used to define surfaces, mechanical properties, optical and thermal properties of the materials (as conductivity and specific heat), nodal distribution, radiation couplings (view factors).
Afterwards, a thermal math model has to be devised in order to define the nodes' characteristics, heat sources, conduction couplings, and solver control variables. Generally, the nodes are assumed to be isothermal, and physical properties are hypothesised to be constant within a node. Finally, it is necessary to conduct an environmental analysis to determine the heat exchange that occurs with the environment.

For the project under discussion, the heat exchanges have been evaluated for each system and modelled introducing simplifying hypotheses. Two worst-case conditions of equilibrium have been considered for the steady-state analysis: cold situation, when it is night and the system dissipates the minimum power; and hot case, when the system is in sunlight and the maximum power is being dissipated. Additionally, a transient analysis has been conducted to visualise the temperature oscillations taking into account the thermal inertia of the system's components.

5.6.2 Fisher thermal analysis

Temperature control system

As per the Wind Fish, it has been decided to use an additional device capable of measuring the temperature of the system. Additionally, a subsystem has been implemented in order to turn on/off a heater depending on the value collected by the temperature's sensor. Such system has been built in the form of an internal circuit with a MOSFET[43] that is open/closed as needed.

[43] A MOSFET is a unique type of transistor that is voltage controlled. It presents three terminals, named "gate", "drain" and "source": by applying voltage to the gate, an electrical field is created, which controls the current flow through the channel between the drain and the source.

For the specific application described here, a N-channel Enhancement-mode MOSFET has been used; more precisely, the utilised component is a standard IRFZ24N. A representative picture of its logic principle is illustrated in Figure 37.

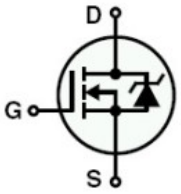

Figure 37: N-channel MOSFET (How to Use the MOSFET, 2023)

This component can operate as a switch: if the voltage difference between the gate and the source is null, then no current flows from the drain to the source; whereas if the voltage applied between the gate and the source is higher than the threshold value, then current can flow from the drain to the source.

For the described project's implementation, the MOSFET circuit has been built with the following logic: the electronic board reads the temperature measured by a dedicated sensor; in case this value is within the operating range of the system (which has been established above $-20°C$)[44], no action is taken; whereas if the collected temperature is lower than the acceptable minimum, the board provides an output voltage to the pin connected to the MOSFET's gate. In this latter case, since the source is connected to the common ground (GND), the voltage difference between the gate and the source is enough (the used MOSFET requires at least $3V$) to close the drain-source circuit, which means that current can flow through it. The drain is connected to the load, which in this case is represented by the heater - powered by separated batteries - so that it is turned on when needed.

A schematic of the circuit is represented in Figure 38. The resistors between the ESP32 signal and the gate are needed to reduce the gate-source voltage to $0V$ when the input signal is open-circuited.

[44] The majority of electronic components used in the project has an operating temperature range of $-40°C \div 85°C$; however, it is commonly chosen to fall within a narrower range of temperatures, in order to ensure conservative analyses of the proper functioning of the system - also taking into account the presence of lithium-ion batteries, whose charging and discharging cycles shall not occur below $0°C$.

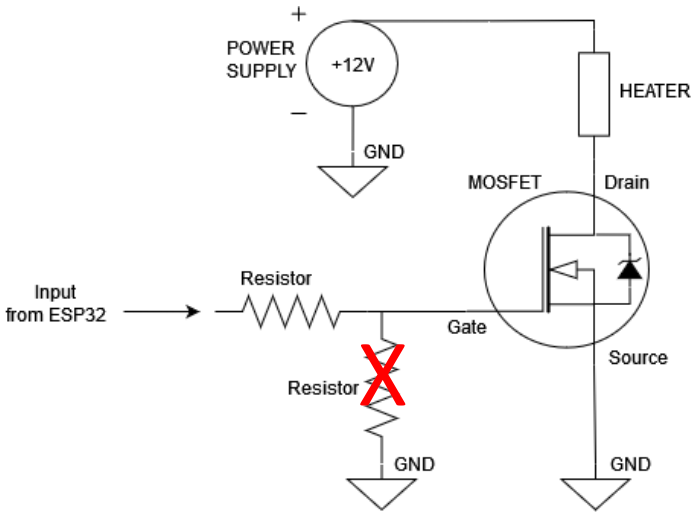

Figure 38: MOSFET circuit[45]

It is important to mention that, since the board goes to sleep periodically, the circuit for the temperature control must be linked to a GPIO (General Purpose Input Output) pin. More precisely, it is necessary to set the pin's output to be kept the same during the board's sleeping time (there exists a hold functionality that can be called to maintain the state during deep sleep).

Regarding the temperature sensor, several options have been explored and tested. Initially, the device evaluated have been a PT100 resistor and a DHT11. As concerns the PT100, this component is a platinum resistance thermometer (thermocouple) which enables simple, precise, and linear temperature measurement capabilities (What is a PT100 Resistor, 2023).
Despite the components' advantages, it was decided not to make use of it due to its considerable space occupation. Additionally, the best way to read data from such sensor is to integrate a digital chip, which was not available - it is however possible to bypass this inconvenience by directly reading the sensor output with ADC pins on the ESP32 board. Anyway, to obtain a very fine precision from the sensor it is necessary to use an amplifier capable of reading the low resistance values (Adafruit PT100 RTD Temperature Sensor Amplifier, 2023).

As for the DHT11, it consists of a humidity sensing component, a NTC (Negative Temperature Coefficient) temperature sensor (or a thermistor - a variable resistor that changes its resistance with temperature's variations) and an IC (Integrated Chip) on the back side of the sensor. It is therefore capable of measuring not only the environmental temperature, but also its relative humidity.

[45] The meaning of the red "X" in the Figure is explained in Section 5.4.1 of the present report.

Some tests have been conducted in order to verify the device's precision and reliability. The main outcome has been that the DHT11 can work only in a range of temperatures among $0°C$ and $50°C$ (DHT11 Humidity & Temperature Sensor, 2023). Since this range does not correspond to the system's operating environment, it was necessary to identify a way to devise this conflict. Two possibilities have been individuated. The first is based on the logic programming of the electronic board[46]. Since the DHT11 does not work below $0°C$, it is necessary that when the board wakes up for the first time during the mission, the temperature is above this threshold, otherwise it will provide no temperature data. Then, the board goes to sleep periodically and takes temperature's measures accordingly. Reasonably, the radiative fluxes (solar flux, albedo, etc.) decrease gradually while the day is ending. Implementing accurate models about the day-night cycle for these quantities, it is possible to identify the temperature cycle to which the electronics is exposed to, and more specifically at which temperature the heater must be turned on. It is fundamental to ensure that such temperature is above $0°C$, otherwise the DHT11 is not capable of measuring it.
The same reasoning would apply for the transition to the day-case: when the temperature reaches a certain value, the board understands that the day is starting and there is no more need for the heater to be on. Again, there is the need for a system that ensures that the temperature is always in the DHT11's operating range; also, the day-case and the night-case must be well separated to distinguish their characteristic ranges of temperature.

The second approach is the one that has been adopted in the actual project, and it lies in the use of a different temperature sensor, characterised by a wider operating range of temperatures.
The sensor BMP280 from Bosch has been integrated within the system. Indeed, the device can operate among $-40°C$ and $+85°C$. The component is shown in Figure 39.

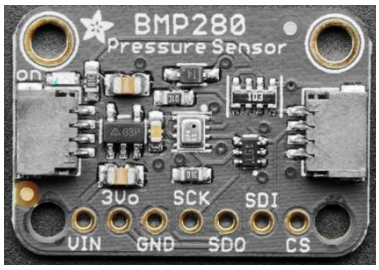

Figure 39: BMP280 (Adafruit BMP280 Barometric Pressure + Temperature Sensor Breakout, 2023)

[46] It is assumed that before the balloon's launch all the electronics is set to sleep for some hours to cover the launch and ascending phases.

This sensor can work with both I^2C and SPI communication, but it has been chosen to adopt the I^2C protocol to reduce the number of necessary wirings. Since the involved pins are the same as for the IMU, it has been necessary to verify that no interference occurred among the devices; the outcome of such tests was positive. To read the sensor's data, it is fundamental to install the Adafruit_BMP280 Library.

It is meaningful to underline that a further possibility could seem to measure the temperature with the electronic components already under use. Indeed, it is known that the ESP32 board has an internal temperature sensor which produces a voltage proportional to temperature and is then converted to digital form by an internal analogue-to-digital converter (though its reading was all the time 128, which according to (ESP32 Internal Temperature Sensor, 2023) corresponds to the sensor's absence - or else it indicates a measure of around $53°C$ which cannot be a meaningful value for the outside temperature), as well as the device used as IMU. However, some experiments have pointed out that for both components the built-in temperature sensor is not intended as an environmental sensor, whereas it can only monitor the chip's internal temperature. Indeed, the performed tests have shown that the digital reading is not representative of the external temperature.

Thermal model

At first, it was necessary to design a thermal model of the system to simulate the worst cold and hot conditions in a steady state. The present Section is focused on the description of the model that has been conceived for the Fisher, schematised in Figure 40.

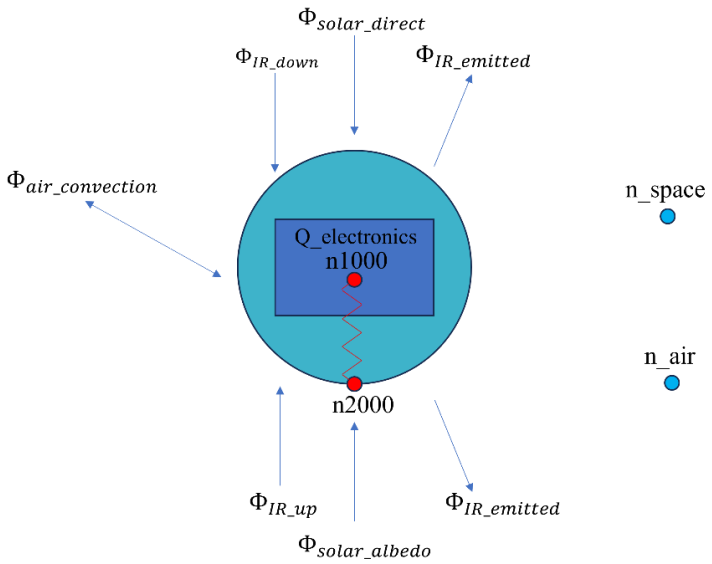

Figure 40: Fisher thermal model

As shown in the above picture, the system is modelled in nodes. More precisely, the electronics is represented by node $n1000$, while the thermal protection is imagined to be a polystyrene sphere which is here represented by node $n2000$. Finally, n_{air} and n_{space} are used to represent the stratospheric environment and free space respectively.

As shown, the electronics box (represented as a blue rectangle in Figure 40) is a source of heat due to power dissipation, $Q_{electronics}$. The other thermal exchanges are represented by:

- the conductive coupling between the electronics $n1000$ and the external sphere $n2000$. This exchange is modelled in TN Solver as a spherical conduction, taking into account the material present among the two nodes, the internal[47] and the external radius.
- the convective exchange between the protective sphere and the external air, flux $\Phi_{air_{convection}}$. Such transfer is simplified as a spherical natural external convection, considering the fluid involved and the sphere's outer diameter.
- the radiation with the external environment, which is constituted by the radiative flux emitted by the system towards the space $\Phi_{IR_{emitted}}$, the direct solar flux $\Phi_{solar_{direct}}$, the albedo flux from the Earth $\Phi_{solar_{albedo}}$, the ascending infrared flux $\Phi_{IR_{up}}$, and the descending one $\Phi_{IR_{down}}$.

  The exposed area considered for the radiation from the Sun and the Albedo is the frontal area (i.e., the surface orthogonal to the incident radiation vector). Whereas the area considered for the radiation towards the sky is the exposed area, for which it has been assumed that half of the sphere's surface emits towards free space n_{space}, and the other half towards the air n_{air} since the system operates in the stratosphere - thus it is not completely exposed to space.

Moreover, a fundamental hypothesis is made in order to simplify the model: the radiative exchange between the electronics and the external protection is considered negligible.

The model has been built in a text file indicating the listed exchanges as different types of conductors (conduction, convection and radiation) and as heat sources. Moreover, the following conditions have been set as reported in the following Table:[48]

[47] Since the coupling is not exactly spherical, the internal radius has been calculated as the average between the minimum and the maximum values.

[48] The indicated values for the boundary conditions and the environmental IR fluxes have been taken from the thermal analysis referenced in (Sesma, 2022) conducted for the BALMAN system.

Table 2: Thermal boundary conditions

	n_{air} temperature	n_{space} temperature	$\Phi_{solar_{direct}}$ flux	$\Phi_{solar_{albedo}}$ flux	$\Phi_{IR_{up}}$ flux	$\Phi_{IR_{down}}$ flux
Night case	$-78.15\ °C$	$-273.15\ °C$	$0\frac{W}{m^2}$	$0\frac{W}{m^2}$	$100\frac{W}{m^2}$	$10\frac{W}{m^2}$
Day case	$-46.15\ °C$	$-273.15\ °C$	$1388\frac{W}{m^2}$	$87\frac{W}{m^2}$	$418\frac{W}{m^2}$	$25\frac{W}{m^2}$

Furthermore, the material properties of polystyrene have been specified as an add on to the material library: in particular, its density ($30\frac{kg}{m^3}$), conductivity ($0.037\frac{W}{m\ K}$) and specific heat capacity ($1380\frac{J}{kg\ K}$) have been indicated. As for the material's emissivity[49], it is assumed that the upper side of the polystyrene sphere is coated with white paint ($\varepsilon = 0.85$), whereas the lower side is coated in black colour ($\varepsilon = 0.90$).

Finally, regarding the worst cold case, it has been considered that the internal power dissipation is about $0.3W$, which corresponds to the system's deep sleep mode; whereas in the hottest condition (monitored in order to verify that there is no risk of overheating), the electronics is assumed to be fully operational and to generate $1.5W$.[50]

The conducted simulations have proven that a heater of 3W is sufficient to maintain the system at an acceptable temperature: indeed, the internal temperature (of node $n1000$) in the worst cold case increases from $-68.02°C$ to $-19.41°C$ by adding the heating source. Whereas for the day case, the internal temperature has resulted to be $+16.29°C$.

As concerns the transient analysis, it is necessary to consider the thermal inertia of the system's components. To do so, the system nodes' characteristics must be specified in terms of specific heat, density and volume. The node $n2000$ is defined by its volume (considering that the protection is not simply a spherical shell, whereas the inside is filled with polystyrene that surrounds the electronics), and the material properties. For node $n1000$ it was instead necessary to determine the characterising quantities: these values have been determined as weighted values considering both the batteries' properties and the electronics ones. More precisely, the

[49] Emissivity represents the ratio of energy emitted by a substance to that emitted by a perfect radiator or by a black body at the same temperature. It is a dimensionless quantity, in the range $[0 \div 1]$.

[50] These values have been determined considering each component's power consumption. Their detailed computation falls out of the scope of the present paper and is reported in auxiliary documents.

nodes' volume and density have been determined taking into account the approximative 3D model designed for the system, reported in Figure 44 of Section 5.7.
The specific heat has been determined as follows:

$$global\_specific\_heat\ \left[\frac{J}{kgK}\right] =$$

$$= \frac{(batteries\_specific\_heat * batteries\_weight + electronics\_specific\_heat * electronics\_weight)}{(batteries\_weight + electronics\_weigth)}$$

It is important to point out that the batteries' specific heat capacity has been taken from the reference sources (Zhang, 2014) and (Taylor, 2023); whereas its density has been precisely determined from the component's datasheet (Primary Lithium Battery - LSH 20, 2023).
The weight of each component has been taken into account, as well as the approximative volume - determined taking into consideration the 3D CAD design shown in Figure 44 of Section 5.7.

The oscillations that characterise the environmental fluxes and the electronics' power dissipation have been modelled as time functions, which the solver accepts in the form of time tables (linear interpolation) or time splines. As regards the boundary conditions, the sky temperature is assumed to be always the same, whereas the air temperature is considered constant at the average value between day and night case. Concerning the electronics' dissipation, the mean value between the two worst cases is taken into account.
Focusing on the heater, its on/off cycle has been modelled with the function $tstatQ$, which operates as a heat source applied to a desired node only when the temperature of a specified node is below the programmed threshold value.

The outcomes of the transient analysis have shown that the internal temperature stays around $-5 \div -4°C$ for $n1000$ and $-35 \div -34°C$ for $n2000$ during the day/night cycle.

5.6.3 Nacelle thermal analysis

Temperature control system

In the case of the nacelle, the temperature control is achieved through a different strategy.
In this case, the thermal subsystem is planned to be completely autonomous from the main board: the independency is achieved thanks to the use of a patch temperature sensor that monitors the electronics' working environment. Such device is sensible to temperature's

changes and works as a switch: for the specific component under use, when the temperature is above $0°C$, the switch is open (no current is flowing); whereas when the temperature is below $-15°C$, the circuit closes. If directly connected to this device (and to an external power supply of $12V$), the heater can only be turned on when the temperature decreases below the threshold value.

The switch and heater devices are shown in Figure 41.

Figure 41: Heater (on the right) and thermal switch (on the left)

This choice has been made since the board is already continuously busy due to the interrupt function that constantly checks the encoder status, so it has been considered better to not overload it with an additional circuit for the temperature control.

Thermal model

Again, it was necessary to design a thermal model of the system to simulate the worst cold and hot conditions in a steady state.

The present Section focuses on the description of the conceived model, shown in Figure 42.

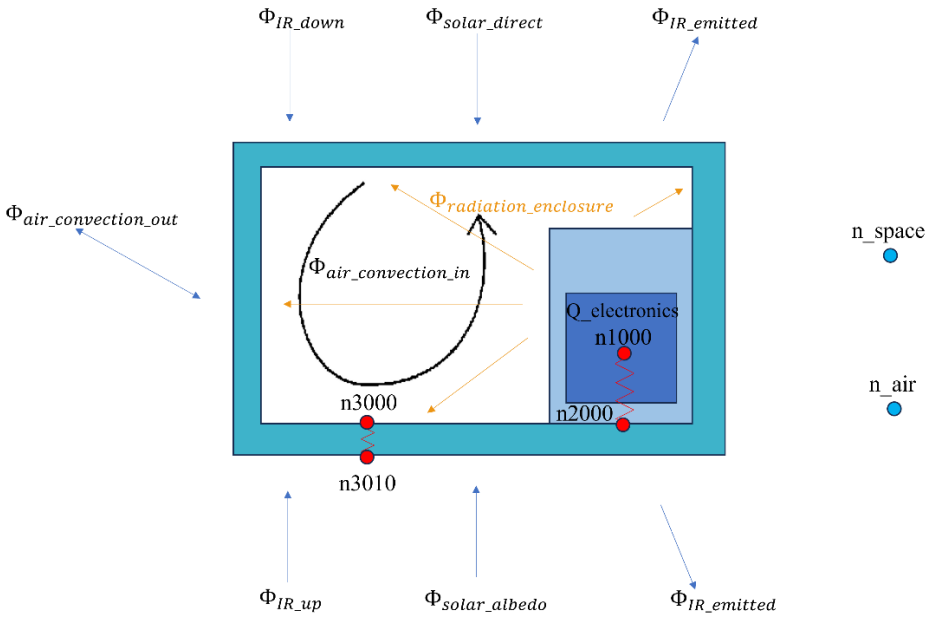

Figure 42: Nacelle thermal model

Evidently, even this system is modelled in nodes: the electronics is represented by node $n1000$, while the thermal protection is imagined to be constituted of two polystyrene boxes which are here illustrated as node $n2000$ and $n3000$. Finally, n_{air} and n_{space} are used to represent the stratospheric environment and free space respectively.

As shown, the electronics box (represented as a dark blue rectangle in Figure 42) is a source of heat due to power dissipation, $Q_{electronics}$. The other thermal exchanges are represented by:

- the conductive coupling between the electronics $n1000$ and the inner box $n2000$. This exchange is modelled in TN Solver as a cartesian wall conduction, taking into account the material present among the two nodes, the coupling's thickness and the area of contact.
- the conductive coupling between the inner box $n2000$ and the outer case $n3010$. This exchange is modelled in TN Solver as the one just described.
- the convective exchange between the protective case $n3010$ and the external air n_{air}, flux $\Phi_{air_{convection_{out}}}$. Such transfer depends on the fluid involved and the box dimensions. It is simplified as the combination of multiple natural external convections: two horizontal plates representing the upside and downside surfaces, plus a vertical surface to simplify the lateral surface.
- the convective exchange among the two polystyrene boxes, flux $\Phi_{air_{convection_{in}}}$. This exchange is a natural internal convection that is modelled as vertical rectangular enclosure.

More precisely, two convective cells $A1$ and $A2$ are taken into account, as shown in the picture below.

The same outcomes are achieved in case only one vertical enclosure is taken into account and the dimensions are set as the average of the real ones, as observed during some verification tests.

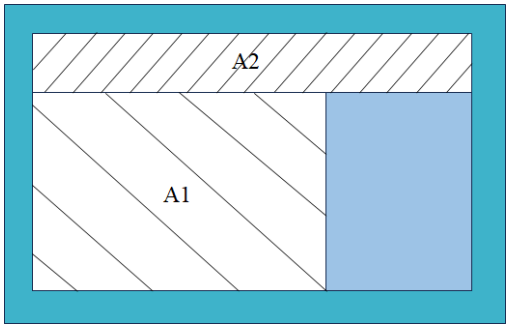

Figure 43: Natural internal convection schematisation

- the radiation with the external environment, which is constituted by the radiative flux emitted by the system towards the space $\Phi_{IR_{emitted}}$, the direct solar flux $\Phi_{solar_{direct}}$, the albedo flux from the Earth $\Phi_{solar_{albedo}}$, the ascending infrared flux $\Phi_{IR_{up}}$, and the descending one $\Phi_{IR_{down}}$. In analogy with the simplification adopted for the Fisher, it has been assumed that only the upside face of the box emits towards free space n_{space}: since the system operates in the stratosphere, it is not completely exposed to space; additionally, considering that the presented system will be surrounded by other elements present in the nacelle, this approximation is assumed acceptable.
- the radiation between the inner polystyrene box and the outer case. This exchange is modelled as a radiation enclosure, to define which it has been crucial to determine the view factor among the interested surfaces. Indeed, it is assumed that the radiative heat exchange between two surfaces is determined by the view factor, which depends on surface properties and enclosure geometry (McAdams, 1954). The view factor between two surfaces i and j is generally defined by the formula (J. H. Lienhard IV, 2016): $F_{ij} = \frac{1}{A_j}\int\int \frac{cos\theta_i cos\theta_j}{\pi r^2} dA_i dA_j$.

  For the specific case described here, only two surfaces have been considered: one surface which is representative of all the outer case inside faces, here referenced as A_{3000}; and one surface that is illustrative of the outside faces of the inner box, A_{2000}. Therefore, four view factors were determined $F_{3000-3000}$, $F_{3000-2000}$, $F_{2000-2000}$ and $F_{2000-3000}$. To do so, it was necessary to consider the summation and reciprocity principles: the first concept states that

the sum of all the view factors related to a surface is one, $\sum_{j=1}^{n} F_{ij} = 1$; the second one affirms that $A_i F_{ij} = A_j F_{ji}$. Observing that the inner box faces do not radiate towards each other, it is quite intuitive to notice that $F_{2000-2000} = 0$, and for the summability principle $F_{2000-3000}$ must be equal to 1. Given that the surfaces A_{2000} and A_{3000} are known from the 3D mechanical design of the nacelle's system (see Figure 45 in Section 5.7), it was possible to determine $F_{3000-3000}$ and $F_{3000-2000}$.

The basic principles and hypotheses are the same taken into consideration for the Fisher model, described in the previous Section. Again, the radiative exchange among the electronics and the inner polystyrene box is not taken into account.
For the worst cold case, it has been considered that the internal power dissipation is about $0.5W$, which corresponds to the system's deep sleep mode; whereas in the hottest condition the electronics is assumed to be fully operational and to generate $3W$.[51]

The conducted simulations have proven that a heater of 5W is sufficient to maintain the system at an acceptable temperature: indeed, adding the heating source the internal temperature in the worst cold case increases from $-66.98°C$ to $-20.66°C$ for $n1000$, and from $-69.76°C$ to $-27.74°C$ for $n2000$. Whereas for the day case, the internal temperature has resulted to be $+20.09°C$ for $n1000$ and $+16.23°C$ for $n2000$.

Finally, the transient analysis has shown that the temperature stays around $-10 \div -9°C$ for $n1000$. It has to be mentioned that the transient analysis is only capable of providing rough results, which must be compared with the outcomes of verification tests performed in a thermal chamber.

5.7 Mechanical design

The two subsystems have been mechanically designed, in order to have a general idea about their sizing and to complete the thermal protection's analysis. To this aim, it has been necessary to take into account each component's dimensions and also the number of required batteries.

The activity of designing has been performed through the software FreeCAD, which illustrations are reported in Figures 44 and 45, where the electronics assemblies are represented

[51] These values have been determined considering each component's power consumption. Their detailed computation falls out of the scope of the present paper and is reported in auxiliary documents.

in the form of rectangular grey boxes. From the pictures it is also possible to visualise the batteries, designed in the shape of orange cylinders. The heater is illustrated as a thin yellow parallelepiped, whereas other components are shown in different colours (the Li-Ion battery and the solar charger in the Wind Fish are represented in the shape of a green and a purple parallelepiped respectively, while the motor driver in the nacelle is shown as a small blue box).

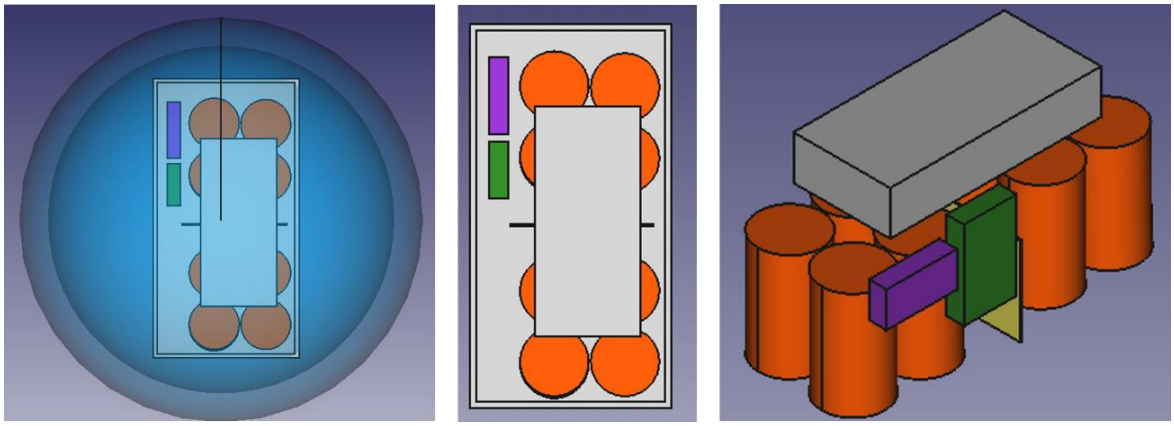

Figure 44: Wind Fish 3D CAD scheme

The thermal protections are illustrated as blue boxes. The Wind Fish is designed as a sphere of diameter $290mm$ with an average thickness of $72mm$; the external case of the nacelle is sized as $460mm \times 345mm \times 340mm$ with a thickness of $20mm$, and the internal box has a total volume of $330mm \times 130mm \times 170mm$ and a thickness of $10mm$. The two cases designed for the system in the nacelle have been manufactured by the CNES technician Remi Cousinet.

As it can be observed from Figures 44 and 45, the intent is to place the electronics assembly above the heater, which is planned to be located next to the batteries. In fact, since the specific heat of the cells is very high - which means their thermal inertia is big - they tend to keep the warmth for a long period of time once they have been heated.

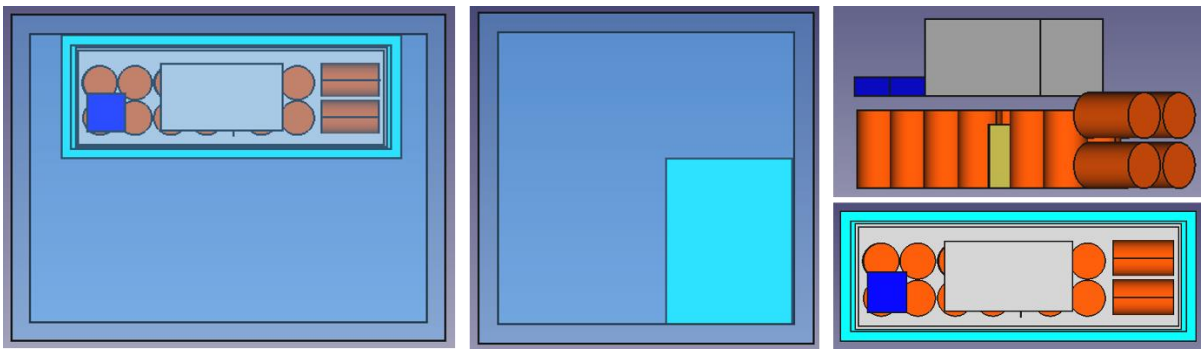

Figure 45: Nacelle 3D CAD scheme

6. Discussion

The present Chapter aims at providing a global review of the work that has been performed during the described End of Studies Project.

To do so, a critical viewpoint on the actual project's evolution and an analysis of the obtained results is given in Section 6.1. Later, Section 6.2 provides a description of the next steps to be followed to achieve the project's final goal.

6.1 Critical viewpoint

Regarding the project's actual evolution, it has been possible to achieve several of the programmed objectives, especially as regards the first phase described in Section 3.2.1 of the present paper.

From the computational point of view, two different algorithms for the wind's determination have been implemented and their results have been compared with data provided by a flight simulator, showing a satisfactory accuracy which is generally better in the wind direction rather than in its intensity, as deeply described in Section 4.2.3.
It is important to note that the initial intent was to perform all the computations at the software level within the electronic board in the balloon's nacelle. Therefore, it was required to translate the two algorithms implemented as MATLAB scripts into C/C++ libraries. Nevertheless, this was found not possible due to the algorithms' complexity, which is not supported by automatic converters. The solution to this problem has been identified in executing the two programs on ground with MATLAB. Although this might be considered not ideal, it can be agreed that the balloon trajectory must inevitably be controlled on the ground, which represents in any case a fundamental segment in the overall system. Consequently, even though it adds some complexity, running the calculation programs on the ground does not significantly modify the system's operationality, thus it does not constitute an unacceptable issue.

As regards the electronics assemblies, it was possible to develop two integrated and interference-free systems, comprehensive of all the required devices and able to record and send useful information.

Since the aim of the project is to develop prototypes, several tries have been attempted to properly connect the different devices. This activity has sometimes caused the permanent damage of certain components, due to the lack of already existing documentation and examples of application.
In order to avoid the same issue, it is recommended to verify the operating ranges of each device in terms of input and output currents before connecting them to other components, taking into account their datasheets, when available, and also making use of an electrical tester to check the real signals' intensity.

After the electronics verification on a breadboard, the corresponding PCBs have been designed and printed. The first versions have been printed with the company's drilling machine, with the aim of maintain low costs for their production; however, they have shown to be inoperative due to several problems, as mentioned in Section 5.4.1. The final version of the layouts has been ordered from a professional supplier and has been successfully tested. This shows that the best choice would have been to order the PCBs directly from an external provider, so as to avoid a waste of time and effort, and to prevent the further delay caused by delivery times.

Concerning the thermal control systems, the steady-state and transient simulations have been carried out for the two systems in the Wind Fish and in the gondola, showing that the use of common heaters active during the night should be sufficient to maintain the electronics assemblies in the operating range of temperature. The results obtained from the performed simulations are considered consistent with data from real missions and simulations of similar systems. Nevertheless, it must be mentioned that these are only approximate analyses, since the dimensions of the system have been defined on the basis of preliminary 3D CAD designs - the two systems have been mechanically designed to have a better visualisation of their sizes. More realistic and reliable simulations require the knowledge of the actual dimensions and physical characteristics of the ultimate system.
Even though the first prototype for the nacelle's assembly has been manufactured, the thermal simulation remains inaccurate since it does not take into account the complete assembly, which includes the reeling system and holes in the protective boxes to allow the cable's deployment.

6.2 Future perspectives

At the software level, the next step in the verification of the implemented algorithms would be their ground validation with real data provided by operative sensors - instead of the flight simulator. This would enable the realistic analysis and comparison of the methods' accuracy, as well as the possibility to integrate the reading of the GNSS module and of the IMU, and to observe if the results are improved consequently. Moreover, the in-flight validation of the two programs during test campaigns could complete the certification process before the actual application of the developed system.
Finally, a possible improvement could be to identify a strategy to enable the conversion of the codes into C/C++ language, eventually transferring the MATLAB script into Python.

At the hardware level, the purpose for the future is to perform a thorough environmental test campaign of the developed system. More precisely, the two prototypes must be subjected to structural and thermal tests. The validation must be planned within a thermal chamber, in order to verify that their temperature's oscillation is consistent with the one predicted by the simulations, as well as to examine whether the devised thermal control system is suitable for maintaining the operating temperature in the electronics' acceptable range (the correct functioning of the circuits that turn on the heaters must be verified).

The correlation between the predictions of the theoretical model and the results of the simulation will also enable the refinement of the mechanical designs (the one for the Wind Fish and the one for the balloon's nacelle), as well as the final sizing of the power supply system. Consequently, the following step in the project's development is the prototypes' manufacture. As for the system in the gondola, it is necessary to verify that the developed boxes are suitable for real application and that the electronics assembly works properly within the two thermal protections that have been already built.
As regards the system in the Fisher, the intent is to produce the protective box in the shape of a sphere, to ensure that the maximum drag is generated by the wind probe, as previously mentioned. Additionally, the purpose is to design and manufacture a rudder of the appropriate size in order to guarantee that the wind sensor orients itself according to the direction of the wind, as assumed by the implemented computations. These considerations make explicit the supplemental complexity of the Fisher's mechanical design, which therefore requires to perform some further activities and analyses. Specifically, it is required to implement the

system’s mass balance so as to ensure that it stays in equilibrium and is not subject to excessive structural stress or mechanical vibrations.
Furthermore, after the Wind Fish prototype is completed, it will be necessary to implement the definitive calibration of the Inertial Measurement Unit.

Finally, once the two systems are both manufactured, test campaigns performed both on ground and during flight will enable the ultimate validation of the system’s operability in the real working environment.

Conclusion

From the description and analysis carried out in the previous Chapters of this dissertation, it is possible to derive some final remarks.
Overall, the internship has achieved many of the objectives of the project within which it is contextualised. As already mentioned, it was possible to implement two calculation programs for the determination of the wind speed and intensity below a stratospheric balloon.
To do this, it was necessary to choose the most suitable components considering the requirements in terms of limiting costs, occupied space and additional weight, but also the compatibility between the working environment and the operational constraints of each component.

The chosen sensors were appropriately tested and programmed in order to provide relevant information for the wind's determination. In addition, two communication systems had to be implemented so as to enable the transmission of the measured data to the mission control centre - and thus allow the monitoring of the mission -, one between the Wind Fish and the gondola, and one between the gondola and the ground station. To this end, the operating logic schemes of the two subsystems had to be studied and programmed in detail, as well as the time intervals required to complete each activity.
The electronics integration's effectiveness has been successfully tested by verifying the proper functioning first of each component separately, and then of the complete assembly of devices.

Given that the stratosphere represents a hostile operating environment for the electronic components, a thermal control system based on the use of polystyrene boxes and heaters was envisaged. Moreover, thermal models of the two systems were devised and theoretical simulations were carried out to verify the correct operation under the worst-case conditions (extreme cold situation and extreme heat case). Although the results obtained are consistent with the actual operating environment and coherent to other simulations, the final validation of the thermal protection would require simulations performed within a thermal chamber, as well as the correlation of the experimental evidence with the predictions of the theoretical model.
Due to the limited availability of time and personnel in charge of these tests, it was not possible to proceed with the mentioned activities of verification.

In addition, during the internship period it was possible to develop only a preliminary mechanical design, this also because of the interdependence between thermal analysis and the actual physical sizing of the system.
The first example for the assembly in the gondola was built, whereas the probe has not been manufactured yet. This activity must be performed in the future, taking into account not only the thermal aspects, but also the need to devise a directing system according to the wind and consequently to ensure the mass balance of the system.

Once the first prototypes are completed, it will be essential to proceed with the validation tests both on the ground and in flight, not only to verify the effectiveness of the calculations implemented for the determination of the wind, but also to monitor the structural strength of the two assemblies.

Glossary (acronyms)

Abbreviation	Definition
ACHAB	Analysis Code for High Altitude Balloons
BALMAN	Ballon manœuvrable
CAD	Computer-Aided Design
CIRA	Centro Italiano Ricerche Aerospaziali
COTS	Commercial Off The Shelf
CNES	Centre National d'Études Spatiales
DARPA	Defense Advanced Research Projects Agency
DC	Direct Current
DoD	Depth of Discharge
DoF	Degrees of Freedom
GNSS	Global Navigation Satellite System
GPIO	General Purpose Input Output
GPS	Global Positioning System
HAPS	High-Altitude Platform Systems
IC	Integrated Chip
I^2C	Inter-Integrated Circuit
IDE	Integrated Development Environment
IMU	Inertial Measurement Unit
IR	Infrared Radiation
ISA	International Standard Atmosphere
LEO	Low Earth Orbit
Li-Ion	Lithium Ion
LIDAR	LIght Detection And Ranging
LoRa	Long Range Wide Area
MATLAB	MATrix LABoratory

MEMS	Micro Electro-Mechanical Systems
MOSFET	Metal Oxide Semiconductor Field Effect Transistor
NCEI	National Centres for Environmental Information
NGDC	National Geophysical Data Centre
NMEA	National Marine Electronics Association
NOAA	National Oceanic and Atmospheric Administration
NTC	Negative Temperature Coefficient
PCB	Printed Circuit Board
PID	Proportional Integral Derivative
RADAR	Radio Detecting And Ranging
RTC	Real Time Clock
SBAS	Satellite Based Augmentation System
SBD	Short Burst Data
SINBAD	Scientific Balloon Analysis Model
SMA	Sub Miniature version A
SoC	System on a Chip
SPI	Serial Peripheral Interface
Strat-OAWL	Stratospheric Optical Autocovariance Wind Lidar
ULP	Ultra Low Power
WMM	World Magnetic Model

Bibliography and Web references

38S6G5-B-G24N-Imprimante Incrémentale à Distance. (n.d.). Retrieved from AliExpress: https://fr.aliexpress.com/item/1005004359395872.html

5V 28BYJ-48 Stepper Motor + ULN2003 Driver Board. (2023, March). Retrieved from Cytron Marketplace: https://my.cytron.io/c-motor-and-motor-driver/p-5v-28byj-48-stepper-motor-plus-uln2003-driver-board

Adafruit BMP280 Barometric Pressure + Temperature Sensor Breakout. (2023, June). Retrieved from Adafruit Industries: https://learn.adafruit.com/adafruit-bmp280-barometric-pressure-plus-temperature-sensor-breakout

Adafruit PT100 RTD Temperature Sensor Amplifier. (2023, June). Retrieved from Adafruit: https://www.adafruit.com/product/3328

al., L. E. (2021). A reel-down instrument system for profile measurements of water vapor, temperature, clouds, and aerosol beneath constant-altitude scientific balloons. *Atmospheric Measurement Techniques*.

Andrea, P. (2023, June). *L'importanza dei driver motori*. Retrieved from EMC Elettronica: https://it.emcelettronica.com/limportanza-dei-driver-motori

Arc Length. (2023, May). Retrieved from LibreTexts Mathematics: https://math.libretexts.org/Bookshelves/Calculus/Map%3A_Calculus__Early_Transcendentals_(Stewart)/08%3A_Further_Applications_of_Integration/8.01%3A_Arc_Length

Arduino Pitot Tube Wind Speed and Airspeed Indicator - Theory and Experiments. (2023, March). Retrieved from MakerPortal: https://makersportal.com/blog/2019/02/06/arduino-pitot-tube-wind-speed-theory-and-experimenthttps://makersportal.com/blog/2019/02/06/arduino-pitot-tube-wind-speed-theory-and-experiment

ArduPilot - AP_Declination. (2023, March). Retrieved from GitHub: https://github.com/ArduPilot/ardupilot/blob/master/libraries/AP_Declination/AP_Declination.h

AZ-Delivery. (n.d.). Wemos ESP32 Lolin32 Board BOOK.

Bellavia S., M. M. (2002). *STRSCNE: A Scaled Trust-Region Solver for Constrained Nonlinear Equations.* Florence, Italy: Dipartimento di Energetica, University of Florence.

Benedetta Morini, M. P. (2010). *TRESNEI, a Matlab trust-region solver for systems.* Springer Science and Business Media.

BN-220 GPS Module + Antenna Datasheet. (2023, March). Retrieved from Beitian: https://www.beitian.com/en/

Catenary. (2023, May). Retrieved from Wikipedia, The Free Encyclopedia: https://en.wikipedia.org/w/index.php?title=Special:CiteThisPage&page=Catenary&id=1168330438&wpFormIdentifier=titleform

Christian Kanzow, N. Y. (2004). Levenberg-Marquardt methods with strong local convergence properties for solving nonlinear equations with convex constraints. *Journal of Computational and Applied Mathematics*, 375-397.

CN306518650 Li-Ion Mini Solar Charger Module. (2023, June). Retrieved from ThinkRobotica: https://thinkrobotics.com/products/cn3065-18650-li-ion-mini-solar-charger-board-module

Computing tilt measurement and tilt-compensated eCompass. (2023, March). Retrieved from STMicroelectronics: https://www.st.com/content/st_com/en.html

D., M. (1963). An Algorithm for Least-Squares Estimation of Nonlinear Parameters. *SIAM - Society for Industrial and Applied Mathematics*.

DARPA Tests Wind Sensor for Stratospheric Balloons. (2019). *DEFENSE TECHCONNECT - The Innovation Source for National Security*.

Department Balloons, C. (2022, January 13). *Intro-PDR_FV.*

DHT11 Humidity & Temperature Sensor. (2023, June). Retrieved from Mouser Electronics.

Difference Between I2C vs SPI. (2023, July). Retrieved from Prodigy Technovations: https://prodigytechno.com/i2c-vs-spi/

Differential GPS: What It Is and How to Use It Effectively. (2023, March). Retrieved from GISGeography: https://gisgeography.com/differential-gps/

Digital compass. (2023, April). Retrieved from Open source software and hardware avionics: https://avionicsduino.com/index.php/en/digital-compass/

E., K. (1996). *Understanging GPS: Principles and Applications.* Artech House.

Earth Atmospheric Model - Metric Units. (2023, May). Retrieved from National Aeronautics and Space Administration: https://www.grc.nasa.gov/www/k-12/airplane/atmosmet.html

ESP32 Internal Temperature Sensor. (2023, June). Retrieved from The engineering projects: https://www.theengineeringprojects.com/2022/01/esp32-internal-temperature-sensor.html

ESP32 Projects. (2023, April). Retrieved from The Engineering Projects: https://www.theengineeringprojects.com/2022/01/esp32-internal-temperature-sensor.html

ESP32 SPI Communication. (2023, March). Retrieved from Random Nerd Tutorials: https://randomnerdtutorials.com/esp32-spi-communication-arduino/

ESP32 with DC Motor and L298 Motor Driver - Control Speed and Direction. (2023, July). Retrieved from Random Nerd Tutorials: https://randomnerdtutorials.com/esp32-dc-motor-l298n-motor-driver-control-speed-direction/

H., N. (2012). Wind Energy. *Comprehensive Renewable Energy*.

Helical antenna. (2023, June). Retrieved from Wikipedia - The Free Encyclopedia: https://en.wikipedia.org/wiki/Helical_antenna

High Speed LDO Regulators, High PSRR, Low noise, ME6211 Series. (2023, June). Retrieved from MicrOne: http://www.microne.com.cn/

Holfmann-Wellenhof B., L. H. (1992). *Global Position System - Theory and Practice.* Springer - Verlag.

How GPS Receivers Work - Trilateration vs Triangulation. (2023, March). Retrieved from GISGeography: https://gisgeography.com/trilateration-triangulation-gps/

How to use cup anemometer. (n.d.). Retrieved from mrc Laboratory-Instruments: https://www.mrclab.com/how-to-use-cup-anemometer

How to Use the MOSFET. (2023, June). Retrieved from OscarLiang: https://oscarliang.com/how-to-use-mosfet-beginner-tutorial/

Huafei Du, J. L. (2019). Flight performance simulation and station-keepind endurance analysis for stratospheric super-pressure balloon in real wind field. *Aerospace Sciene and Technology*.

Improved magnetometer calibration. (2023, April). Retrieved from Sailboat Instruments: http://sailboatinstruments.blogspot.com/2011/09/improved-magnetometer-calibration-part.html

International Standard Atmosphere. (2023, May). Retrieved from Flight Mechanics for Pilots: https://agodemar.github.io/FlightMechanics4Pilots/mypages/international-standard-atmosphere/

Introduction to CN3065 Mini Solar Charger. (2023, June). Retrieved from The engineering knowledge: https://www.theengineeringknowledge.com/introduction-to-cn3065-mini-solar-charger/

Iridium Network. (2023, April). Retrieved from Iridium: https://www.iridium.com/

J. H. Lienhard IV, a. J. (2016). *A Heat Transfer Textbook.* Cambridge, Massachussetts.

K., L. (1944). A Method for the Solution of Certain Problems in Least Squares. *Quarterly of Applied Mathematics*.

L293D Motor Driver Module. (2023, July). Retrieved from FEC - Future Electronic Corporation: https://www.fec-electrotech.com/products/620c13ba6dcfe60016016550

(2009). *Le magazine d'information du centre national d'études spatiales .*

Lithium Ion Battery Charger for Solar-Powered Systems. (2023, June). Retrieved from Consonance: http://www.consonance-elec.com/

LoRa SX 1276/77/78/79. (2023, March). Retrieved from Semtech: https://www.semtech.com/

LSM9DS1 - iNEMO inertial module. (2023, March). Retrieved from STMicroelectronics: https://www.st.com/content/st_com/en.html

LSM9DS1 - iNEMO inertial module: 3D accelerometer, 3D gyroscope, 3D magnetometer. (2023, march). Retrieved from STMicroelectronics: https://www.st.com/content/st_com/en.html

Magnetic Field Calculators. (2023, March). Retrieved from NOAA - National Centers for Environmental Information: https://www.ngdc.noaa.gov/geomag/calculators/magcalc.shtml#declination

Maruca BA, M. R. (2017). Overview of and first observations from the TILDAS High-Altitude Balloon Mission. *Atmospheric Measurement Techniques*, 1595-1607.

McAdams, W. H. (1954). *Heat Transmission.* New York: McGraw-Hill.

Mini Solar Panel - model 11585. (2023, June). Retrieved from AZ-Delivery.

MS4525DO Measurement Specialties. (2023, March). Retrieved from Measurement Specialties - MEAS: https://www.te.com/usa-en/products/brands/meas.html?tab=pgp-story

Ozyagcilar, T. (2015). *Implementing a Tilt-Compensated eCompass using Accelerometer and Magnetometer Sensors.* Applications Engineer.

Pitot Tube Wind Speed and Airspeed Indicator - Theory and Experiments. (2023, March). Retrieved from Maker Portal: https://makersportal.com/blog/2019/02/06/arduino-pitot-tube-wind-speed-theory-and-experiment

Pixhawk PX4 Differential Airspeed Sensor Kit - Pitot Tube. (2023, March). Retrieved from Robotisan: https://www.robotistan.com/pixhawk-px4-differential-airspeed-sensor-kit-pitot-tube

Power Supply. (2023, April). Retrieved from RockBLOCK Guides: https://docs.rockblock.rock7.com/docs/power-supply

Pratap Misra P., E. P. (2006). *Global Positioning System: Signals, Measurements, and Performance.* Ganga-Jamuna Press.

Primary Lithium Battery - LSH 20. (2023, June). Retrieved from Saft batteries: https://www.saft.com/

Ra-01 Specification. (2019). Retrieved from Ai-Thinker.

RockBLOCK 9603 - Datasheet Small. (2023, March). Retrieved from Ground Control.

RockBLOCK 9603. (2023, April). Retrieved from Ground Control: https://www.groundcontrol.com/en/

Save energy on the ESP32 with Deep Sleep. (2023, April). Retrieved from uPesy: https://www.upesy.com/blogs/tutorials/how-to-use-deep-sleep-on-esp32-to-reduce-power-consumption#

Sesma, S. S. (2022). *ANALYSE THERMIQUE SIMPLIFIEE DES PIECES POLAIRES ENVELOPPE - BALMAN.*

T. L. Bergman, A. S. (2011). *Introducion Heat Transfer .* New York: John WIley & Sons.

Taylor, N. (2023, June). *Specific Heat Capacity of Lithium Ion Cells.* Retrieved from Battery Design: https://www.batterydesign.net/specific-heat-capacity-of-lithium-ion-cells/

Techical data - series E192. (2023, June). Retrieved from micromotors: https://www.micromotors.eu/

TNSolver - A Thermal Network Solver. (2023, June). Retrieved from Heat Transfer: http://www.heattransfer.org/ME331/

Tournie, G. (2023). *Journal d'essai préliminaire - Treuil Strato.* Toulouse.

Using The Logic Level Converter. (2023, April). Retrieved from sparkfun: https://learn.sparkfun.com/tutorials/retired---using-the-logic-level-converter

Valérian Jewtoukoff, R. P. (2016). On the Prediction of Stratospheric Balloon Trajectories: Improving Winds with Mesoscale Simulations. *The Bulletin of the American Meteorological Society (AMS)*, 16029-1647.

What is a PT100 Resistor. (2023, June). Retrieved from Allectra: https://www.allectra.com/news/what-pt100-resistor/

What is Heat Transfer? (2023, July). Retrieved from Simscale: https://www.simscale.com/docs/simwiki/heat-transfer-thermal-analysis/what-is-heat-transfer/

WMM Software and Coefficients. (2023, March). Retrieved from NOAA - National Centers for Environmental Information: https://www.ncei.noaa.gov/products/world-magnetic-model

Zhang, W. Z. (2014). Experimental study if the heat generations of Li/SOCl2 and Li/SO2 batteries using a phase-change measurement method. *Journal of Thermal Analysis and Calorimetry*. Retrieved from https://link.springer.com/article/10.1007/s10973-013-3603-4/tables/1

Appendix A

Comparison of the implemented algorithms

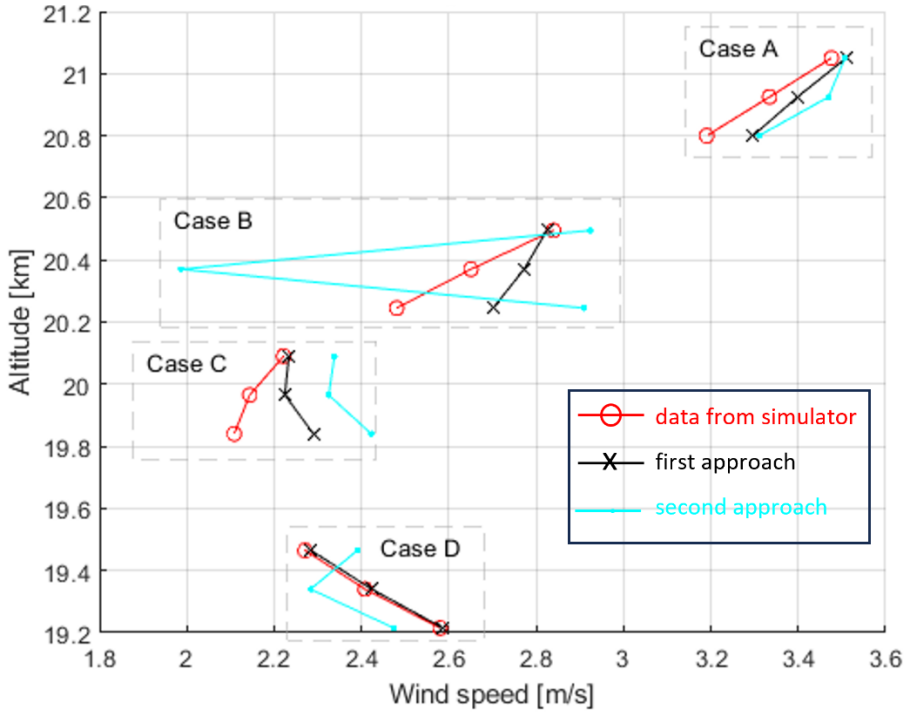

Figure 46: Comparison of wind speed for L=125m

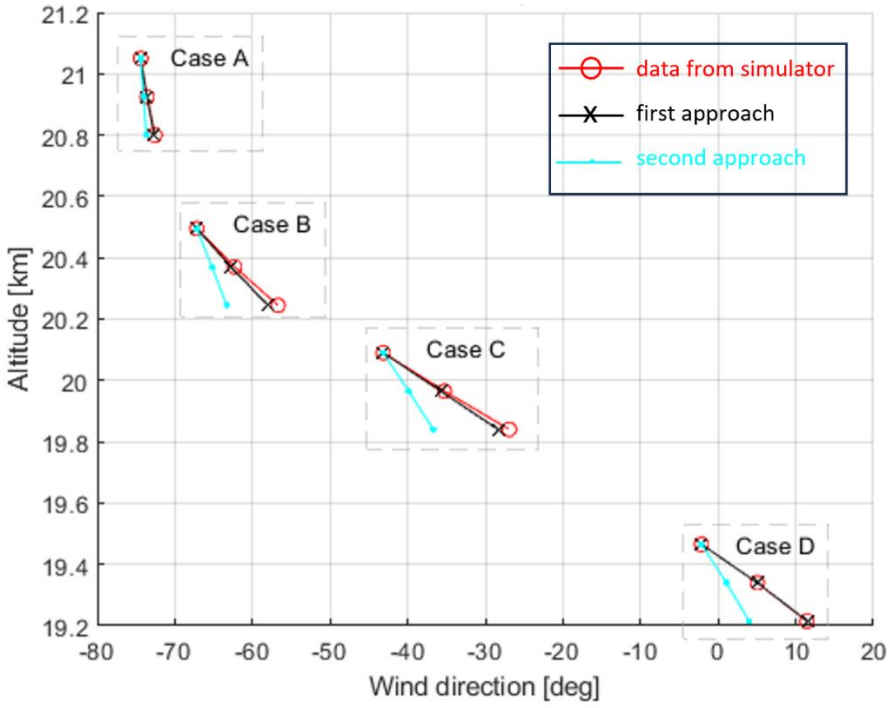

Figure 47: Comparison of wind direction for L=125m

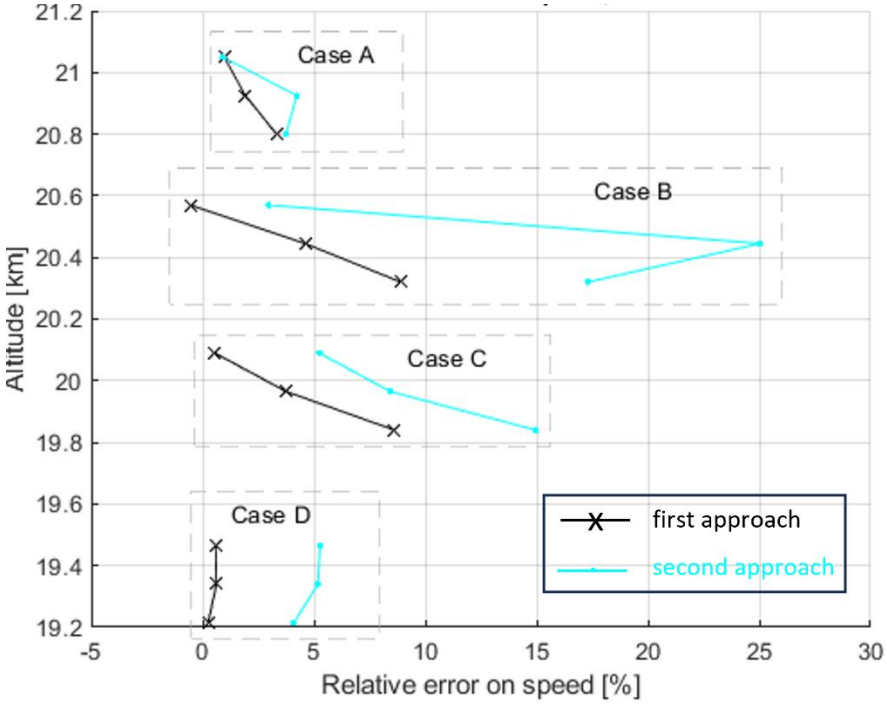

Figure 48: Comparison of relative errors on wind speed, L=125m

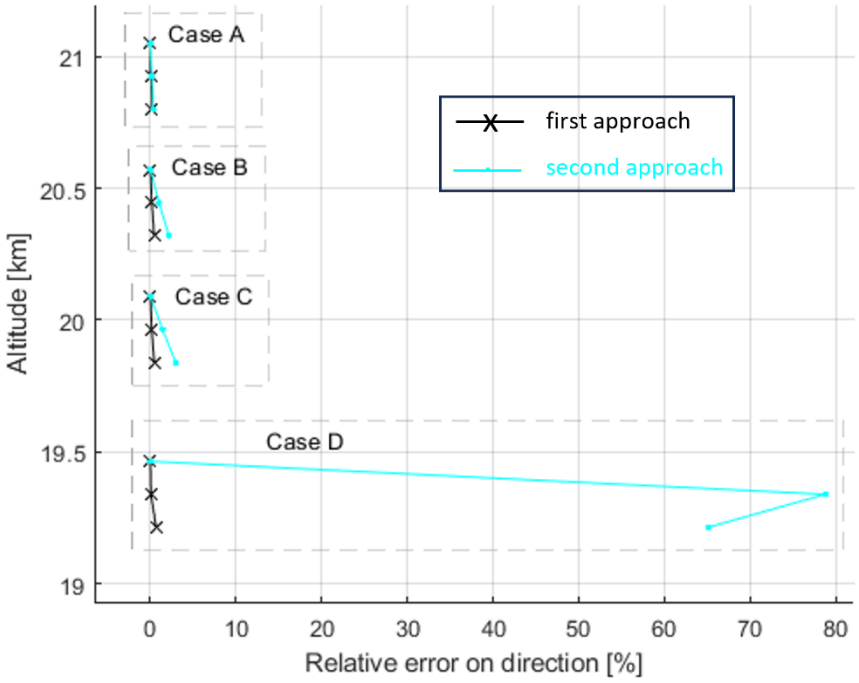

Figure 49: Comparison of relative errors on wind direction, L=125m

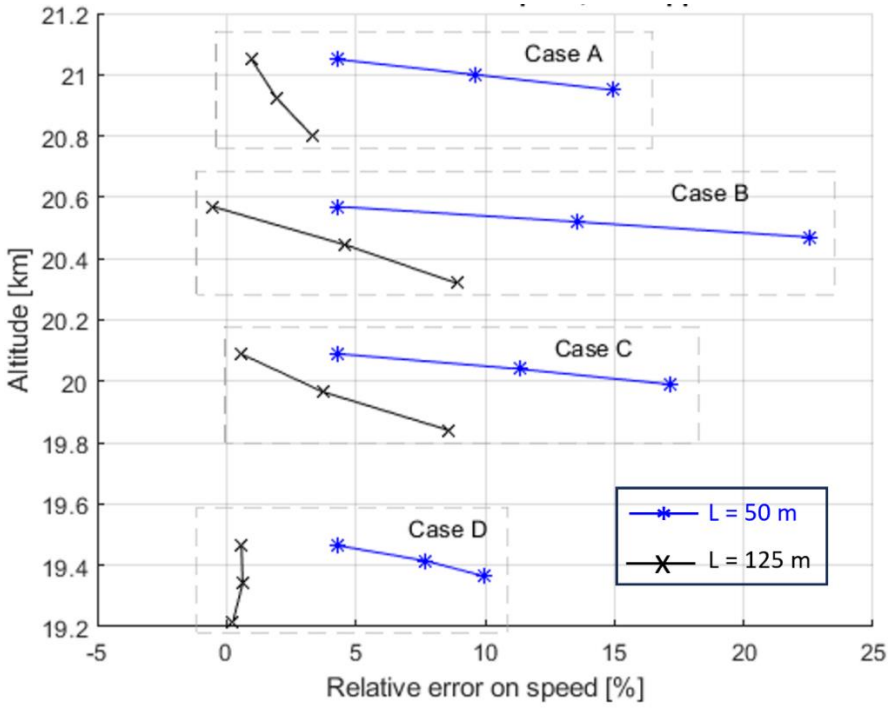

Figure 50: Comparison of relative errors on wind speed for different L, first approach

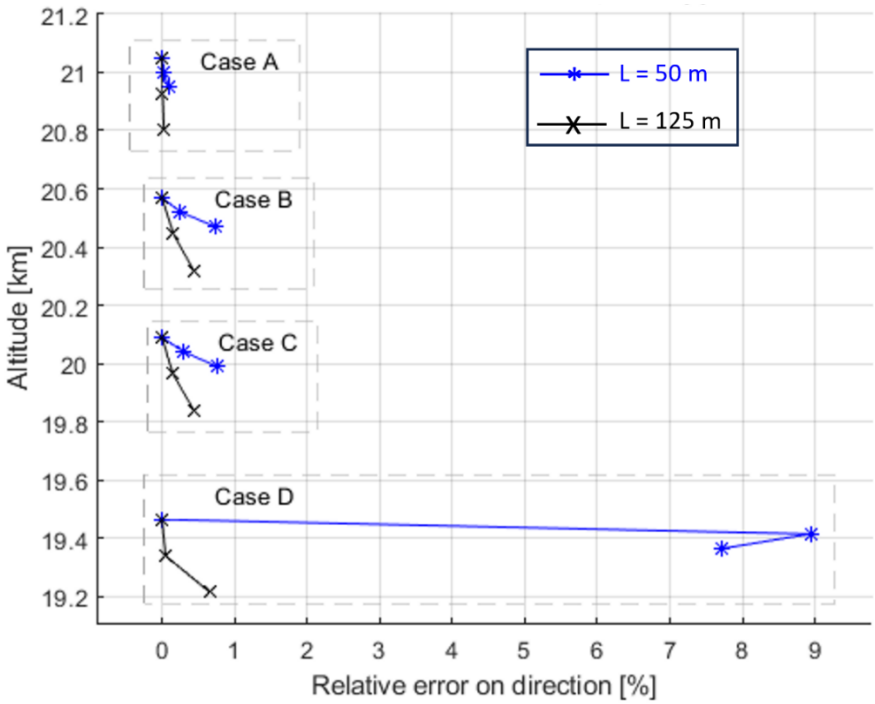

Figure 51: Comparison of relative errors on wind direction for different L, first approach

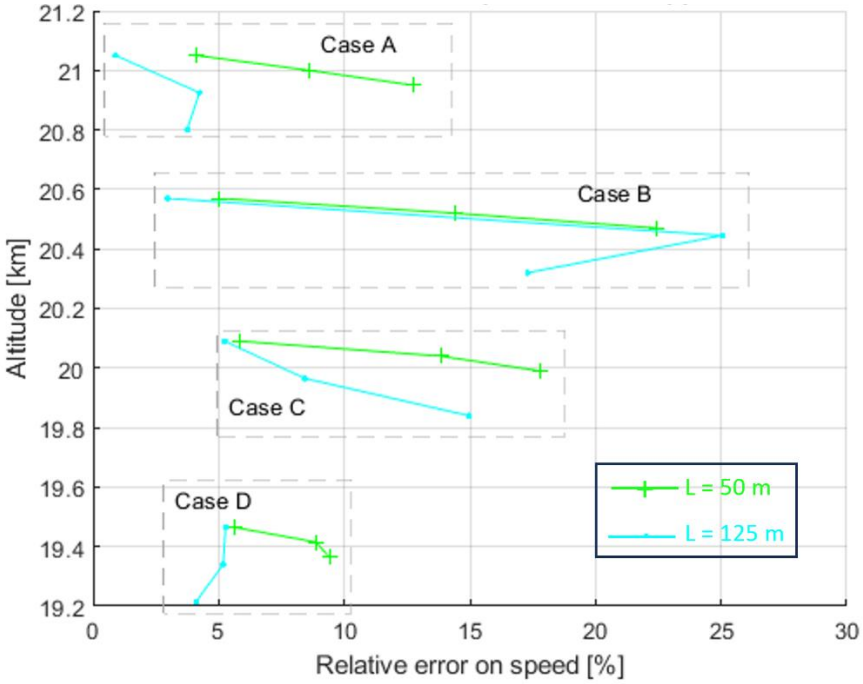

Figure 52: Comparison of relative errors on wind speed for different L, second approach

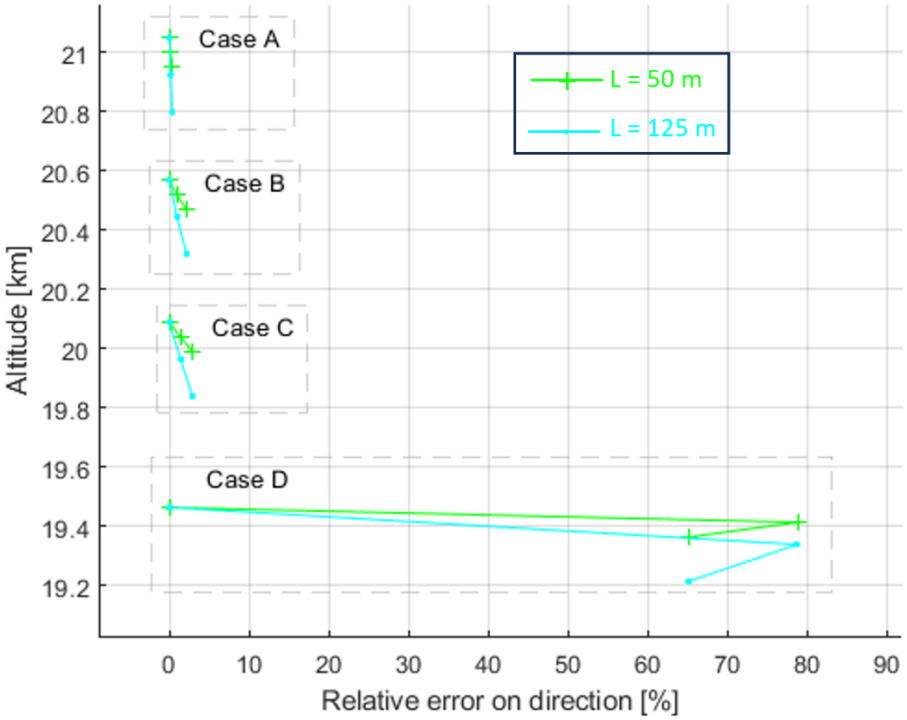

Figure 53: Comparison of relative errors on wind direction for different L, second approach

Appendix B

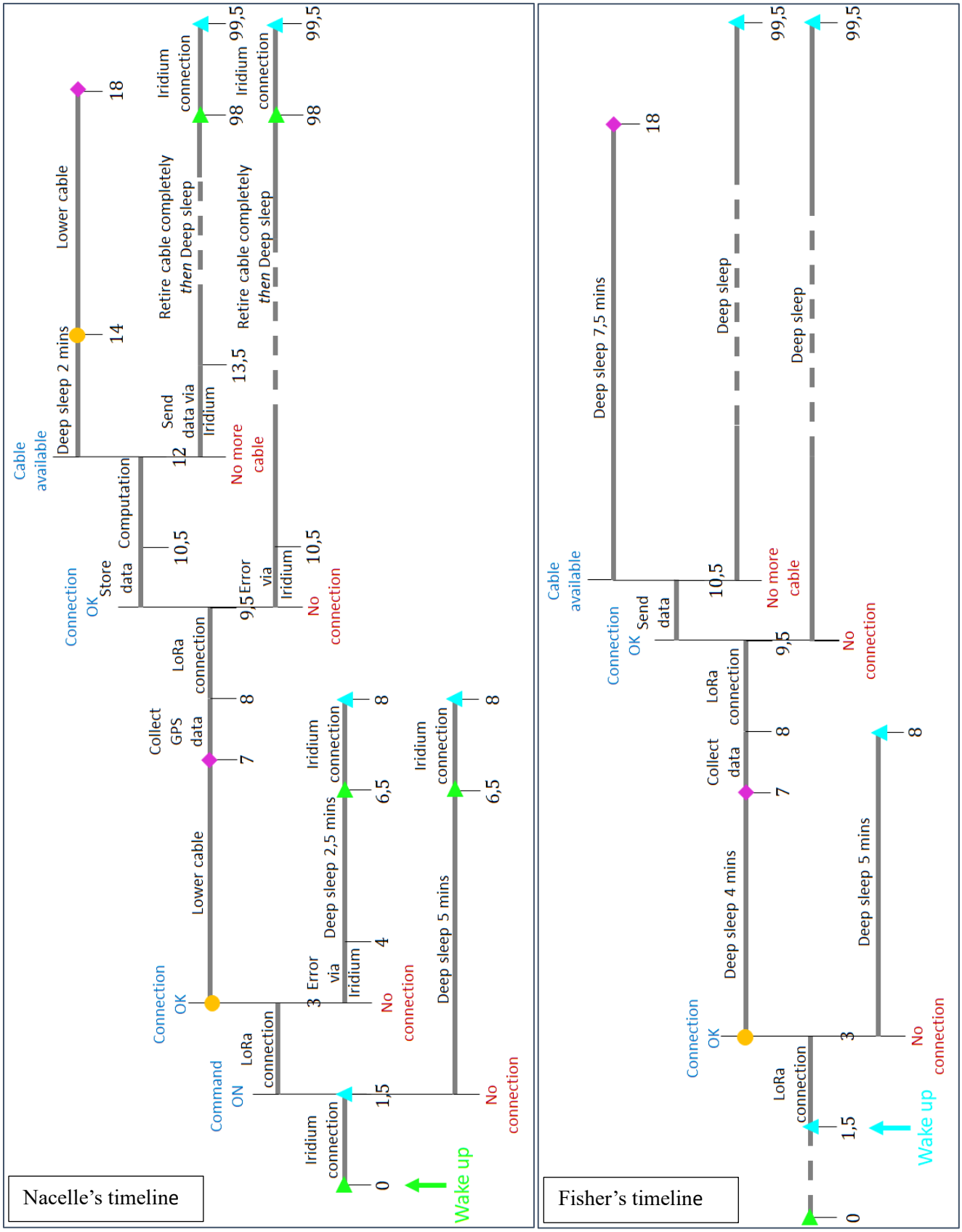
Nacelle's timeline
Wake up
Command ON
Iridium connection
0
LoRa connection
1,5
Connection OK
Lower cable
Collect GPS data
7
LoRa connection
8
Store data
Computation
10,5
Deep sleep 2 mins
Lower cable
14
18
Send data via Iridium
12
13,5
No more cable
Retire cable completely then Deep sleep
Iridium connection
98
Iridium
99,5
Cable available
Connection OK
Error via Iridium
3
No connection
Deep sleep 2,5 mins
Iridium connection
4
6,5
8
Deep sleep 5 mins
Iridium connection
6,5
8
Error via Iridium
9,5
No connection
10,5
Retire cable completely then Deep sleep
Iridium connection
98
Iridium
99,5
Fisher's timeline
Wake up
Deep sleep 7,5 mins
18
Deep sleep 4 mins
Deep sleep 5 mins
Deep sleep
Deep sleep
99,5
99,5
Cable available
Connection OK
Send data
10,5
No more cable
9,5
No connection
Collect data
7
LoRa connection
8
Connection OK
LoRa connection
1,5
0
3
No connection
8

Appendix C

PCBs schematics

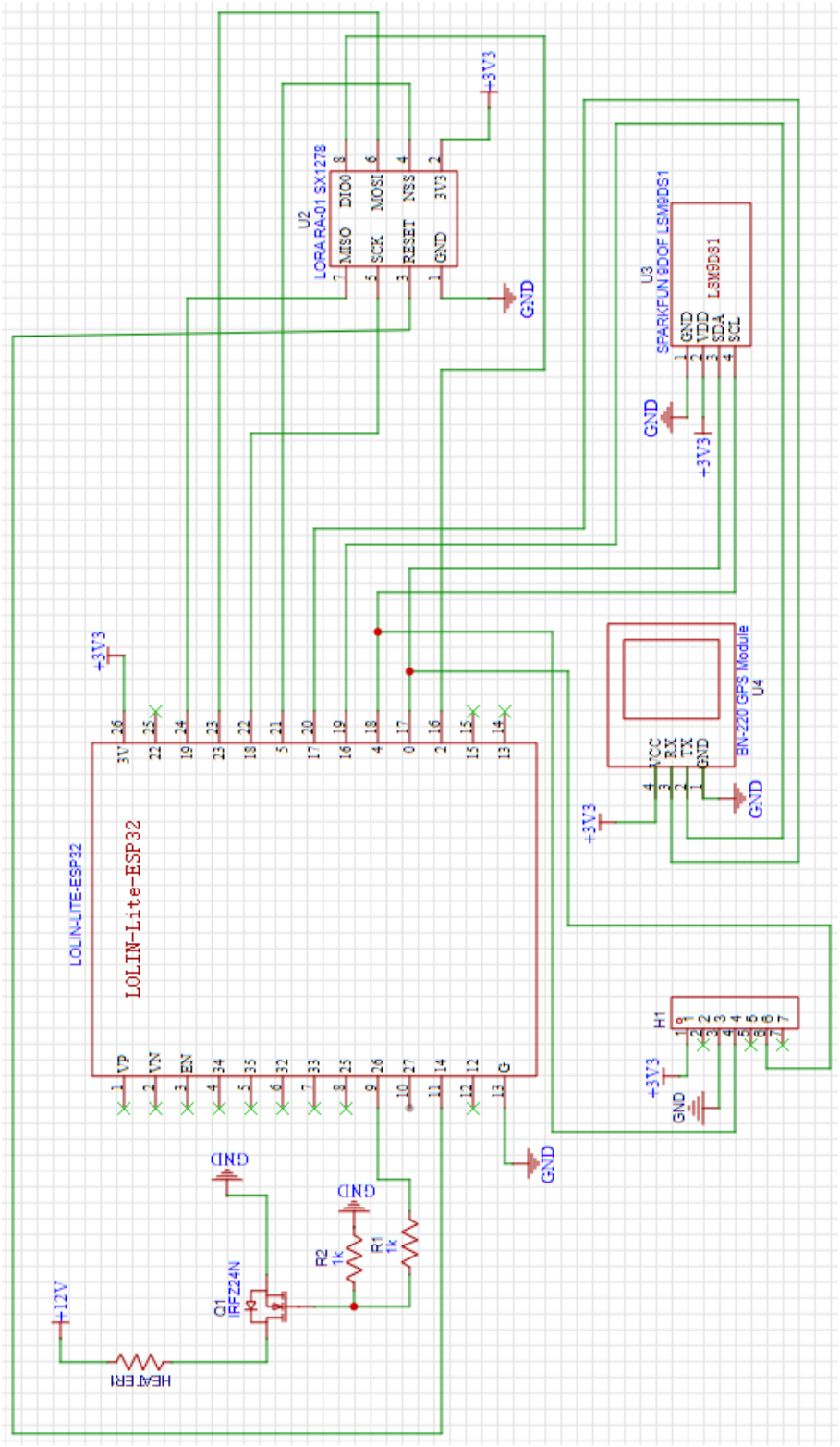

Figure 54: Wind Fish PCB schematic - from EasyEDA project

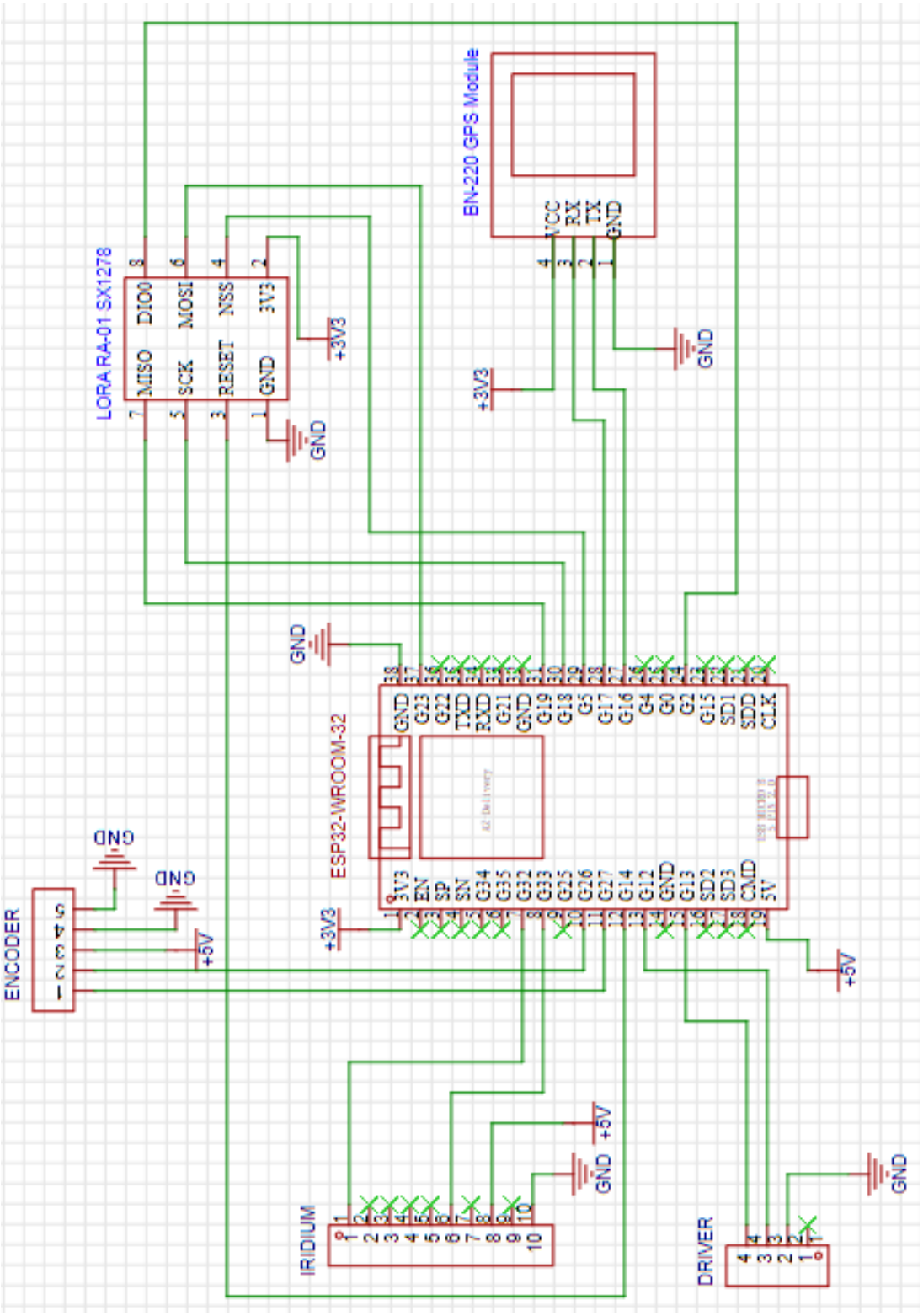

Figure 55: Nacelle PCB schematic - from EasyEDA project